IAEA-TECDOC-572

NUCLEAR DATA FOR RADIATION DAMAGE ASSESSMENT AND RELATED SAFETY ASPECTS 1989

PROCEEDINGS OF AN ADVISORY GROUP MEETING
ORGANIZED BY THE
INTERNATIONAL ATOMIC ENERGY AGENCY
AND HELD IN VIENNA, 19–22 SEPTEMBER 1989

FOREWORD

Radiation damage in materials is a field of increasing importance because the number of reactor service years is growing very fast. There were 429 nuclear power units working in the world as of July 1989. Despite the absence of new orders in the US and the after-Chernobyl slow down of atomic power reactor construction in the USSR the overall number of reactor units in the world is still growing and the total number of reactor operation years grows now by more than 1 year a day. It means that more and more reactor units (or their components) come to the end of their design service life and the problems connected with their exchange or extension of the service life become more and more important.

The Nuclear Data Section of the IAEA has been involved in the field of nuclear data for radiation damage assessment for about twenty years. Its programme on reactor neutron dosimetry resulted in the creation of the International Reactor Dosimetry File (IRDF) in 1982. This file is being updated constantly by NDS, the last version is now IRDF-85 and the creation of the next version is underway. Another activity of the NDS in this field is the international intercomparison exercise REAL, several rounds of the exercise were run and the results of these activities were discussed by the participants at the meeting.

The first Advisory Group Meeting on Nuclear Data for Radiation Damage Assessment and related Safety Aspects was convened by NDS eight years ago in October 1981. The present meeting was a second one on this topic and it was intended to summarize the progress and status of nuclear data for radiation damage assessment since the first meeting.

The participants have emphasized that since the first meeting a number of spallation neutron sources were put into operation and many material radiation damage studies are conducted now at these facilities. The distinguishing feature of spallation neutron sources is that the neutron energy spectra which they produce in most cases have a high energy component which may give a significant contribution to radiation damage. The proper understanding of radiation damage experiments in these neutron fields requires a better knowledge of nuclear data at high neutron energies.

These ideas were formulated in detail in the conclusions and recommendations of the participants which are contained in this report.

Another new issue was the need for activation cross-section data of long-lived isotopes. This topic is also considered in the conclusions below.

EDITORIAL NOTE

CONTENTS

CHARACTERIZATION OF NEUTRON REACTOR ENVIRONMENT, SURVEILLANCE AND NUCLEAR DATA (Session I)

HIGH ENERGY NEUTRON DOSIMETRY AND RADIATION DAMAGE CALCULATIONS (Session II)

REAL-88 RESULTS AND PROSPECTS (Session III)

CONCLUSIONS AND RECOMMENDATIONS

CHARACTERIZATION OF NEUTRON REACTOR ENVIRONMENT, SURVEILLANCE AND NUCLEAR DATA

(Session I)

Chairman

L.R. GREENWOOD
United States of America

EXPERIMENTAL AND THEORETICAL INVESTIGATIONS FOR WWER PRESSURE VESSEL NEUTRON EXPOSURE EVALUATION IN CZECHOSLOVAKIA

B. OŠMERA
Nuclear Research Institute,
Řež, Czechoslovakia

Abstract

A sixty degree symmetry sector of VVER-440 and VVER-1000 mock-ups in radial direction was realized in the LR-0 experimental reactor at the NRI Řež. Suitable geometrical conditions and technical arrangements of the LR-0 enable us to construct full-scale physical models of the VVER type reactors in radial direction from the core to the biological shielding of the reactor. This mock-ups represent the core periphery and radial shielding heterogeneities of the VVER-type reactors. The neutron spectrum was measured by proton recoil methods at the edge of the core, surveillance capsule position, on pressure vessel inner and outer walls. Neutron spectra calculations were performed by means of one- and two-dimensional transport codes ANISN and DOT-3.5 using data cross section libraries EURLIB-4, VITAMIN-C and CASK. The intercomparison of measured and computed data was done for differential spectra and integral quantities.

The precise physical model makes it possible to obtain direct experimental estimation of some quantities for the power reactors such as fast neutron spectra at "crucial points" (surveillance specimen position, inner and outer PV wall) and some space-energy indexes for radiation damage monitoring.

I. Introduction

The radiation damage evaluation and prediction is a necessary part of safety and economy analysis of any WWER power reactor. Knowledge of the space-energy distribution of neutron flux impining on a reactor pressure vessel is required for the evaluation of the radiation damage . Since 1980 a great attenation has been paid to the investigation of the neutron field parameters near the vicinity of the pressure vessel (PV). The experimental and theoretical studies began in the frame of the contract between Škoda Concern and N.R. I., IAE Moscow joined the work later.

The reactor characteristics cannot be always calculated wiht sufficient reliability and it is necessary to measure the needful quantities not only in the particular reactor but also in benchmark mock-ups from its components or fulscale low power assemblies of the reactor .

To rech demanded quality in the energy-space neutron flux density distribution measurements and monitoring the corresponding neutron spectrometers and methods were developed and improved /2/. Further progress wad reached since the Working Group on Reactor Dosimetry (WGRD) at the Czechoslovak Atomic Energy Commision has been established in 1980 /3/. Some published results associated with the WGRD activity could be found for example in /4, 5, 6/. During the Reactor Dosimetry Specialist reeting, held in Prague, Mart 27 - 28, 1985 /7, 8/ and Czechoslovak Reactor Dosimetry Seminar, Held in Prague, October 20 - 22, 1987 /9/ organized vy WGRD, the problems of the progress in this field have been discussed and corresponding recommendations and conclusions have been adopted.

Since 1983 the main effort has been concentrated on the WWER power reactor mock-up experiments on the LR-0 experimental reactor assembly.

A sixty degree symmetry sector of VVER-440 and VVER-1000 mock-ups in radial direction was realized in the LR-0 experimental reactor at the NRI Řež. Suitable geometrical conditions and technical arrangements of the LR-0 enable us to construct full-scale physical models of the VVER type reactors in radial direction from the core to the biological shielding of the reactor. This moc-ups represent the core periphery and radial shielding heterogeneities of the VVER-type reactors. The neutron spectrum was measured by proton recoil methods at the edge of the core, surveillance capsule position, on pressure vessel inner and outer walls. Neutron spectra calculations were performed by means of one- and two-dimensional transport codes ANISN and DOT-3.5 using data cross section libraries EURLIB-4, VITAMIN-C and CASK. The intercomparison of measured and computed data was done for differential spectra and integral quantities /11, 12/, fig. 1. 2.

The precise physical model makes it possible to obtain direct experimental estimation of some quantities for the power reactors such as fast neutron spectra at "crucial points" (surveillance specimen position, inner and outer PV wall) and some space-energy indexes for radiation damage monitoring.

The VVER mock-ups at the LR-0 experimental reactor could be also utilized for experimental investigation into different ways of decreasing the PV radiation loading (such as rearran-

gement of the core, steel shielding cassettes at the edge of the core, etc.). The series of this experiments have started this year.

The Light Water Experimental Reactor LR-0

The LR-0 reactor was designed for research on neutron-physical parameters of active zones of the pressurized water reactors of the VVER type. A multi-purpose design of the technology equipment allows accomplishment of experiments with VVER-1000- or VVER-440-type assemblies in symmetric or nonsymmetric arrangements with the standard or variable pitch in the triangular core lattice. Measurements may be performed with absorption clusters in VVER-1000-type assemblies shifted to desired heights, one chosen absorption cluster can be moved in the course of an experiment. The core is controlled mainly by changing moderator level in the reactor vessel. Thus, clean cores without absorption elements may be simulated. The H_3BO_3 concentration in the moderator may by of 0 to 12 g H_3BO_3 per 1 H_2O, the moderator may be heated up to 70 $^{\circ}C$. The heat from uranium fission in fuel elements is dissipated into the moderator. The termal power of the reactor is limited to 5 kW for 1 hour and the thermal neutron flux density in the centre of the reactor core to 10^{13} $m^{-2}s^{-1}$ /1/.

II. Description of the WWER-440 Mock-up and Experiment

The WWER-440 symmetry sector (60°) from the core periphery area to the inner region of the biological shield with the ionization chamber channel modelled on the LR-0 facility is seen on Fig. 1. The core and radiation shielding models (steel faceted belt, core basket, barrel and water leyer) were located inside the aluminium tank of the LR-0, the pressure vessel (steel) and biological shielding simulators were outside the tank. The LR-0 tank wall thickness is 16 mm.

The fuel composition in the core was chosen in such a way that the radial-azimuthal power distribution within its periphe-ry area, where the fast neutron source important in the radia-tion damage of the reactor vessel is formed, was close as much as possible to the equilibrium power distribution in the core pheripheral area of the commercial VVER-440 (standard loading).
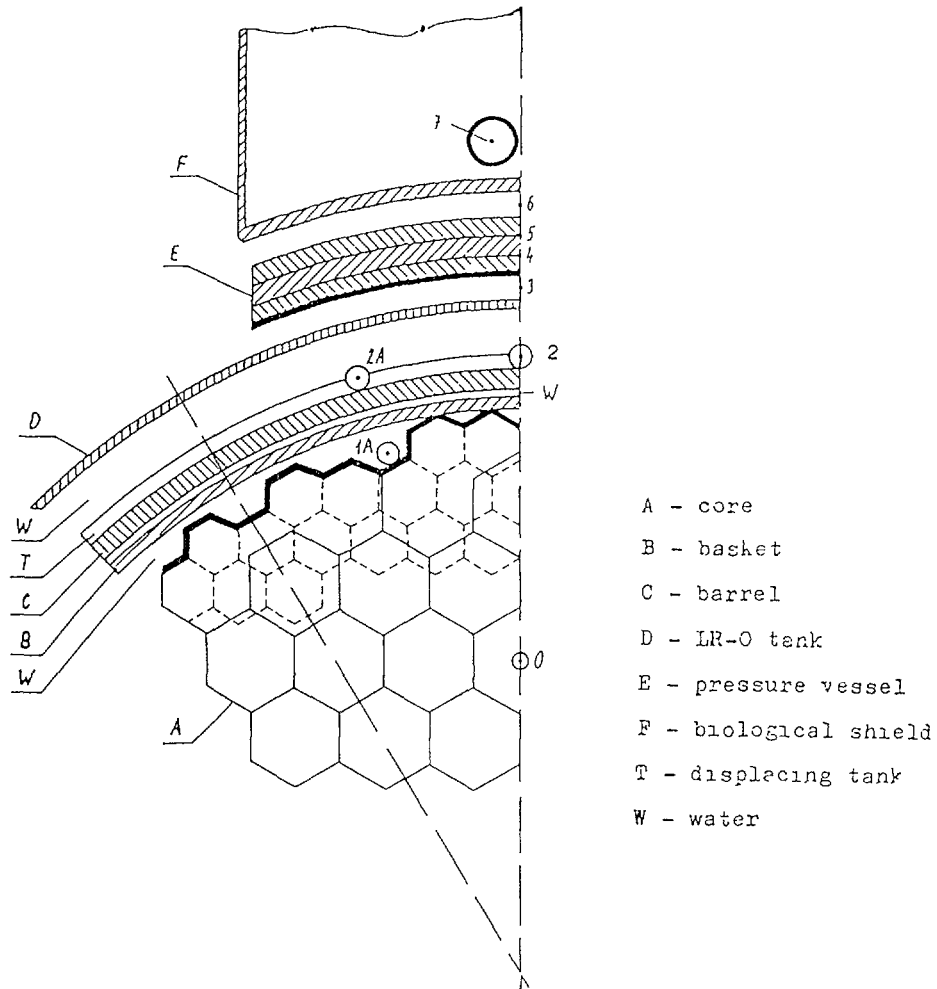
FIG 1 Schematic view of the WWER-440 mock-up
(numbers show measurement points)

A – core
B – basket
C – barrel
D – LR-O tank
E – pressure vessel
F – biological shield
T – displacing tank
W – water
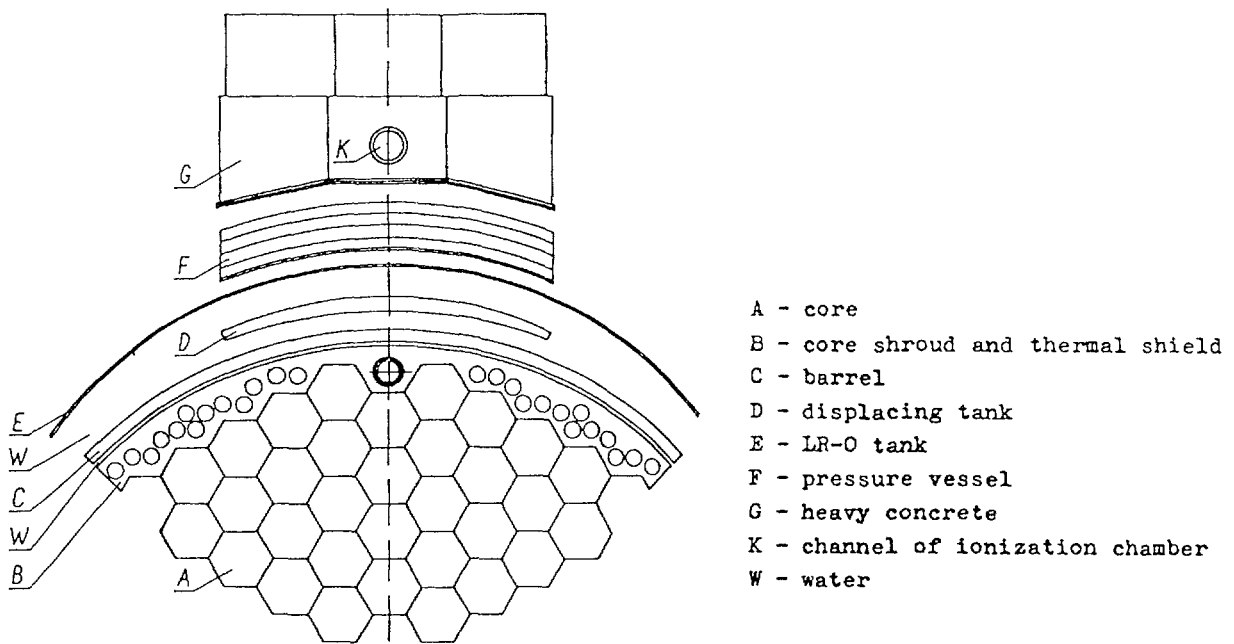
FIG 1a Schematic view of the WWER-1000 mock-up

A – core
B – core shroud and thermal shield
C – barrel
D – displacing tank
E – LR-O tank
F – pressure vessel
G – heavy concrete
K – channel of ionization chamber
W – water

The region of the maximum value of the fast neutron flux density incident on the pressure vessel is on the mock-up symmetry axis. The active mock-up core height is 125 cm.

For simulation of the water density reduction which takes place in the VVER-440 operation conditions the steel displacing tank is placed in the space between the barrel and the LR-0 tank.

The pressure vessel consists of three identical layers which can be successivelly shifted in radial direction in order to form an additional 65 mm air gap layer for the spectrometric measurements "over the vessel thickness".

The azimuthal length of the pressure vessel and biological shielding models was twice smaller than the core and the basket and barrel models. However, the pressure vessel and shielding models could be shifted in azimuthal direction for performing mesurements within the 30° azimuthal range.

The power distribution in the core was measured by means of the fuel element gamma activity (about 600 elements).

Measurements of differential energy distribution of the fast neutron flux density were carried out within the energy range of 10 keV - 10 MeV and 100 keV - 10 MeV respectivity at selected points of the mock-up (see Fig. 2). The following proton recoil detectors were used:

- a scintillation detector with a 10 x 10 mm stilben crystal for measurements within the 0,5 MeV - 10 MeV energy interval
- a 40 diameter sphere proportional hydrogen-filled counter, gas pressure 981 kPa, for measurements within the 0,3 MeV - 1,4 MeV energy interval (NOK 1045 chamber)
- a similar counter, the hydrogen pressure of 3S2,4 kPa, for measurements within the 0,01 MeV - 1,0 MeV interval (SP-2 chamber). The method of PSD was used to decrease the gamma background below 120 keV.

During the measurements in the water layer between the barrel and the LR-0 tank the spectrometer was set in the displacing tank using the cylindrical experimental channel. (Using the channel only, the Spectrum is perturbed /10/.) All the measurements were carried out at the central plane of the model core in four or five overlapping energy ranges depending
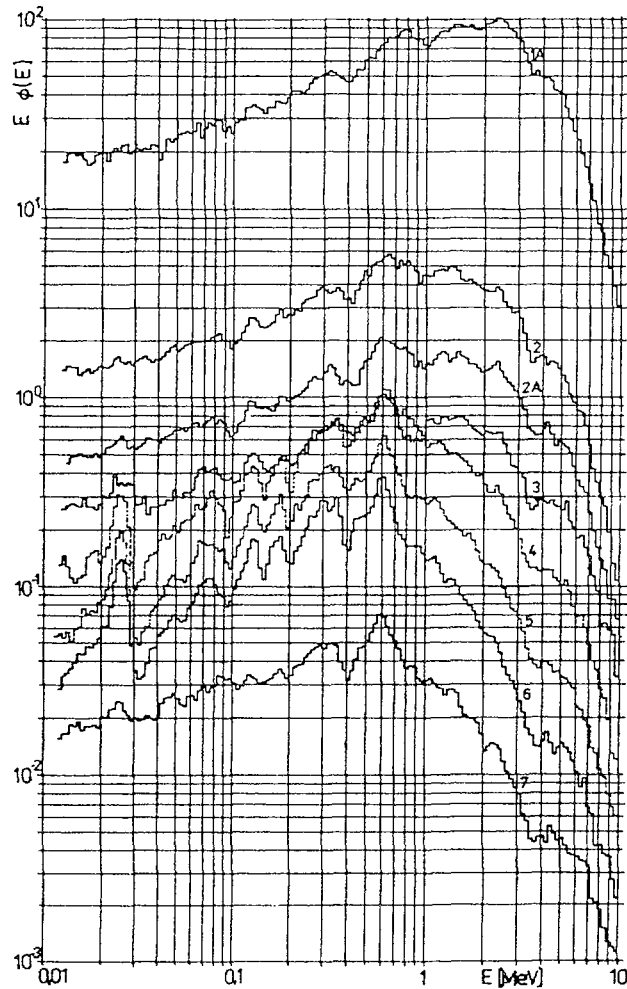
FIG. 2. Measured neutron spectra normalized to ϕ (E > 1 MeV)
in point 3, spectrum 2, measured in dry channel.

on the choice of the detectors and the amplification parameters
of this output signals. To perform the whole set of the spectra
measurements the LR-0 power changed within 0,1 W - 3 kW.

The experimental results (50 logarithmically equidistant
points per decade) were smoothed by using the cubic parabola
which was drawn through 5 - 9 points depending on the statis-
tical spread. The statistical uncertainties of smoothed neutron
flux density spectra are reparted in /10/.

Activation measurements were performed at positions of pro-
ton recoil measurements using different types of activation de-
tectors.

The measured spectra are presented on Fig. 2 /8, M.Holman/,
the azimuthal distributions on Fig. 3 /10, 12/.

14
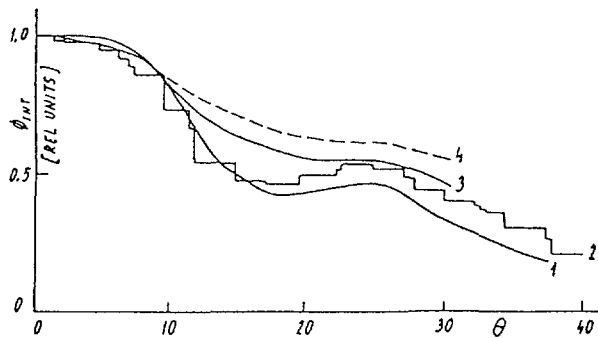
Azimuthal distribution of the fast neutron flux
density: 1 - behind the pit, $^{58}Ni(n,p)^{58}Co$;
2 - the same, calculation; 3 - before the pressure
vessel, $^{115}In(n,n')^{115m}Ih$, and the proton recoil
detector in the integrated mode; 4 - behind the
pressure vessel, the proton recoil detector in the
integrated mode.

FIG. 3.

Calculations

The calculations of the fast neutron flux characteristics
were carried out using the approximated formula for the neutron
flux density calculation in 3-D geometry based on 1D and 2D
calculations (in the r, r-θ and r-Z geometries) /13, 14, 15/.
For 1D calculation of the neutron flux density the ANISN code
/16/ was used, the 2D calculations were performed by the DOT-III
code /17/. In the calculations the cross-section libraries
DLC-23/CASK, VITAMIN-C and EURLIB-4 /18, 19, 20/ were used.
S_8P_3 approximation, 1 - 3 cm step in steel-water composition,
0,5° step in the azimuthal range weighted difference scheme,
were used. The distribution of neutron source density over
the core was specified on the basis of experimental investiga-
tions of fuel element power density distribution in the core
and calculations.

Table 1 lists the experimental and calculation values
of the normalized integral neutron flux densities at points
2, 3, 6 of the mock-up /10, 12/.

The results were obtained at a water layer thickness of
12 cm (which corresponds to a water density of 770 kg/m^3).
The calculation values were obtained in S_8P_3 - approximation
using the cross-section library DLC-23/CASK.

15

TABLE 1 RELATIVE INTEGRAL ENERGY DISTRIBUTIONS OF NEUTRON FLUX DENSITIES

Measure- ment point	Experiment or cal- culation	E_{min}, MeV				
		0.11	0.55	1.1	3.0	5.0
2	Exp.	35.9	20.3	10.9	2.16	0.648
2	Cal.	38.1	20.8	11.0	2.1	0.66
3	Exp.	2.65	1.62	1.0	0.267	0.105
3	Cal.	2.56	1.57	1.0	0.26	0.10
6	Exp.	0.603	0.256	0.096	0.0147	0.0058
6	Cal.	0.69	0.26	0.1C	0.0154	0.0062

Figs. 4 shows the normalized calculation and exprimental differential energy spectra at points 3 and 6. In these cal- culations the EJRLIB-4 cross-section library was used /12, 1C/. More detailed analysis of the results could be found in /12,1C/.

III. Conclusions

The investigations carried out for the first time on the models the VVER reactor types represent the first important stage of research work an quality assessment of radiation load of VVER reactor type pressure vessels.

Since 1986 the experimental data of the VVER-440 mock-up (standard core) measurements have been adopted for the evalua- tion of the neutron dosimetry data in surveillance specimen programme /21/. The neutron spectra at the surveillance speci- men point, PV inner and outher walls in the central plane of the core together with the corresponding space-energy indexee were recommended for further use in this type of reactor with the standard core loading (modelled in mock-up). Simultaneously the data of the LR-0 experiments were widely used for the eva- lution of the neutron flux measurements at the PV outer wall of power reactors by activation detectors /22/.

DETECTOR 6
1 - EXP. . CALC.: 2 - EUR.
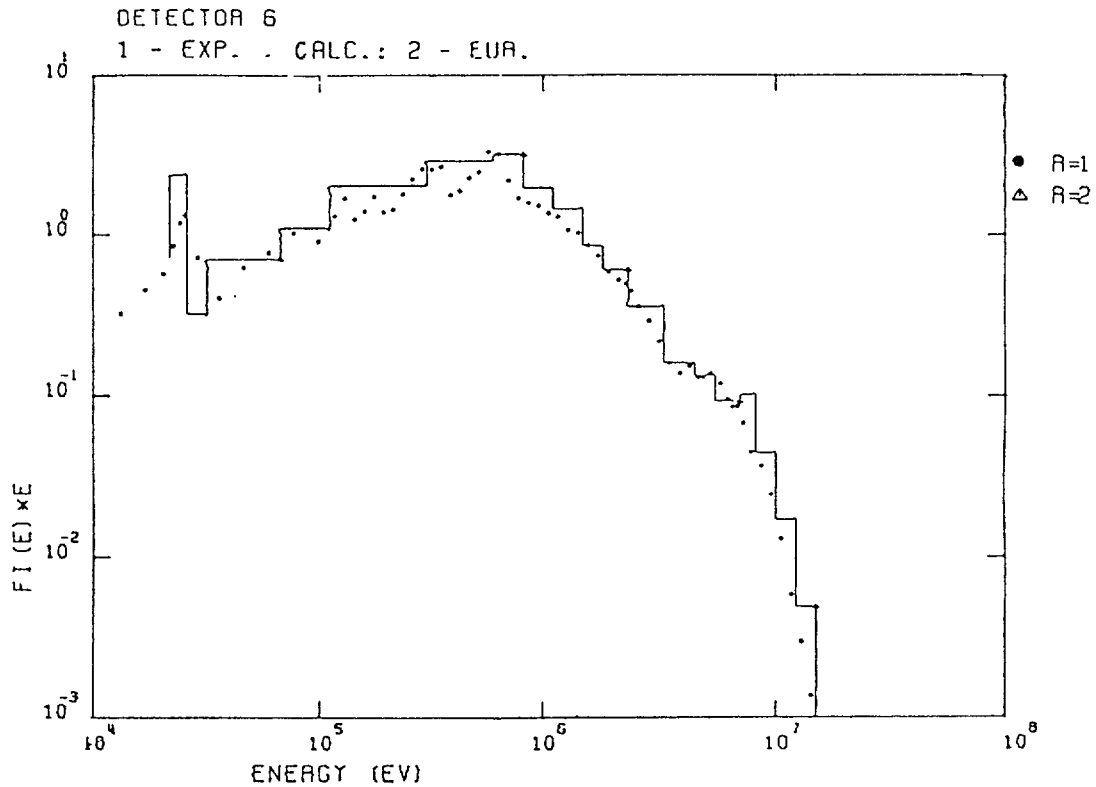
Differential energy spectrum of the neutron flux

density Ø (E)E at point 6. ... - experiment,

⌐ - calculation (EURLIB-4).

DETECTOR 3
1 - EXP. . CALC.: 2 - EUR.
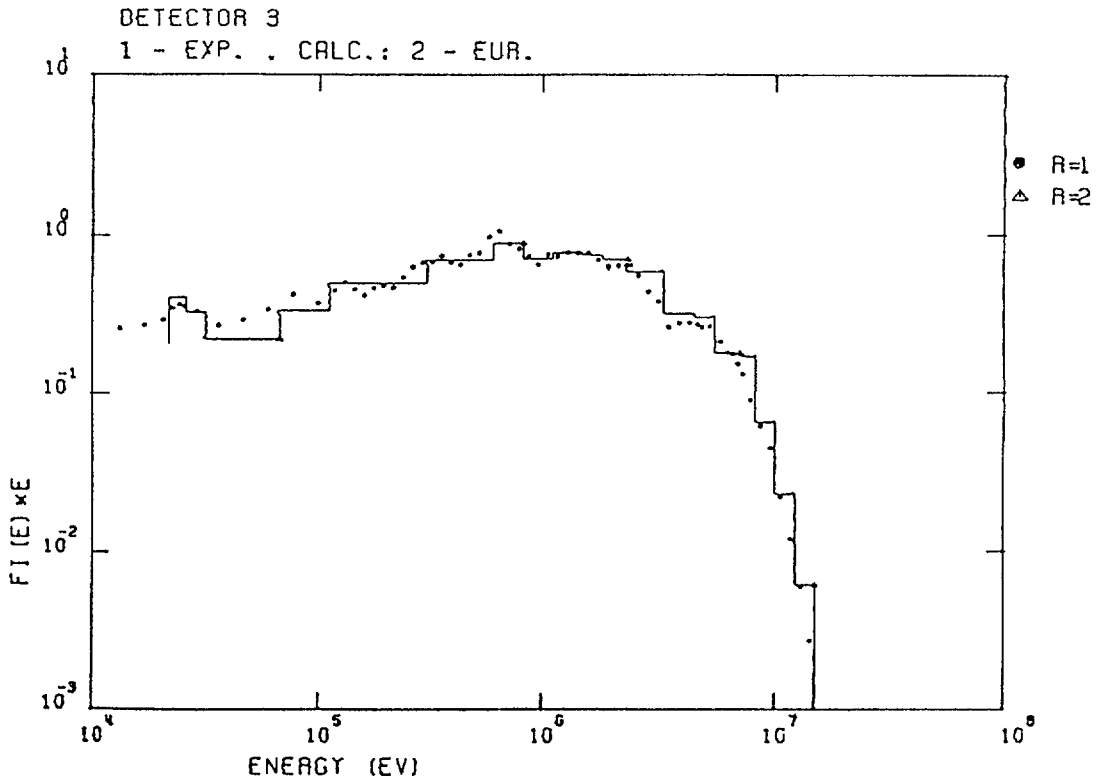
Differential energy spectrum of the neutron flux

density Ø (E)E at point 3. ... - experiment,

⌐ - calculation (EURLIB-4).

FIG. 4.

17

The corresponding space-energy indices are reported in Table 2 (9, M. Holman/. These indices were used for the evaluation an neutron flux density estimation in nuclear power plant at PV (O) in point corresponding to the mock-up experiment /22,9/.

TABLE 2

SPECTRAL INDEX

Point		E [MeV]					
		0,1	0,5	1	2	3	5
SB	E	3,04	1,80		.406	.180	0,054
(a)	C	3,00	1,81	1	.415	.184	0,056
R=163,5 cm	E/C	1,01	0,99		0,98	0,98	0,96
PV(I)	E	2,49	1,59		0,486	0,247	0,098
TN (b)	C	2,31	1,53	1	0,521	0,262	0,099
R=177, 1 cm	E/C	1,08	1,04		0,93	0,942	0,99
PV(O)	E	5,35	2,60		0,302	0,128	0,047
TN (e)	C	5,87	2,71	1	0,286	0,115	0,043
R=192 cm	E/C	0,91	0,96		1,06	1,11	1,09

SB: surveillance box; PV(I): pressure vessel inner surface; PV(O): pressure vessel outer surface; E: experiment; C: calculation.

SPACE INDEX R_j/R_i ϕ (E > 1 MeV)

R_j [cm]	163,5	
R_i [cm]	177,1	192
	a/b	a/e
E	8,2	79,4
C	8,65	73,44
E/C	0,95	1,08

SPACE INDEX R_j/R_i ϕ (E > 0.5 MeV)

R_j [cm]	163,5	
R_i [cm]	177,1	192
	a/b	a/e
E	9,2	55
C	10,2	49
E/C	0,9	1,12

TABLE 2a. 90% ENERGY RESPONSE INTERVALS OF MONITORS

Monitor/ Point	SB E /MeV/	PV (I)	PV (0)
+ 54 Fe (n,)	2.2-7.7	2.3-8.7	2.1-8.7
+ 63 Cu (n,)	4.9-11.1	5.2-11.7	5.2-11.6
+ 93 Nb (n, n′)	0.63-5.2	0.69-6.2	0.475-5.1
++ 115 In (n, n′)	0.92-5.6	1.0-6.5	0.76-5.7

+ SB monitors,   ++ mock-up detector
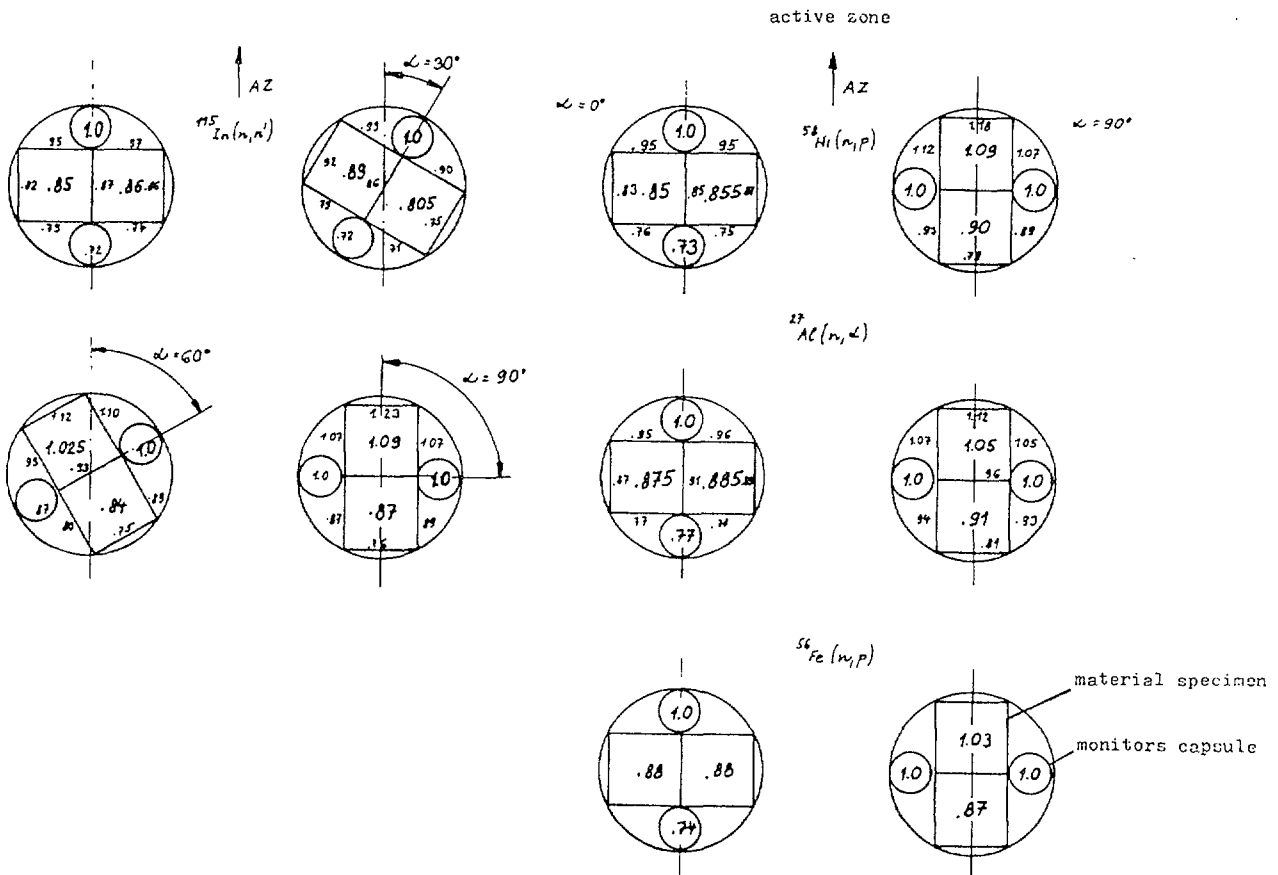
FIG. 5. Relative distribution of fast neutron flux density in SB depending on SB orientation during irradiation.
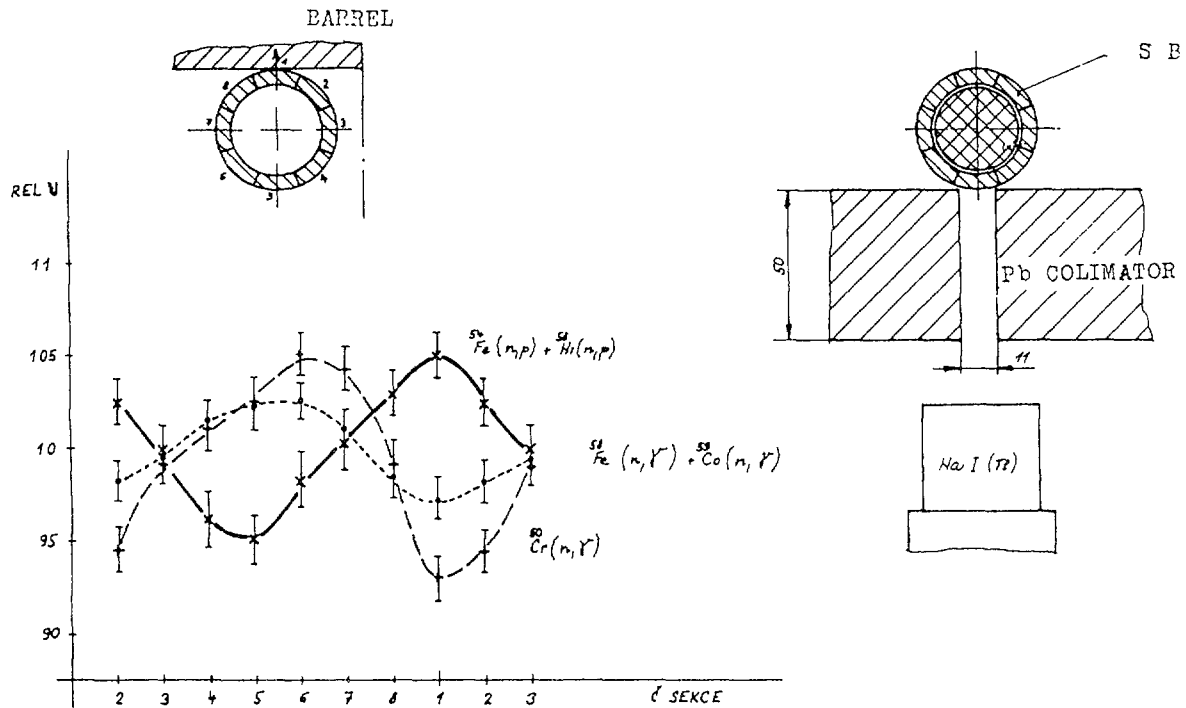
FIG. 6. Azimuthal distribution of SB activation.

To evaluate the surveillance specimen monitors it is
neccesary to take into account real geometry and reevalute the
corresponding space index. A systematic error is coused by
undefined azimuthal position of the monitors in SB during
irradiation. The neutron flux distributions were studied
in a physical model at ŠR-0 reactor (Škoda). The results
are presented on Figures 5, 6 /9, F. Vychytil/. To complete
the problem of error propagation in neutron flux monitoriong
/23/ with full error matrix it is necessary to estimate the
corresponding matrixes of the measured and calculated spectra
(relating sensitivity studies needs the cross section error
matrixes). The mock-up program an LR-0 reactor is being
acompcanied by benchmarks in sphere and slab geometry (iron,
iron-water with Cf^{252} source) which have been extensively
used for the spectrometers intercalibration. The last but not
least part of this work is the fluence monitoring at PV (0)
by means of activation detectors. The standardized procedure
of monitoring including an effective computing method
should be the goal of this programme.

20

TABLE 3

NEUTRON FLUXES IN THE NORD NUCLEAR POWER PLANT (GDR)

E_p/MeV/ point		0,1	0,5	1	2	3	5
SB	E	4,68+16	2,77+16	1,54+16	6,25+15	2,77+15	8,31+14
	C	4,26+16	2,57+16	1,42+16	5,90+15	2,61+15	7,95+14
(a)	E/C	1,10	1,08	1,08	1,06	1,06	1,04
PV(I)	E	4,65+15	2,97+15	1,87+15	9,08+14	4,62+14	1,83+14
(b)	C	3,81+15	2,52+15	1,65+15	8,60+14	4,32+14	1,63+14
	E/C	1,22	1,18	1,13	1,05	1,07	1,12
PV(O)	E	1,04+15	5,03+14		5,85+13	2,52+13	9,08+12
(e)	C	1,14+15	5,25+14	1,94+14	5,54+13	2,23+13	8,34+12
	E/C	0,91	0,95		1,05	1,13	1,09

SB: surveillance box; PV(I): pressure vessel inner surface; PV(O): pressure vessel outer surface.

INTEGRAL CROSS-SECTIONS

Detector Point	$\bar{\sigma}\ (E > 1MeV)\ \mathrm{cm}^2$ 93,Nb(n,ń)	54Fe(n;p)	63Cu(n, α)	58Ni(n,p)	55Mn(n,2n)
SB	2.238-25	7,49-26	5,53-28	-	- -
PV(O)	2.359-25	5,863-26	6,668-28	7,921-26	3,925-28
	46Ti(n,p)				
	-				
PV(O)	9,887-27				

TABLE 4. STATISTICAL UNCERTAINTIES (PERCENT) OF SMOOTHED NEUTRON FLUX DENSITY SPECTRA

Measurements Point	Energy Range, MeV				
	0.012-0.12	0.12-0.8	0.8-2.4	2.4-7.0	7.0-10.0
2	5-10	2-10	2-20	1-10	2-20
3	10-25	3-20	2-15	2-10	15-30
6	2-25	1-10	2-6	1-20	10-25

REFERENCES

/1/ Sochor, Q. : The Experimental Reactor LR-O. Jaderná energie, 30, 1984, N°. 7, pp. 243-247

/2/ Ošmera, B., et al., Neutron Spectra Measurements and Neutron Flux Monitoring for Radiation Damage Purposes. Report ÚJV 5081-R, Řež, 1979

/3/ Petr, J., Ošmera, B. Report on establishing of the Working Group pn Reactor Dosimetry of the CAEC (in Czech), Jaderná energie, Col. 27, p. 116 (1981)

/4/ Ošmera, B. et al., The Activity of the Czechoslovak Working Group on Reactor Dosimetry in the Period from 1980 to 1983; Proceedings of the Fifth ASTM-EURATOM Symposium on Reactor Dosimetry, Volume, 2, p. 967

/5/ Ošmera, B. et al., Neutron Spectra Measurements in WWR-S Reactor. Proceedings of the Fourth ASTM-EURATOM International Symposium on Reactor Dosimetry, NUREG/CP-0029-VI, Vol. 1, US Nuclear Regulatory Commission, Washington, DC, p. 587, 1982

/6/ Brumovský, M. et al., Effect of Uncertainties in Neutron Spectra and Fluence Determination on the WWER Pressure Vessel Lifetime Prediction. Proceedings of the Advisory Group Meetkings on Nuclear Data for Radiation Damage Assesment and Related Safety Aspects, IAEA-TECDOC-263, Vienna, p. 193, 1982

/7/ Neutron spectrometry and Reactor Dosimetry. Proceedings of the Reactor Dosimetry Specialist Meeting. Invited papers. W.G.R.D. Prague, 1985 (in Czech)

/8/ Neutron Spectrometry and Reactor Dosimetry Proceeding of the Reactor Dosimetry Specialist Meeting. Mars 27-28, 1985, W.G.R.D. Prague, 1985 (in Czech)

/9/   Reactor Dosimetry. Proceedings of the Czechoslovak
Seminar, October 20-22, 1987.
W.G.R.D. Prague, 1988 (in Czech)

/10/   Ošmera, B. et al. : Experimental Validation of Neutron
Calculations for VVER Pressure Vessel Radiation Load
Evaluation. Reacotr Dosimetry: Methods, Applications
and standardization. ASTM STP 1001, 1989, p. 130

/11/   Ošmera, B. et al.: Experimental and Theoretical Inves-
tigations of the Neutron Flux Distribution Outside the
Core of VVER-1000 Reactor Type. 7th International
Conference on Radiation Shielding, 12 - 16 September,
Bournemouth, UK

/12/   Ošmera, B., et al., Mock- up Experiments for the Deter-
mination of the Radiation Loading of the WWER Reactor
type Pressure Vessel. Report ÚJV 7797, Řež, 1986
(in Russian, restricted distribution)

/13/   Brodkin, E.B., Kozhevnikov, A.N., Khrustalev, A.V.
Determination of Characteristics of the Neutron Field
Affecting on the WWER Reactor Vessel. In : Proc. 6th
Intern. Conf. Rad. Shielding, 1983 Tokyo, Japan, CONF-
850538, vol. 2, pp. 1055-2060

/14/   Brodkin, E.B., Khrustalev, A.V., Methods for calculation
of characteristics of the neutron flux in the WWER-440
near-vessel space. In "Voprosy atomnoi neuki i tekhniki.
Seriya: Fizika i tekhnika yadernykh reaktorov, 1986,
vyp. 4, S. 50 (in Russian)

/15/   Borodin, A V., Brodikin, E.B., Vikhrov, V.I. et al. :
Calculation and experimental studies of the neutron flux
in the WWER-440 near vessel space. In "Voprosy atomnoi
nauki i tekhniki, Seriya: Fizika i tekhnika yadernykh
reaktorov", 1985, vyp. 4, S. 72 (in Russian)

/16/   Engle, W.W., Jr., A Users Manual for ANISN, K-1693, 1967

/17/   Rhoddes, W.A., Mynatt, F.R. The DOT-III Two-Dimensional
         Discrete Ordinates Transport Code, ORNL-TM -4280, 1973

/18/   40 Group Coupled Neutron and Gamma Rays Cross Section
         Data. RSIC DATA LIBRARY DLC-23, 1973

/19/   RSIC DATA LIBRARY COLLECTION VITAMIN-C (DLC-41),
         ORNL, 1979

/20/   Gaglioti, E. et al., EURLIB-4, Standard Shielding Library
         for Fission and Fusion Technology, 1980

/21/   Ošmera, B. : Recommended Neutron Dosimetry Data for the
         Evalution of the WWER-440 Surveillance Programme.
         Interlaboratory notes - June 1986. Unpublished.

/22/   Mehner, H.C., Ošmera, B. et al., Ex-Vessel Dosimetry
         at WWER-440. 6th ASTM Reactor Dosimetry Symposium
         Jackson Hole, 1987

/23/   Ošmera, B., Štěpánek, V. : The Determination of the
         Error in ronitoring the Neutron Flux and Fluence in
         a Nuclear Reactor. Jaderná energie 33, 1987, N° 8-9,
         p. 304

SOLID STATE TRACK RECORDER PRESSURE VESSEL SURVEILLANCE NEUTRON DOSIMETRY AT COMMERCIAL NUCLEAR POWER REACTORS

F.H. RUDDY, J.G. SEIDEL
Westinghouse Science and Technology Center,
Pittsburgh, Pennsylvania,
United States of America

Abstract

Solid State Track Recorder neutron dosimetry methods developed under the U.S. Nuclear Regulatory Commission Light Water Reactor Pressure Vessel Surveillance Dosimetry Improvement Program have been applied for pressure vessel surveillance dosimetry at commercial nuclear power reactors. More than 800 SSTR neutron dosimeters have been deployed at twelve different power reactors during twenty-two cycles of operation. More than 300 SSTR have been analyzed, and results with uncertainties in the 2-5% range have been generally obtained.

Several new areas of application of SSTRs for radiation damage assessment for safe routine operation or extended life operation of power reactors are planned and these applications are discussed.

---

1. INTRODUCTION

In 1977 the United States Nuclear Regulatory Commission established the Light Water Reactor Pressure Vessel Surveillance Dosimetry Improvement Program. Among the dosimetry methods developed under this program for light water reactor pressure vessel surveillance is the use of Solid State Track Recorders (SSTRs). The status of the development of SSTR neutron dosimeters was reported at the last meeting in this series.[1] Since that time SSTR neutron dosimeters have been used for pressure vessel surveillance dosimetry at commercial nuclear power reactors by a number of U.S. Utilities.

One of the key accomplishments in the extension of SSTR neutron dosimetry methods to the higher neutron fluences characteristic of pressure vessel surveillance dosimetry applications was the development of methods to produce ultra low-mass fissionable deposits.[2] A second key development was the establishment of routine automated track scanning methods for SSTRs.[3] The overall validity and accuracy of these techniques for high fluence SSTR neutron dosimetry have been verified by irradiations in U.S. National Institute of Standards and Technology (formerly National Bureau of Standards) standard neutron fields. These results are described in a separate paper at this conference.[4]

2. REACTOR CAVITY SSTR NEUTRON DOSIMETRY

Dosimetry sets containing radiometric foils and flux wires as well as SSTR neutron dosimetry are deployed at power reactors in key locations outside of the pressure vessel in the annular gap or reactor cavity region. These dosimetry sets are placed during maintenance outages and left in place during the operating cycle until the next outage, at which time the dosimetry set is retrieved for analysis and replaced with dosimetry for the subsequent operating cycle. To date, SSTR neutron dosimeters have been deployed for a total of 22 operating cycles at twelve different power reactors. Of the twelve reactors, one is entering its fourth cycle of operation with SSTR neutron dosimetry in place and two are in their third operating cycle.

A typical SSTR neutron dosimetry set consists of separate aluminum and cadmium covered ^{235}U and ^{239}Pu dosimeters and cadmium covered ^{237}Np and ^{238}U dosimeters or a total of six SSTR-fissionable deposit pairs per set. To date, a total of more than 800 SSTRs have been deployed in nuclear power reactors and more than 300 have been analyzed. Fission reaction rates have been measured with uncertainties

that are generally in the 2-5% range, and, with the exception of one damaged dosimetry set, more than 96% of the fissionable deposits have been found to be reusable in subsequent dosimetry cycles.

3. OTHER PLANT LIFE EXTENSION RELATED SSTR APPLICATIONS

SSTR neutron dosimeters offer advantages for other applications related to the emerging field of nuclear plant life extension (PLEX). SSTR neutron dosimetry has been applied at neutron fluence rates as low as 3×10^{-4} n/cm^2/sec[5] and can be applied accurately up to fluences of about 5×10^{18} n/cm^2.[6] In addition to pressure vessel surveillance, other possible areas of SSTR dosimetry application include:

(1) Reactor Vessel Support Surveillance

(2) Equipment Qualification (EQ) Surveillance

(3) Reactor Vessel Internals Monitoring

3.1 REACTOR VESSEL SUPPORT STRUCTURE SURVEILLANCE DOSIMETRY

Recently, fluence rate effects on neutron embrittlement were deduced from analyses conducted as part of the pressure vessel materials surveillance program at the High Flux Isotope Reactor at Oak Ridge National Laboratory.[7,8] Materials tests revealed that the embrittlement rates of several ferritic carbon steels were higher than anticipated for the corresponding neutron fluences, presumably due to the much lower fluence rate in HFIR compared to metallurgical test reactors. An immediate concern is that the fluences and fluence rates obtained in the HFIR specimens are similar to those anticipated for the support structures for reactor pressure vessels. Indeed, a need for neutron dosimetry to evaluate potential neutron-induced embrittlement in vessel support structures has been identified.[8,9]

In most cases, the neutron fluxes received by support structures are much less than those obtained at cavity dosimetry locations. Whereas the sensitivity of radiometric dosimetry decreases with neutron fluence, SSTR neutron dosimetry is less difficult at the fluences anticipated in support structure neutron dosimetry because of less stringent low-mass requirements for the SSTR fissionable deposits. Therefore, SSTR neutron dosimetry offers a proven and immediately available method for addressing dosimetry concerns related to pressure vessel support surveillance.[10]

3.2 EQ SURVEILLANCE

Degradation due to aging and service wear limits the life of many reactor components that are located within reactor containment. The useful life of these components is shortened by aging effects that are generally accelerated by the effects of radiation exposure and elevated temperatures. Pre-use qualification tests use worst case conditions with respect to radiation and temperature. Maintenance and/or replacement of these components are often based on conservative assumptions regarding the reactor operating environment. SSTR neutron dosimetry provides a means to obtain data to verify that equipment qualifications with respect to neutron exposure are not exceeded either during routine or extended life service.[10]

Because the neutron fluxes to be monitored are of the order of 10^6 n/cm^2/sec, the much higher sensitivity of SSTR neutron dosimeters relative to radiometric flux foils makes SSTRs the method of choice for EQ surveillance dosimetry.

3.3 REACTOR VESSEL INTERNALS MONITORING

Irradiation effects on core structural elements have recently become a subject of concern due to the potential effects of irradiation-assisted stress corrosion cracking on grid plates, core plates, and on

top guides, control rods, and control rod drive assemblies.[11] Because the anticipated neutron fluxes are in the range from 10^{11}-10^{12} n/cm^2/sec, the use of SSTR neutron dosimeters is limited to rather short exposure times due to the present SSTR upper fluence limit of about 5 X 10^{18} n/cm^2. However, methods are currently under development at the Westinghouse Science & Technology Center that should extend the present high fluence limit to a significantly higher level. Therefore, imminent applications of SSTR neutron dosimetry in core structural element monitoring are anticipated. These developments in SSTR technology should also open other fields of SSTR application such as the use of SSTR neutron dosimeters in replacement reactor surveillance capsules.

4. CONCLUSIONS

SSTR neutron dosimeters provide a useful and versatile means for obtaining data for radiation damage assessment. Among the many advantages of SSTR neutron dosimetry are:

(1) SSTRs have a wide range of sensitivity ranging from cosmic ray-induced neutron background up to about 5 x 10^{18} n/cm^2.

(2) Because SSTRs are passive devices, they can be deployed and retrieved during plant outages, thereby reducing the radiation doses to required support personnel. During operation, no support personnel or electronics are necessary.

(3) SSTRs measure integrated neutron exposure. Detailed time history corrections are not needed.

(4) SSTR neutron dosimeters can be deployed in harsh β/γ and

temperature environments. SSTRs are totally insensitive to

β/γ background and have been used at temperatures in the

680-830°F range.[12]

(5) SSTRs can be miniaturized, introducing minimal

perturbations into the neutron field being measured.

(6) SSTR neutron dosimetry is a high accuracy technique.

Uncertainties in the 2-5% range are obtained routinely in

cavity dosimetry measurements,[13] and, with care,

uncertainties less than 1% can be obtained.[14]

(7) SSTRs are a permanent record. An SSTR retains the tracks

produced during a neutron dosimetry exposure, and the SSTR

can be stored as a permanent Quality Assurance record for

time periods relevant to the routine or extended life

operation of a reactor.

The use of SSTR neutron dosimetry for reactor pressure vessel

surveillance has become commonplace, and extended applications in other

radiation damage assessment areas related to safe routine operation or

extended life operation of nuclear power plants are planned.

REFERENCES

1. F. H. Ruddy, R. Gold, and J. H. Roberts, "Pressure Vessel Surveillance Dosimetry Using Solid State Track Recorders," in Nuclear Data for Radiation Damage Assessment and Related Safety Aspects, IAEA-TEC-DOC-263, Vienna, (1982), p. 109.

2. F. H. Ruddy, "Neutron Dosimetry in High Intensity Fields: A Review," Nuclear Tracks and Radiation Measurements 11, 197 (1986).

3. F. H. Ruddy, A. E. Manhardt, and J. G. Seidel, "Analysis of Solid State Track Recorders with the Westinghouse Research and Development Center Automated Track Counter "in Reactor Dosimetry: Methods, Applications, and Standardization, ASTM STP 1001, American Society for Testing and Materials, Philadelphia, p. 676 (1989).

4. F. H. Ruddy and E. D. McGarry, "Benchmark Referencing of Ultra Low-Mass Solid State Track Recorder Neutron Dosimeters in NBS Standard Neutron Fields," IAEA Advisory Group Meeting on Nuclear Data for Radiation Damage Assessment and Related Safety Aspects, Vienna, Austria, Sept. 19-22, 1989.

5. F. H. Ruddy, J. H. Roberts, and R. Gold, "Applications of Solid State Track Recorder Neutron Dosimetry for Fuel Debris Location in the Three Mile Island Unit 2 Makeup and Purification Demineralizers," Nuclear Tracks 8, 473 (1984).

6. F. H. Ruddy and J. G. Seidel, "Solid State Track Recorder Pressure Vessel Surveillance Neutron Dosimetry at Commercial Light Water Reactors," in Reactor Dosimetry: Methods, Applications, and Standardization, ASTM STP 1001, American Society for Testing and Materials, 1989, p. 175.

7. R. D. Cheverton, F.B.K. Kam, R. K. Nanstad, and G. C. Robinson, "An Embrittlement Rate Effect Deduced from HFIR that May Impact LWR Vessel Support Life Expectancy," in Nuclear Power Plant Life Extension, ISBN 0-89448-139-8, American Nuclear Society, Volume 1, p. 98 (1988).

8. R. D. Cheverton, W. E. Pennell, G. C. Robinson, and R. K. Nanstad, "Impact of Radiation Embrittlement on the Integrity of Pressure Vessel Supports for Two PWR Plants," NUREG/CR-5320 (ORNL/TM-10966), January 1989.

9. R. L. McCoy, "NUPLEX: Oconee Vessel Support," in Nuclear Power Plant Life Extension, ISBN 0-89448-139-8, American Nuclear Society, Volume 1, p. 99 (1988).

10. F. H. Ruddy, "The Use of Solid State Track Recorders for Plant Life Extension Related Neutron Dosimetry," in Nuclear Power Plant Life Extension, ISBN 0-89448-139-8, American Nuclear Society, Volume 2, p. 386 (1988).

11. C. Z. Serpan, "NRC Research in Aging and Extended Life for LWR Primary Systems," Trans. ANS 55, 266 (1987).

12. F. H. Ruddy and J. H. Roberts, "Solid State Track Recorder Fission Rate Measurements at High Neutron Fluence and High Temperature," Nuclear Tracks and Radiation Measurements 11, 193 (1986).

13. F. H. Ruddy and J. G. Seidel, "Pressure Vessel Surveillance at Commercial Light Water Reactors Using Solid State Track Recorder Neutron Dosimetry," Nuclear Tracks and Radiation Measurements 15, 491 (1988).

14. R. Gold, R. J. Armani, and J. H. Roberts, "Absolute Fission Rate Measurements with Solid State Track Recorders," Nuclear Science and Engineering 34, 13 (1968).

BENCHMARK REFERENCING OF ULTRA LOW-MASS
SOLID STATE TRACK RECORDER NEUTRON DOSIMETERS
IN NBS STANDARD NEUTRON FIELDS

F.H. RUDDY
Westinghouse Science and Technology Center,
Pittsburgh, Pennsylvania

E.D. McGARRY
National Institute of Standards and Technology,
Gaithersburg, Maryland

United States of America

Abstract

Ultra low-mass fissionable deposit fabrication techniques
developed for light water reactor pressure vessel surveillance
dosimetry with solid state track recorders have been verified
through irradiations in standard neutron fields at the National
Institute of Standards and Technology (formerly NBS). Excellent
agreement has been obtained between independent absolute
calibrations of the fissionable deposits based on ultra low-mass
radiochemical spiking techniques and on the response to a known
neutron fluence in the standard neutron field. The status of and
the results of standard irradiations carried out to date are
described.

1. INTRODUCTION

The status of the development of Solid State Track Recorders

(SSTRs) for high fluence neutron dosimetry was described at the

preceding meeting in this series,[1] and the present status is described

elsewhere in these proceedings[2]. SSTRs have now been used for pressure

vessel surveillance dosimetry in more than 22 cycles of operation at

commercial power reactors.

A key to the successful use of SSTR neutron dosimetry for this

purpose is the development of techniques to produce ultra low-mass

fissionable deposits[3]. SSTR neutron dosimeters are deployed in the

reactor cavity region of power reactors and are typically left in place

for one operating cycle. During that time the dosimeters are exposed to

fast neutron fluences in the range (2-5) x 10^{16} n/cm^2. In order to

obtain accurate results, SSTR track densities must be kept below about 10^6 tracks/cm^2 [4].

This is accomplished by limiting the mass of the fissionable deposit so that track densities in the range from about 5×10^3/cm^2 to 5×10^5/cm^2 result. The deposit masses required to accomplish this purpose are contained in Table 1.

Table 1. Required Fissionable Deposit Masses for SSTR Cavity
Neutron Dosimetry

Isotope	Cover	Deposit Mass (grams/cm^2)
^{239}Pu	Al	1.3×10^{-13}
^{239}Pu	Cd	6.3×10^{-13}
^{235}U	Al	1.9×10^{-13}
^{235}U	Cd	9.5×10^{-13}
^{237}Np	Cd	4.7×10^{-10}
^{238}U	Cd	3.2×10^{-9}

The masses of these deposits are much less than those conventionally used in SSTR neutron dosimetry. For example, 1.3×10^{-13}g/cm^2 of plutonium corresponds to only 3 atoms per square μm of surface area.

Special isotopic spiking techniques have been developed[3] for absolute mass calibrations of these deposits. Selected deposits have been irradiated under controlled conditions in standard neutron fields at the National Institute of Standards and Technology (NIST - formerly the National Bureau of Standards) to verify the absolute mass calibrations by testing the response of ultra low-mass SSTR neutron dosimeters in known neutron fields. The results of these benchmark irradiations are contained in this report.

2. EXPERIMENTAL

NIST (formerly NBS) maintains standard neutron fields (or benchmark fields) to supply calibration irradiations and certified fluence standards. Two different types of irradiations were carried out at NIST. Isotopes with threshold neutron responses (^{237}Np and ^{238}U) were irradiated in the NIST cavity fission source, and isotopes with primarily thermal neutron responses (^{235}U and ^{239}Pu) were irradiated in a thermal neutron field.

2.1 ^{235}U FISSION SPECTRUM IRRADIATIONS

The NIST Cavity Fission Source (see Figure 1) provides a ^{235}U thermal-neutron induced fission spectrum in a 30-cm diameter cavity of the NIST research reactor. The foils to be irradiated are positioned inside of a cadmium pill box which is sandwiched between two ^{235}U driver discs. When the reactor is operated at maximum power (20 megawatts), the ^{235}U spectrum fluence rate is 4×10^{10} n/cm^2-s. Fluences are based upon the known source strength of a standard ^{252}Cf field relative to the ^{235}U field by comparisons of irradiated nickel foils. First the nickel foils are irradiated in the californium spectrum and their activity is used to validate the efficiency calibration of a germanium gamma-ray counter. The nickel foils are then included in each Cavity Fission Source irradiation as fluence monitors. The NIST reactor is operated at predetermined fixed fractions of 20 MW for cycles lasting about three weeks. The fluence rate is normally very constant (±2%) but it is monitored during each ^{235}U irradiation by a separate fission chamber and when necessary power-time variations are taken into account. Certified fluences are normally reported to an accuracy of 1.5-2%[5].
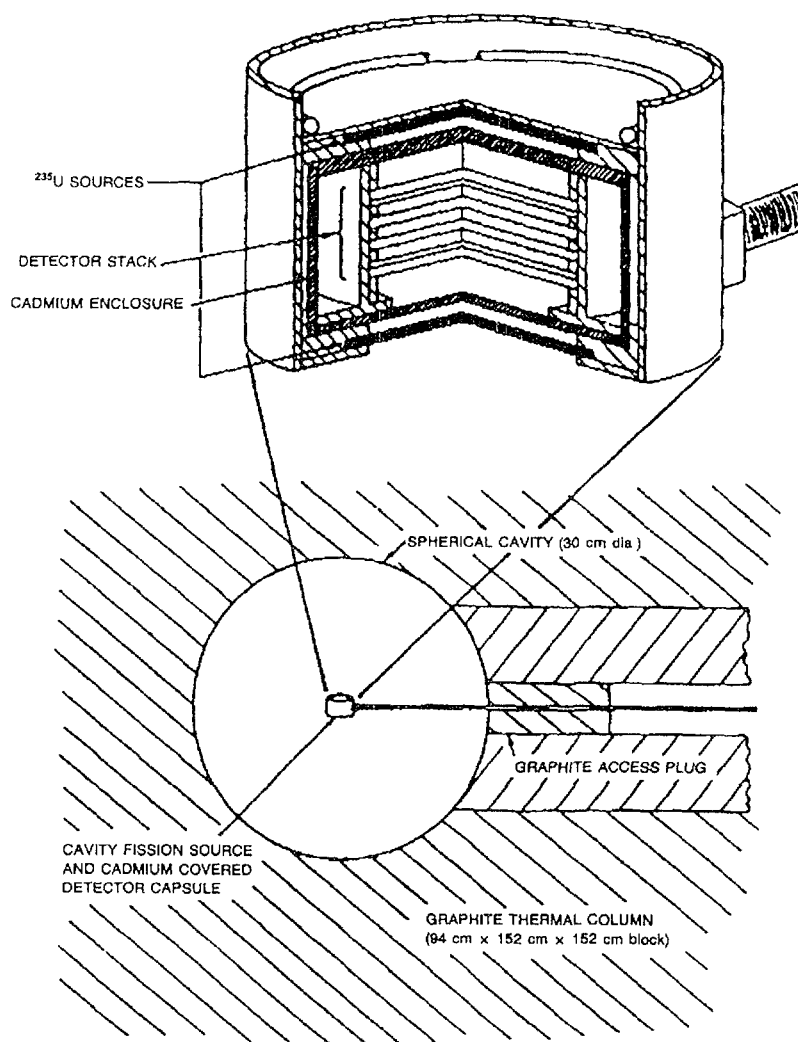
Figure 1. ^{235}U Cavity fission source. Upper view: relative positions of
neutron sensor foils, fission disks and cadmium enclosure. Lower
view: the assembly in the thermal column of the NBS reactor.

Fission neutron return spectra for spherical cavities in
graphite have been studied extensively by means of neutron transport
calculations and by experiments accomplished to develop standard neutron
fields in spherical geometries[6,7]. For the 30-cm diameter cavity at
NIST, the response of threshold fission detectors to neutrons returning
from the cavity walls is less than 0.3% of the uncollided fission
neutron fluence from the fission source disks; for detectors with
thresholds above 1 MeV, the response to the wall-returned neutrons is
less than 0.1%. The Cavity Fission Source is generally not used to

irradiate low-energy-sensitive integral dosimeters such as ^{235}U and ^{239}Pu.

The ^{235}U fission disks and the internal structure of the cadmium pill box are shown in the upper half of Figure 1. Small perturbations to the ^{235}U fission spectrum (which result in less than 5% total corrections) come from scattering and absorption in the structure of the Cavity Fission Source, but the effects of scattering dominate. The scattered neutrons may be separated into two categories:

(1) Neutrons which are scattered into the dosimeters that are being irradiated within the pill box. These neutrons come from scattering in the fission disks, in the cadmium pill box, and in the aluminum top-hat-shaped assembly. This inscattering is essentially independent of position of the dosimeter in the stack. These scattered neutrons may produce more activity in the dosimeters than would occur in an unperturbed fission spectrum. Because the fluences reported by NIST are for an unperturbed ^{235}U fission spectrum at the locations of the SSTRs or nickel fluence monitors, scattering corrections are applied to each measured reaction rate.

(2) Neutrons which interact with other foils in the dosimeter stack. Again the scattering effects dominate, but the effects are both a function of position and the number of foils in the stack. Nearest neighbors are most significant and the effects decrease rapidly with distance. The correction factors are larger for the lower energy thresholds and Figure 2 shows the calculated factors as a function of effective threshold of various common threshold dosimeters. Corrections for the nickel and SSTR dosimeter stack are for a cadmium pill box containing four nickel foils with three SSTRs between them. Depending upon the relative positions and type of threshold, the integrated correction factors that are applied to the measured reaction rates may
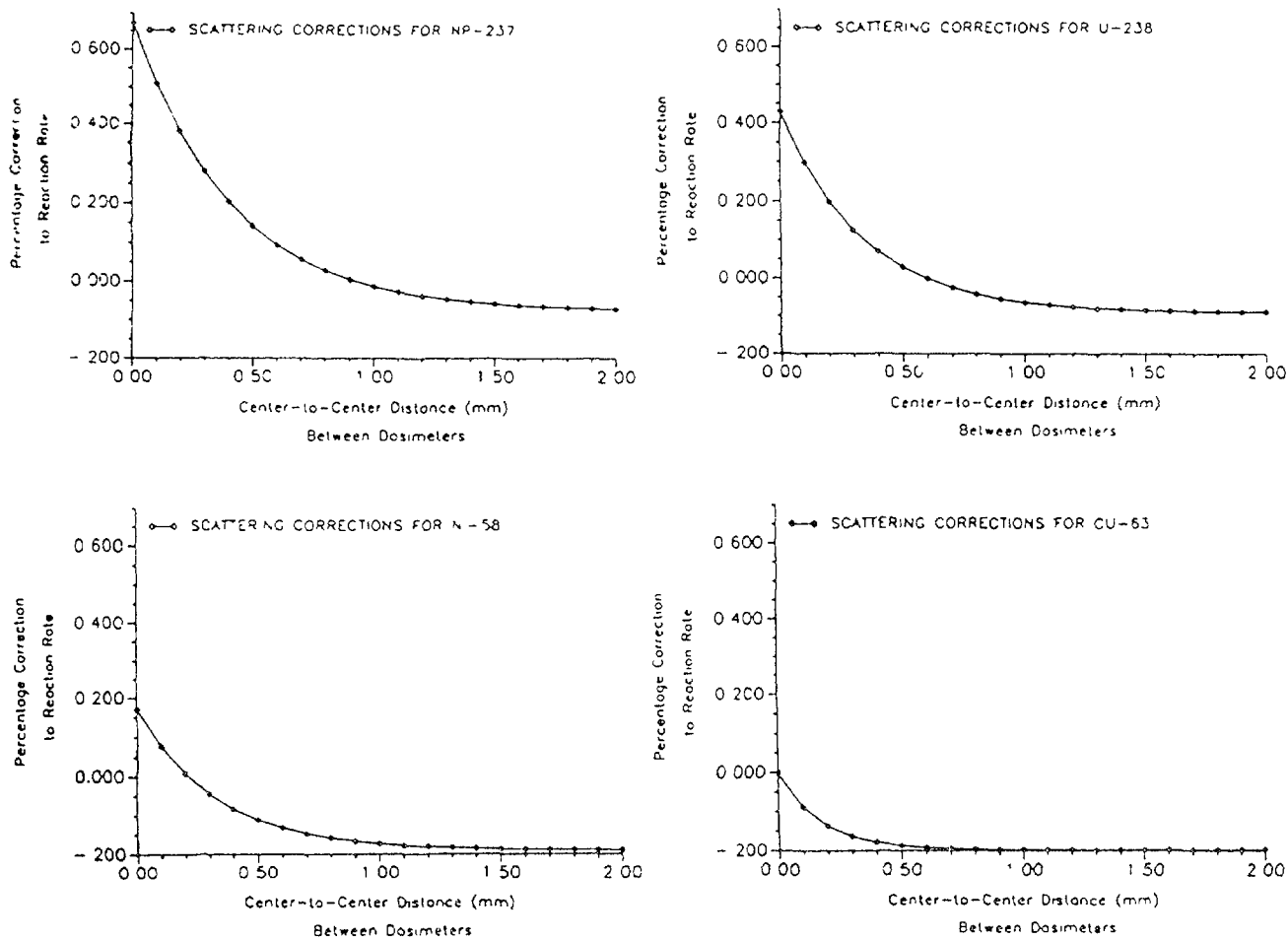
Figure 2.

The functions used to account for scattering effects for various kinds of dosimeters in different foil-stack configurations are shown for four different threshold reactions: $^{237}Np(n,f)FP$, $^{238}U(n,f)FP$, $^{58}Ni(n,p)^{58}Co$, and $^{63}Cu(n,a)^{60}Co$. The respective thresholds of these reactions are approximately 0.6 MeV, 1.0 MeV, 3.0 MeV, and 5.5 MeV. A calculation which accounts for material types, foil thicknesses, and distances between a particular dosimeter and its nearest neighbors is done to derive the net integrated scattering effects for each dosimeter.

be both greater than or less than unity. These corrections are determined by Monte Carlo neutron transport calculations.

Total net corrections for these two types of scattering and the particular irradiation geometry have been applied for all irradiated SSTR deposits. These corrections include the wall-return spectrum corrections factors of 0.997 for ^{237}Np and 0.999 for ^{238}U and the $^{58}Ni(n,p)^{58}$ Co reactions.

38

2.2 SSTR THERMAL IRRADIATIONS

As mentioned, SSTR dosimeters with low-energy neutron response were not exposed in the Cavity Fission Source but in a thermal neutron field at the center of the 30-cm graphite cavity in the NIST Reactor thermal column. As opposed to specifying certified fluences, the thermal irradiations specified ^{235}U fission rates. This was accomplished by irradiating an SSTR package back-to-back with a ^{235}U fission deposit of known mass, 96 nanograms ($\pm 1.5\%$). The known-mass deposit is an active electrode in a fission chamber which looks very much like the cadmium pill box mounted in the aluminum holder in the Cavity Fission Source. The irradiations were carried out by placing the fission chamber containing the monitor deposit and one SSTR package into the cavity before the boral curtain at the thermal column was raised. The fission chamber was then made operational on a predetermined time cycle and the curtain was raised. By monitoring the fluence rate, the stability of the irradiation as well as the desired duration could be determined. The total sum of the monitored fissions provided the basis for determination of the fluence rate at the SSTR package.

Determination of fluence gradients and perturbation effects are still in progress so final data for the thermal irradiations are not available at this time.

3.   RESULTS

Radiometric analysis of the ^{58}Co content of the nickel flux foils were used to determine the neutron flux at the locations of the nickel foils. The magnitudes of the fluxes were plotted as a function of foil position in order to determine the corresponding fluxes at the locations of the SSTR neutron dosimeters by interpolation. Figure 3 is a plot of typical neutron flux results for an irradiation in the NIST
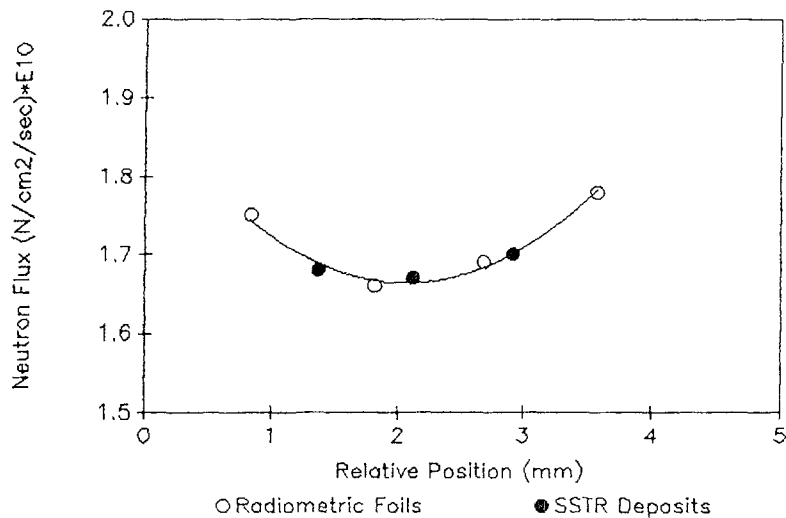
Figure 3. Neutron fluxes as derived from Ni-^{58}Co flux foils plotted as a function of foil location. The fluxes obtained at the locations of the SSTR neutron dosimeters by interpolation are also plotted.

cavity neutron source. The SSTR fluxes were corrected for the radial gradient (0.500" diameter nickel foils and 0.250" diameter fissionable deposits were used) and for neutron scattering as discussed previously. After the irradiation, the SSTRs were etched in 49% HF for one hour at 22.0°C to reveal the tracks which were counted both manually by two independent scanners and with the Westinghouse R&D (now Science & Technology Center) automated track counter[4]. The known irradiation time was used to calculate the total fast neutron fluence, which was used with the number of fissions derived from the track count to derive a deposit mass. The neutron-induced fission cross sections used were 312 mb (±2.3%) for ^{238}U and 1359 mb (±2.1%) for ^{237}Np.

The deposit masses derived from the NIST irradiations are compared with the masses obtained from radiometric spiking calibrations in Table 2. In general, the overall agreement of the masses derived from the NIST benchmark irradiations and those derived from the independent radiometric mass calibrations is quite good. A slight bias (4%) exist between the NIST and radiometric mass scales. The cause for this discrepancy is being investigated although its overall impact on the 2-5% uncertainty requirement for reactor cavity dosimetry is minimal.

Table 2

Overall Comparison of Fissionable Deposit Masses Derived
From NIST Benchmark Neutron Irradiations and
By Ultra Low-Mass Radiometric Spiking Techniques

Isotope	Spike Solution[a]	Mass (nanograms) RM[b]	Mass (nanograms) NIST[c]	Mass Ratio RM/NIST
^{238}U	HEDL-12	8.01	7.60	1.054
^{238}U	HEDL-12	4.34	4.24	1.024
^{238}U	HEDL-K1	1.63	1.53	1.065
^{238}U	HEDL-13	1.58	1.59	0.994
^{238}U	HEDL-13	1.64	1.61	1.019
^{238}U	HEDL-13	2.06	2.16	0.954
^{238}U	W R&D-5	17.07	16.16	1.056
^{237}Np	HEDL-8	3.63	3.42	1.061
^{237}Np	HEDL-7	0.315	0.310	1.016
^{237}Np	HEDL-7	0.302	0.268	1.127
^{237}Np	W R&D-7	4.88	4.65	1.049
^{238}U	HEDL-12	2.88	2.74	1.051
^{237}Np	HEDL-8	0.667	0.634	1.052
^{238}U	W R&D-9	1.73	1.62	1.068
^{237}Np	W R&D-8	7.48	7.36	1.015
			Average	1.040 ± 0.038

[a]HEDL spike solutions were prepared and calibrated at the Hanford
Engineering Development Laboratory. W R&D spike solutions were
prepared and calibrated at the Westinghouse Science & Technology
Center.

[b]Mass determined by ultra low-mass radiometric spiking techniques.

[c]Mass determined from fissions produced in an irradiation in an NBS
standard neutron field.

4. DISCUSSION AND CONCLUSIONS

Typical plots of SSTR track density as a function of position are shown in Figure 4 for SSTRs exposed to the same fissionable deposit in a power reactor cavity exposure and in the NIST Cavity Neutron Source. It can be seen that the track density distributions are quite similar, indicating that the mass distribution of the deposit did not

DEPOSIT #1288 ^{237} Np 3 63 x 10^{-9}g
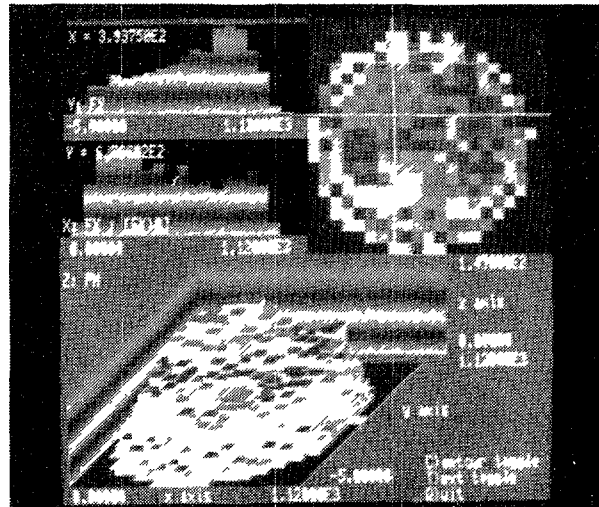
CAVITY IRRADIATION
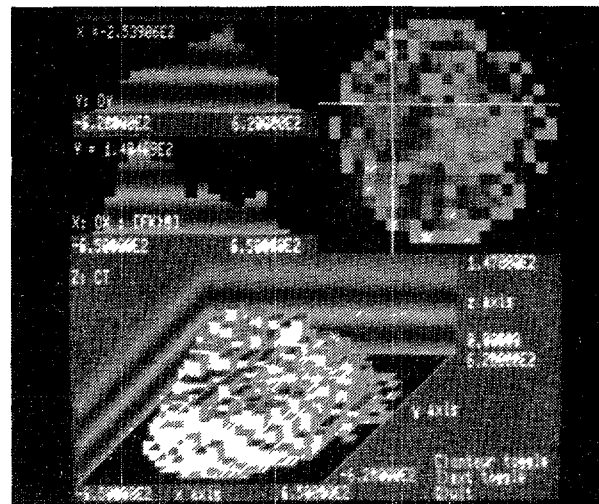
NBS BENCHMARK IRRADIATION

Figure 4. Track density distribution obtained from SSTRs in contact with the same ultra low-mass fissionable deposit irradiated for one cycle in the cavity region of a power reactor and in the NIST cavity neutron source. Isometric contour plots, and selected slices of the track count (z) vs microscope field position (x and y) are shown.

undergo an observable change in the time between the start of the power reactor cavity exposure and the end of the NIST Cavity Neutron Source exposure.

The general agreement between the independent absolute radiometric mass calibrations (Westinghouse STC) and the masses derived by benchmark field neutron irradiations (NIST) is encouraging and serves as an overall verification of the radiometric spiking methods[3] used to calibrate the ultra low-mass fissionable deposits used in SSTR neutron dosimetry and of the track scanning techniques[4] used to analyze the exposed SSTRs.

REFERENCES

1. F. H. Ruddy, R. Gold, and J. H. Roberts, "Pressure Vessel Surveillance Dosimetry Using Solid State Track Recorders," in Nuclear Data for Radiation Damage Assessment and Related Safety Aspects, IAEA-TEC-DOC-263, Vienna, (1982), p. 109.

2. F. H. Ruddy and J. G. Seidel, "Solid State Track Recorder Pressure Vessel Surveillance Neutron Dosimetry at Commercial Nuclear Power Reactors," IAEA Advisory Group Meeting on Nuclear Data for Radiation Damage Assessment and Related Safety Aspects, September 19-22, 1989.

3. F. H. Ruddy, "Neutron Dosimetry in High Intensity Fields: A Review," Nuclear Tracks and Radiation Measurements 11, 197 (1986).

4. F. H. Ruddy, A. E. Manhardt, and J. G. Seidel, "Analysis of Solid State Track Recorders with the Westinghouse Research and Development Center Automated Track Counter "in Reactor Dosimetry: Methods, Applications, and Standardization, ASTM STP 1001, American Society for Testing and Materials, Philadelphia, p. 676 (1989).

5. G. P. Lamaze and J. A. Grundl, "Activation Foil Irradiation by Reactor Cavity Fission Sources," NBS Special Publication 250-14, U.S. Department of Commerce's National Institute of Standards and Technology, Gaithersburg, Maryland, (March, 1988).

6. J. A. Grundl, "Cavity Fission Spectra," Trans. Am. Nucl. Soc. 5, 381, (1962).

7. C. M. Eisenhauer and J. A. Grundl, "Neutron Transport Calculations for the Intermediate-Energy Standard Neutron Field (ISNF) at the National Bureau of Standards," Proceedings International Symposium on Neutron Standards and Applications, NBS Special Publication 493, U.S. Dept. of Commerce, Washington, D.C. (March, 1977).

MEASUREMENT OF LONG-LIVED ISOTOPES AND HELIUM PRODUCTION IN FUSION MATERIALS*

L.R. GREENWOOD
Argonne National Laboratory,
Argonne, Illinois,
United States of America

Abstract

Results are summarized for measurements of the production rates for long-lived radioisotopes and helium in fusion reactor materials. Measurements have been performed at T(d,n) generators, near 14 MeV; at broad-spectrum Be(d,n) accelerator-based neutron fields; and in various fission reactors. These activation data are used to predict the production of these isotopes in fusion reactor materials for waste disposal and maintenance applications. Helium data are needed for the simulation of fusion materials damage in fission reactor irradiations and as a stable product dosimeter. Nuclear data needs and future plans are discussed.

Introduction

Accurate measurements of neutron cross sections are needed for a variety of reactions from threshold to 14 MeV for the prediction of activity levels in fusion reactor materials. Longer-lived activities are of particular interest since they may seriously impact reactor maintenance and the disposal of waste materials. Helium production data is needed for the prediction of the evolution of radiation damage in materials. For many materials and reactions there have been few measurements and we must rely on calculations of the required cross sections. Consequently, we have been involved in measurements of selected reactions at 14 MeV and in integral neutron experiments in reactors and accelerator-based neutron sources.

Activity Measurements at 14 MeV

Neutron irradiations have been conducted at the Rotating Target Neutron Source II at Lawrence Livermore National Laboratory. Samples were placed in the highest flux region near the source for up to 2 weeks and in more remote locations for much longer times with net fluences up to 10^{18} n/cm^2. The neutron energy spectra were calculated, as shown in figure 1.[1] Data have been published[2] for 22 reactions, including many standard dosimetry reactions in the energy range from 14.5-14.9 MeV. More recently, we have focussed on reactions leading to longer-lived isotopes. A list of these reactions with measured cross sections, halflives, and references is given in Table I. Measurements have also been reported[3,4] for the ^{27}Al(n,2n)^{26}Al (7.2x10^5 y) and ^{54}Fe(n,2n)^{53}Fe(β)^{53}Mn (3.7x10^6 y) reactions; however, these are not listed in Table I due to their steep energy dependence near 14 MeV, which makes them highly useful for fusion reactor dosimetry and plasma diagnostics.[5] Activity measurements for the reactions listed in Table I were performed with either gamma, x-ray, or liquid scintillation detectors. The nuclear decay data used for these measurements were adopted from reference 6. In most cases, chemical separations were required to remove shorter-lived, interfering reactions.
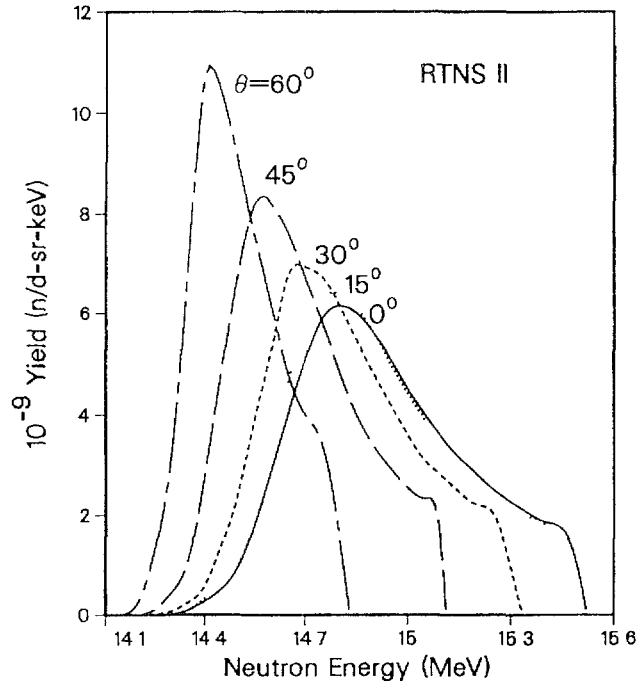
FIGURE 1

Calculated neutron spectra for RTNS II with E_d = 360 keV and a TiT$_2$ target.

Table I· Production of Long-Lived Isotopes near 14.8 MeV

Reaction	σ,mb	$T_{1/2}$,y	C/E[a]	Reference
^{50}V(n,2n)^{49}V[b]	258±39	0 90	2.8	17
^{56}Fe(n,2n)^{55}Fe	454±35	2.7	1 4	18-20
^{63}Cu(n,p)^{63}Ni	54±4	100.	0 91	18-20
^{64}Ni(n,2n)^{63}Ni	958±64	100.	1 2	18-20
^{60}Ni(n,2n)^{59}Ni	104±25	7.5x10^4	6.0	18-20
^{94}Mo(n,p)^{94}Nb	55±6	2.0x10^4	0 82	1
^{Nat}Mo(n,x)^{94}Nb	7.8±0 8	2 0x10^4	-	1
^{92}Mo(n,2n)^{91}Nb	603±119	680.?	0 33	1
^{94}Mo(n,2n)^{93}Mo	550±136	3500.	2.5	17
^{94}Mo(n,x)^{93m}Nb	5.7±0 9	16.1	2 0	17
^{95}Mo(n,x)^{93m}Nb	1.36±0 27	16 1	-	17
^{Nat}Mo(n,x)^{93m}Nb	0 75±0.11	16 1	-	17

[a]Ratio of ALICE calculation/experimental result
[b]Vanadium data at 14.3 MeV

Chemical procedures generally involved ion-exchange reactions, as discussed in the references.

Neutron fluences were determined for each irradiation from dosimetry samples. For shorter runs, the $^{93}Nb(n,2n)^{92m}Nb$ (10 day) reaction was used to determine the fluence assuming a value of 463 mb for the cross section.[7] For longer runs, the fluence was determined by the $^{54}Fe(n,p)^{54}Mn$ reaction using cross sections given in reference 2. These measurements can be used to determine the production of each isotope in fusion reactors, as given in Table II for the STARFIRE reactor design.[8] Such calculations can be directly compared with previous predictions of these activities in fusion materials.

Table II: Comparison with ALICE Calculations

Reaction	Ratio - C/E
$^{50}V(n,2n)^{49}V$	2.8
$^{56}Fe(n,2n)^{55}Fe$	1.4
$^{63}Cu(n,p)^{63}Ni$	0.91
$^{64}Ni(n,2n)^{63}Ni$	1.2
$^{60}Ni(n,2n)^{59}Ni$	6.0
$^{94}Mo(n,p)^{94}Nb$	0.82
$^{92}Mo(n,2n)^{91}Mo(\beta^+)^{91}Nb$	0.33
$^{94}Mo(n,2n)^{93}Mo$	2.5
$^{94}Mo(n,x)^{93m}Nb$	2.0

The pre-compound, statistical model computer code ALICE[9] was used to calculate neutron cross sections for the reactions given in Table I. The calculations and experiments (C/E values) are also compared in Table I and figures 2-4. As can be seen, the agreement is generally only good to about a factor of two. ALICE appears to consistently overpredict the values for (n,2n) cross sections. In the case of $^{92}Mo(n,2n)$ the calculation is only 1/3 of the experiment. As discussed in reference 1, our data is also much higher than other experiments. Consequently, the difference may be due to the uncertainty in the halflife of 680±130 y[6], since a value of 300 years or less would lower the cross section accordingly to be in better agreement with the calculations and other data. Similarly, for $^{60}Ni(n,2n)$ our value is much less than calculations and the systematics of other nickel isotopes. In this case, the halflife is only known to 7.5±1.3 x 10^4 y[6] and a value of 3x10^5 y or longer would raise the measurement to 400 mb or greater, in better agreement with calculations and systematics. We are planning to remeasure the halflife of ^{59}Ni since this is easily made in thermal neutron reactions with ^{58}Ni and the value can be determined by standard mass spectrometry techniques.

Additional materials were irradiated at RTNS II and we plan to measure neutron cross sections for the reactions $^{14}N(n,p)^{14}C$ (5730 y), $^{94}Zr(n,2n)^{93}Zr$ (1.5x10^6 y), and $^{93}Nb(n,2n)^{92}Nb$ (3.6x10^7 y).
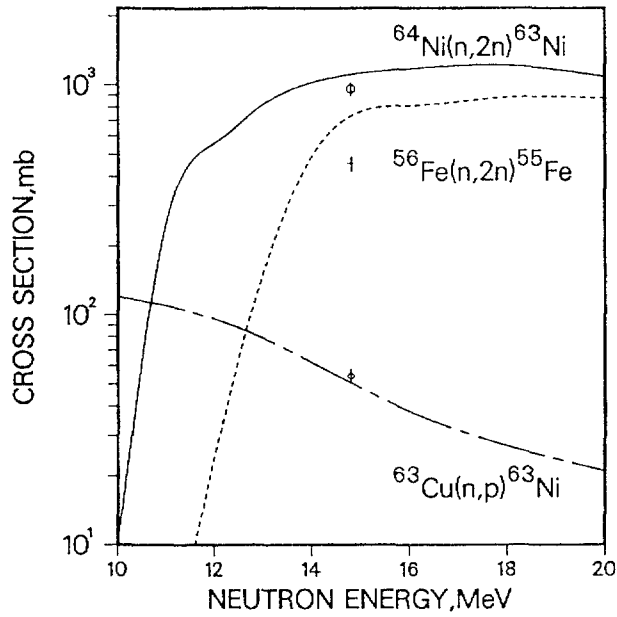
FIGURE 2

Comparison of measured cross sections for the production of ^{63}Ni from ^{63}Cu (diamond) and ^{64}Ni (circle) and for ^{55}Fe from ^{56}Fe (plus) with ALICE calculations (lines).
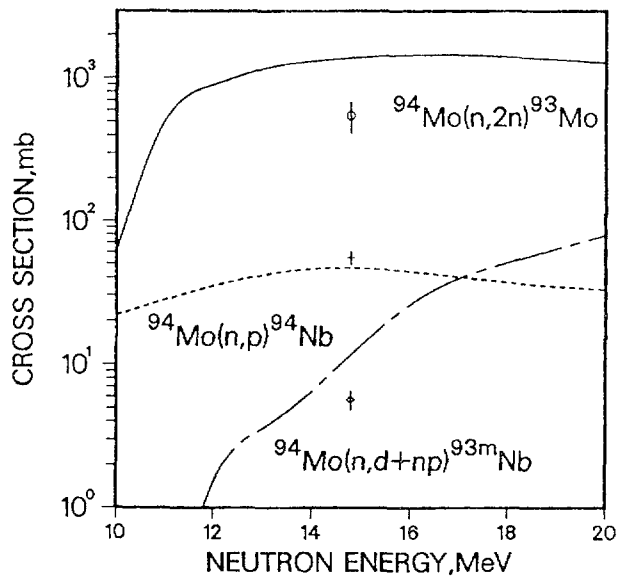
FIGURE 3

Comparison of measured cross sections for the production of ^{93}Mo (circle), ^{94}Nb (plus), and ^{93m}Nb (diamond) from ^{94}Mo with ALICE calculations (lines).
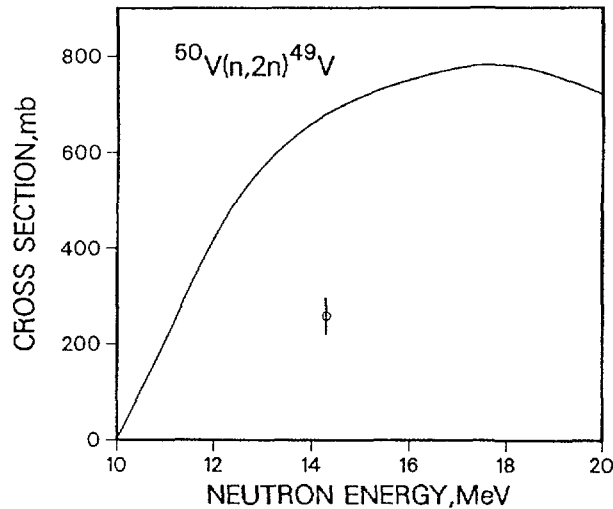
FIGURE 4

Comparison of measured cross section for $^{50}V(n,2n)^{49}V$ (circle) with ALICE calculations (line).

Activity Measurements in Rare Earth Materials

Argonne is collaborating with several other laboratories to measure activities is rare earth materials following a recommendation of the 16th International Nuclear Data Committee meeting in Beijing, PRC, in October 1987. This work is included in a Coordinated Research Program sponsored by the IAEA. The experimenters include J.W. Meadows, D.L. Smith, and the author at Argonne; R.C. Haight at Los Alamos National Laboratory (LANL); and Y. Ikeda at the Japan Atomic Energy Research Establishment (JAERI). Identical packets of foils consisting of copper, silver, europium, terbium, and hafnium, as well as titanium, iron, and nickel dosimeters, were irradiated in a E_d = 7 MeV Be(d,n) neutron field at ANL[10]; a 10 MeV H(t,n)^{3}He field at LANL; and at 14 MeV at the Fusion Neutronics Source Facility at JAERI. The ANL and LANL neutron fields are illustrated in figure 5; the JAERI field is similar to the RTNSII facility shown in figure 1.

Samples have been irradiated and gamma counted from both ANL and LANL. The JAERI irradiations have been completed and analysis will commence shortly. Table III lists preliminary results for several reactions which we have measured; however, the data has not yet been corrected for room-return, target-related background, or multiple scattering. In the case of ^{152}Eu the activity is probably due primarily to the $^{151}Eu(n,\gamma)$ reaction rather than the (n,2n) reaction from ^{153}Eu. Although the thermal flux is quite low at each facility, the thermal cross section of ^{151}Eu is very high (5900 barns). In the case of ^{108m}Ag and $^{178m2}Hf$, more decay time is needed for the decay of interfering silver and hafnium isotopes. When all of the data is available with suitable corrections, it should be possible to adjust the calculated cross sections for these reactions resulting in recommended values for fusion applications.
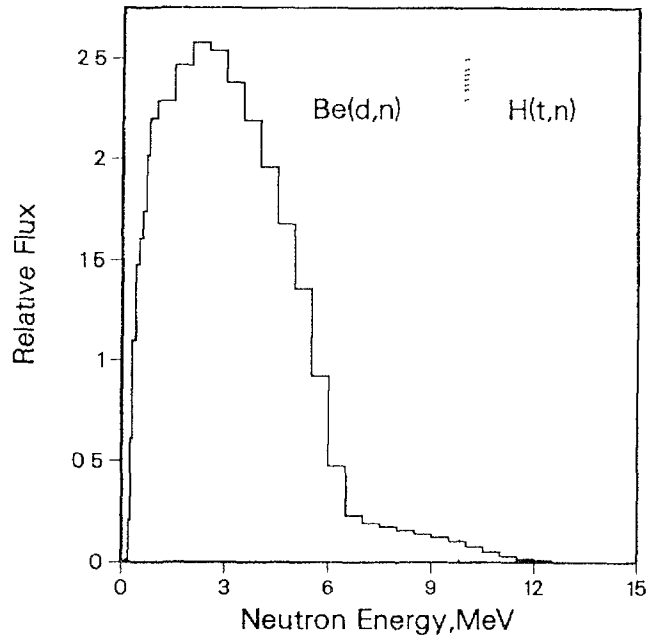
FIGURE 5

Measured neutron spectra for the Be(d,n) neutron field at Argonne and the 10-MeV H(t,n)^{3}He field at Los Alamos.

Table III: Preliminary Results for Rare-Earth Irradiations
(cross sections are listed in millibarns)

Reaction	$T_{1/2}$	LANL-exp	(10 MeV) calc	ANL-exp	Be(d,n) calc
^{107}Ag(n,2n)^{106m}Ag.	8.5 d	5.32	87.	1.41	23.
^{109}Ag(n,2n)^{108m}Ag	127 y	w	151.	w	
^{151}Eu(n,2n)^{150g}Eu	35.8 y	219.	1264.	16.4	18.
^{153}Eu(n,2n)^{152}Eu [+^{151}Eu(n,γ)]^a	13.3 y	529.	647.	344.	17.
^{159}Tb(n,2n)^{158}Tb	150 y	340.	1400.	33.7	54.
^{176}Hf(n,2n)^{175}Hf	70 d	420.	1571.	42.4	34.
^{179}Hf(n,2n)^{178m2}Hf	31 y	w	22.	w	1.
^{180}Hf(n,2n)^{179m2}Hf	25.1 d	3.34	159.	2.93	—

^{a}^{152}Eu partly due to ^{151}Eu(n,γ)
w: indicates waiting for decay of short-lived activities

Additional Measurements at Argonne

In collaboration with D.L. Smith, we are measuring cross sections for the reactions ^{93}Nb(n,n')^{93m}Nb (16.1 y), ^{63}Cu(n,p)^{63}Ni (100 y), ^{60}Ni(n,p)^{60}Co (5.3 y) and a variety of other reactions using the integral Be(d,n) neutron field at Argonne[10] and a limited number of differential measurements using the Li(p,n) reaction. Samples have been irradiated and gamma counted, including dosimetry reactions. Work is now in progress to measure the activity of ^{93m}Nb by x-ray counting and ^{63}Ni by liquid scintillation counting.

Helium Measurements

Helium production is known to be an important parameter in the evolution of the microstructure during the irradiation of fusion materials. Furthermore, helium is especially useful for fluence measurements since it is a stable product. Consequently, we have worked closely with D.G. Kneff of Rockwell International, Canoga Park, CA, USA, for many years to both measure and test helium production cross sections in fission reactors, 14 MeV sources, and broad-spectrum accelerator-based neutron fields. We recently published[11] helium cross sections for 26 elements, 33 isotopes, and for various alloys at 14.8 MeV. Additional materials have been irradiated at RTNS II and at 10 MeV at Los Alamos National Laboratory and analyses are now in progress.

Table IV shows some of our recent results[12] from fission reactors, measured in the High Flux Isotopes Reactor at Oak Ridge National Laboratory. As can be seen, the nickel, iron, and chromium results are in reasonable agreement with calculations based on the ENDF/B-V gas production file.[13] However, nickel[14], iron[15], and copper[16] all have thermal neutron effects whereby transmutation products are found to have significant thermal neutron helium cross sections. The effect in nickel is quite well-known and is used routinely to simulate fusion-like helium production rates in mixed-spectrum fission reactors. The effect in copper is less dramatic since zinc must be produced prior to the onset of helium production. (The effect would be comparable to that for nickel for materials doped directly with zinc.) In iron, there appears to be a small effect due to ^{55}Fe with a thermal (n,α) reaction cross section of about 18 mb. However, more data is needed to sort

Table IV: Helium Production in HFIR
(Ratio of ENDF/B-V Calc./Expt.)

Material	C/E Value	Comments
Nickel	0.95±0.07	Thermal Effect[a]
Iron	0.96±0.06	Thermal Effect?[b]
Chromium	1.06	1 result
Titanium	2.34±0.20	
Niobium	0.73±0.03	
Copper	0.76±0.05	Thermal Effect[c]

[a]Reference 14
[b]Reference 15
[c]Reference 16

out the competing effects from the various iron isotopes. This thermal effect in iron could prove useful for simulating fusion-like conditions in mixed-spectrum reactors, assuming that we use iron enriched in ^{54}Fe or doped directly with ^{55}Fe.

REFERENCES

1. L.R. Greenwood, D.G. Doran, and H.L. Heinisch, Phys. Rev. 34C (1987)76-80.

2. L.R. Greenwood, Influence of Radiation on Materials Properties, ASTM-STP 956 (1987) 743-749.

3. R.K. Smither and L.R. Greenwood, J. Nucl. Mater. 122 (1984) 1071-1077.

4. R.K. Smither and L.R. Greenwood, Damage Analysis and Fundamental Studies Quarterly Progress Report, DOE/ER-0046/17 (1984) 11-13.

5. R.K. Smither and L.R. Greenwood, Rev. Sci. Instrum. 56 (1985) 1078-1080.

6. E. Browne and R.B. Firestone, Table of Radioactive Isotopes, Ed. V.S. Shirley, John Wiley, New York (1986).

7. D.R. Nethaway, J. Inorg. Nucl. Chem. 10 (1978) 1285.

8. STARFIRE: Commercial Tokamak Fusion Power Plant Study, ANL/FPP-80-1 (1980).

9. M. Blann, Lawrence Livermore National Laboratory Report UCID 19614 (1982).

10. D.L. Smith, J.W. Meadows, P.T. Guenther, and L.R. Greenwood, Reactor Dosimetry: Methods, Applications, and Standardization, ASTM STP 1001 (1989) 253-260.

11. D.W. Kneff, B.M. Oliver, H. Farrar IV, and L.R. Greenwood, Nucl. Sci. Eng. 92 (1986) 491-524.

12. D.W. Kneff, L.R. Greenwood, B.M. Oliver, and R.P. Skowronski, J. Nucl. Mater. 141-143 (1986) 824-828.

13. Evaluated Nuclear Data File, Version V, File 533, Gas Production, National Nuclear Data Center, Brookhaven National Laboratory (1979).

14. L.R. Greenwood, D.W. Kneff, R.P. Skowronski, and F.M. Mann, J. Nucl. Mater. 122-123 (1984) 1002-1010.

15. L.R. Greenwood, D.G. Graczyk, and D.W. Kneff, J. Nucl. Mater. 155-157 (1988) 1335-1339.

16. D.W. Kneff, L.R. Greenwood, B.M. Oliver, and R.P. Skowronski, Rad. Effects 92-96 (1986) 553-556.

17. L.R. Greenwood and D.L. Bowers, Specialists' Meeting on Neutron Activation Cross Sections for Fission and Fusion Energy Applications, NEANDC, Sept. 13-15, 1989, Argonne National Laboratory, Argonne, IL, USA.

18. D.L. Bowers and L.R. Greenwood, J. Radio. Nucl. Chem. 123 (1988) 461-469.

19. L.R. Greenwood and D.L. Bowers, J. Nucl. Mater. 155-157 (1988) 585-588.

20. L.R. Greenwood and D.L. Bowers, Reactor Dosimetry: Methods, Applications, and Standardization, ASTM STP 1001 (1989) 508-514.

'LOW-ACTIVATION' FUSION MATERIALS DEVELOPMENT AND RELATED NUCLEAR DATA NEEDS

S. CIERJACKS
KfK–Euratom Association,
Institut für Material- und Festkörperforschung,
Kernforschungszentrum Karlsruhe GmbH,
Karlsruhe, Federal Republic of Germany

Abstract

So-called "low-activation" materials are presently considered as an important means of improving the safety characteristics of future DT fusion reactors. Essential benefits are expected in various problem areas ranging from operation considerations to aspects of decommissioning and waste disposal. Present programs on "low-activation" materials development depend strongly on reliable activity calculations for a wide range of technologically important materials. The related nuclear data requirements and important needs for more and improved nuclear data are discussed.

1. Introduction

With the continuous progress towards break-even DT fusion facilities, more thought has been recently given to the material that will be used in future power-producing reactors. Presently, there are two main goals in materials research for fusion applications which ought to be achieved simultaneously:

1. The development of materials which are resistent to large fluences of fast neutrons with energies $\leq$ 14 MeV.
2. The development of so-called "low-activation" materials (LAMs) in which the neutron-induced activity is as low as possible, but always within acceptable limits.

Thus, in addition to a large variety of engineering property specifications, a broad range of radiological requirements need to be fulfilled for a suitable fusion reactor material, not all of which may be simultaneously satisfied in an optimal manner. The possible development of low-activity materials is due to the fact that the activity produced in a fusion reactor is not intrinsic to the fusion process itself, so that a high degree of control can be exercised by careful selection of suitable structural materials.

Even though a lot of problems still need to be solved, low-activity materials are presently seen, in the broadest terms, as an important means of enhancing the safety and environmental advantages of fusion as an alternative energy source to existing fission reactors. Potential benefits are anticipated in most of the problem areas, ranging from decay heat and accidental releases to aspects of waste disposal. For all aspects of low-activation materials development, the important requirement is that the induced radioactivities, the associated surface γ-dose rates, decay heats and biological hazards need to be well known for a wide span of timescales ranging from the order of minutes/hours (maintenance, decay heat) to

tens/thousends of years (reuse/recycling of material, waste management) and a wide range of potential fusion reactor materials, including critical impurity elements.

In Sect. 2 the safety aspects for which LAMs are beneficial are summarized. The range of nuclear reactions and neutron spectra important for activity calculations are briefly outlined in Sect. 3. Section 4 describes the present status of activity calculations. The nuclear data requirements and the important needs for improved nuclear data are discussed in Sect. 5.

2. Possible Advantages of LAMs for Safety Considerations

The potential advantages of LAMS with respect to fusion reactor safety have been discussed in several recent review papers [1-6]. Some of the safety aspects for which the use of "low-activation" materials is expected to be beneficial are listed in Table I. The relevant ranges of decay times of the activation products are also indicated for each topic.

From the point of view of public acceptance of fusion energy, the most important considerations must be given to those aspects which result in the radiation exposure of the public, in particular, accidental releases and waste disposal. The radiological implications of the remaining areas relate mainly to occupational exposures. These exposures can, however, be considered rather differently, since, at least in normal operations, personnel in nuclear installations works in controlled environments. Here exposures are carefully monitored and maintained within acceptable limits through the adoption of well established radiological protection practices.

Table I.   Fusion reactor safety and environmental aspects for which LAMs are considered to be beneficial

Topic	Relevant timescales for the decay of activation products
Reactor maintenance	Minutes to months
Effluent releases	Hours to years
Accidental releases	Hours to years
Decay heat generation	Minutes to years
Handling of expired components	Days to years
Reuse/recycling of material	Years to tens of years
Waste disposal	Tens to thausends of years

Concerning accidental releases of activated material (for instance as a result of a reactor fire or other conventional accidents), a number of studies have been performed, but much work remains to be done. A realistic modelling of suitable exposure scenarios is rather complex, and requires well agreed methodologies and, in addition to sound technical data, reliable predictions of radiological quantities such as material-specific radioactivities, dose rates and decay heats. Ultimately, the consequences of accidental releases need to be judged according to standard criteria for acceptable exposures, which can be rather different in various national, regional or international regulations and recommendations [7,8].

Regarding decommissioning and waste disposal there is, in principle, a choice between reuse, recycling and permanent disposal of expired components, all of which options strongly depend on the induced radioactivity. In the materials reuse/recycle approach (reprocessing of scrap after a suitable decay period of about 30 to 100 years) it would be favourable if "hands-on" processing of the expired components were permitted. For this purpose, however, the surface γ-dose rates need to range below certain limits (2.5×10^{-5} Sv/h according to European standards [9]). For waste disposal the most desirable option is the deposition of discarded material in near-surface repositories after suitable cooling times. Present calculations indicate, however, that the activation levels of current candidate low-activation steels having the lowest currently attainable impurities of critical elements remain well above the level for which "shallow-land" burial might be considered [3,5]. In case that near-surface disposal must be ruled out, a disposal in deep geological repositories is presently seen as the most likely alternative [1].

3. Nuclear Reactions and Neutron Spectra

Interaction of d-T neutrons and their product particles with the various reactor materials gives a broad range of transmutation products most of which are unstable and subsequently decay by emission of γ-rays, β-particles or weak X-rays. Only very few α-emitters are produced by activation of fusion materials. The diversity of kinematically possible reactions with a single target nuclide is shown in Fig. 1. In addition to all relevant neutron-induced reactions also so-called sequential (x,n) reactions can produce impor-

	N-2	N-1	N	N+1
Z+2				α,n
Z+1		p,n	d,n	
Z	n,3n	n,2n	original nucleus n,n	n,γ
Z-1	n,nt n,tn	n,t n,nd n,dn	n,d n,np n,pn	n,p
Z-2	n,αn n,nα	n,α n,He3n n,nHe3	n,He3 n,pd n,dp	

Atomic number ⟶
Neutron number ⟶
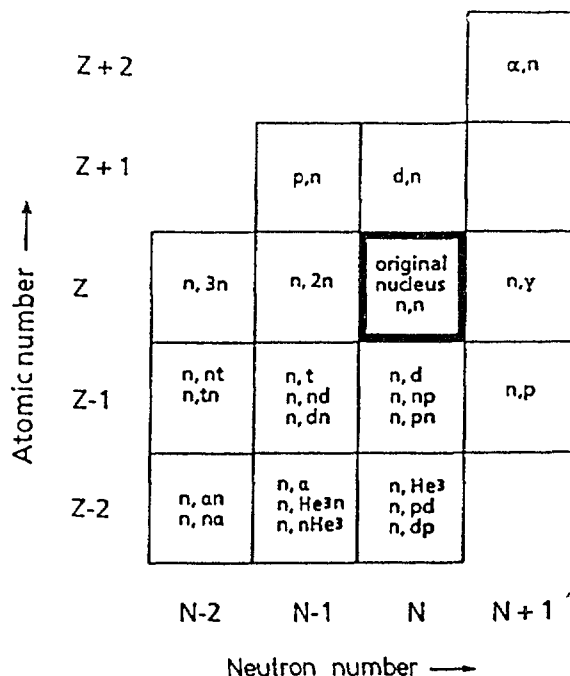
Fig. 1 Kinematically possible neutron-induced and sequential (x,n) reactions for neutron energies $E_n \leq 15$ MeV. Sequential (x,n) reactions are restricted here to the most important types of (p,n), (d,n) and (α,n) processes (see text).

tant radionuclides not achievable in one-step neutron interactions *.
Sequential (x,n) reactions are processes in which charged particles x are
produced in a first-step neutron-induced reaction A(n,x)B, and in which the
emitted charged particles react in a second step by the process A(x,n)C with
the target nucleus A producing the residual nuclide C. In the chart of Fig.
1 only sequential (p,n) (d,n) and (α,n) reactions have been included, which
are the most important ones. Sequential reactions such as (t,n), (^{3}He,n),
or (x,n'p), (x,n'd), (x,n'α), even though often kinematically possible, have
not been included, mainly because of their largely reduced probability.

The neutron flux and spectra depend on the materials used for the various
reactor components and are influenced by the attenuation and moderation
processes as the neutrons are passing through the material. Thus the neutron
spectra are largely dependent on the reactor engineering concept. Figure 2
shows a typical neutron spectrum in the first wall region which is the most
highly-irradiated component of a fusion reactor. The plotted spectrum is that
calculated for the Culham DEMO reactor design concept [10]. It can be seen
that even in the first wall the spectrum is rather soft, exhibiting a broad
distribution ranging from thermal to 14 MeV neutron energy, and only 12.6%
of the spectrum is concentrated in the 14-MeV peak. The large fraction of
neutrons with energies below 14 MeV results mainly from backscattering in
the blanket and in the other reactor components. From the spectral distrib-
ution shown in Fig. 2 it becomes clear that activity studies in fusion
reactors require nuclear cross sections covering the whole energy range from
thermal (or threshold) to more than 14 MeV.
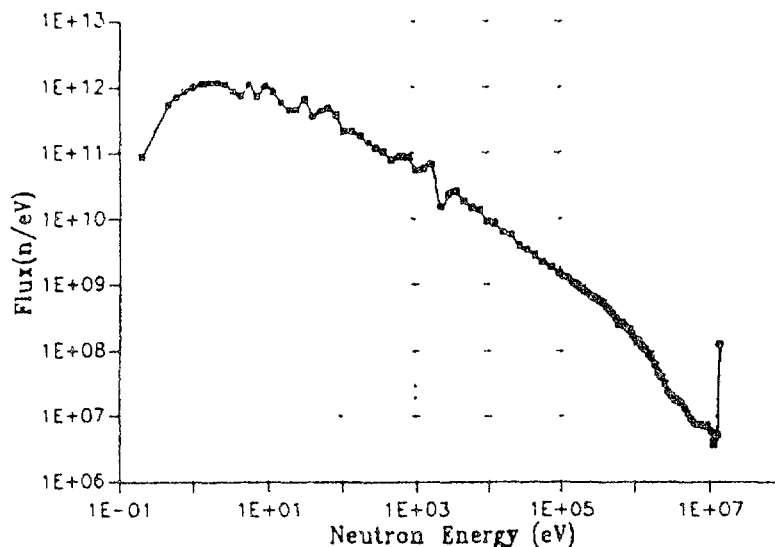
Fig. 2   First wall neutron spectrum for the Culham DEMO reactor design con-
cept (solid breeder). Only 12 6% of the spectrum is concentrated in
the 14 MeV peak. (From Ref. 12).

* In order to avoid misunderstandings, it should be mentioned that nuclides
created by sequential (x,n) reactions can, of course, be produced by mul-
ti-step neutron interactions. But these typically require long reaction
chains with at least one or two intermediate β⁻-decays which give, in gen-
eral, negligible inventories.

4. Present Status of Activity Calculations

Neutron-induced activities, their related surface γ-dose rates, decay heats and biological hazards can be calculated, if the neutron flux level, the neutron spectrum, the reactor operational scenario, the detailed composition of the material and the relevant nuclear data are all well known. For reliable predictions it is essential that all kinematically-allowed nuclear reaction channels are taken into account. Thus it is important to consider not only primary, but also sequential neutron-induced reactions, i.e. reactions that occur due to the presence of large amounts of radioactive or stable nuclides produced as a result of nuclear transmutations with the original nuclides of the reactor material. A typical example of this kind is the production of ^{41}Ca ($T_{1/2}=1.03\times10^5$ y) which dominates the element activity of titanium after a decay time of about 5×10^3 y [11]. In this case ^{41}Ca is chiefly produced through the reaction chain $^{46}Ti(n,\alpha)^{43}Ca(n,2n)\rightarrow$ $^{42}Ca(n,2n)^{41}Ca$, where ^{43}Ca and ^{42}Ca are stable intermediate nuclei.

For calculations of neutron-induced radioactivities in fusion reactors there exist presently several activation codes which require two major nuclear data libraries, one containing multigroup reaction cross sections, and the other nuclear decay data [12-14]. Most of these can already provide fairly good radiological predictions for a wide range of technologically important materials. A typical example of recent calculations with one of these codes is given in Fig. 3. The diagram shows the calculated activities versus cooling time for twelve elements irradiated in a first wall spectrum typical of a DEMO reactor [10]. The results were obtained from recent KfK calculations [15] using the UKACT1 and UKDECAY2 libraries as the primary input to the UK inventory code FISPACT [12,16]. A wall loading of 5 MW m^{-2} for 2.5 years was assumed. The enormous differences in the activity levels as a function of cooling time clearly demonstrate the necessity for a careful selection of elements (and critical element impurities) to be used as possible constituents of fusion reactor structural materials.

While all of the existing activation codes are largely complete with respect to neutron interactions, sequential (x,n) reactions have, to our knowledge, been ignored in all previous work. The KfK group has recently shown, at least for protons, deuterons and α-particles, that these processes can significantly contribute to the integral radiological quantities [17]. One stressing example of this kind is the production of ^{26}Al ($T_{1/2}=7.2\times10^5$ y) through the sequential reaction $^{23}Na(n,z\alpha) \rightarrow {}^{23}Na(\alpha,n)^{26}Al$ (z stands for any particle other than α). This is illustrated in Fig. 4 which shows the integral surface γ-dose rate of sodium as a function of the time after irradiation. In order to suitably separate the effect of sequential (x,n) reactions, the dose rates were calculated twice: Once with and once without including these reactions, while leaving all other conditions unchanged. In this way the difference of the two curves in Fig. 4. is a good measure of the contribution of sequential reactions to the total induced dose rates. As can be seen the effect is most pronounced in the time range beyond ~100 years, where the top curve is governed by the ^{26}Al activity. The bottom curve (excluding (x,n) reactions) shows also a wide plateau in the region 10^2-10^6 years, but this results from neutron-induced reaction chains leading to ^{10}Be ($T_{1/2}=1.6\times10^6$ y). Inclusion of the sequential $^{23}Na(\alpha,n)^{26}Al$ reaction in the calculation gives by 9 orders of magnitude higher dose rates in this range. It even places the long-time dose rates significantly above the "hands-on" level of 2.5×10^{-5} Sv/h [9].
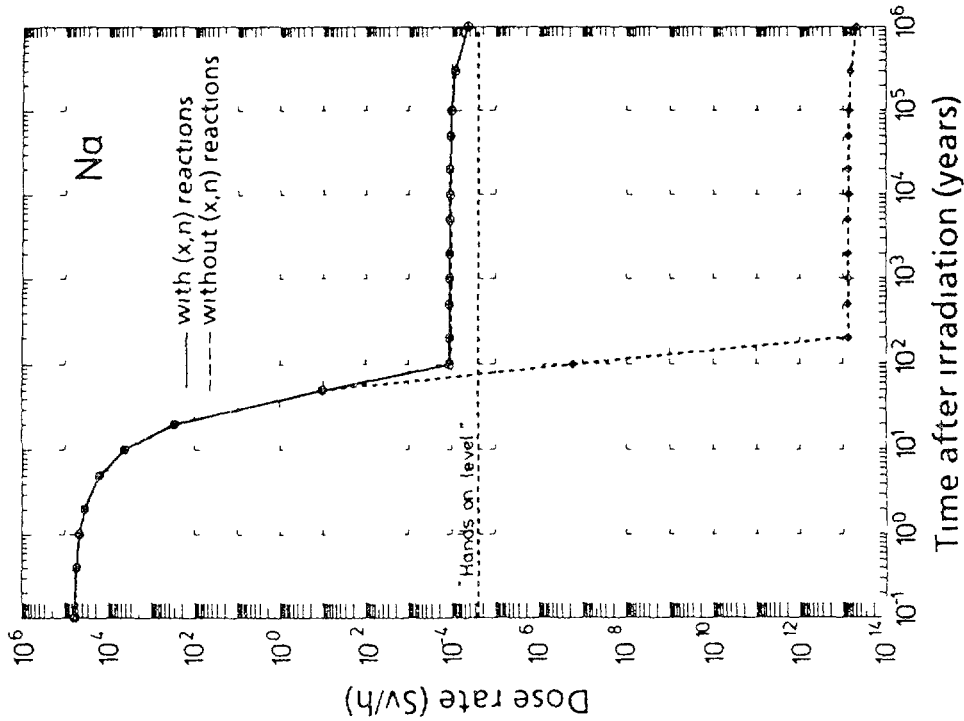
Fig 4

Calculated dose rate versus cooling time for Na The difference between the two curves is a measure of the contribution of the ^{26}Al activity ($T_{1/2}=7$ 2×10^5 y) produced by the sequential reaction ^{23}Na$(\alpha,n)^{26}$Al
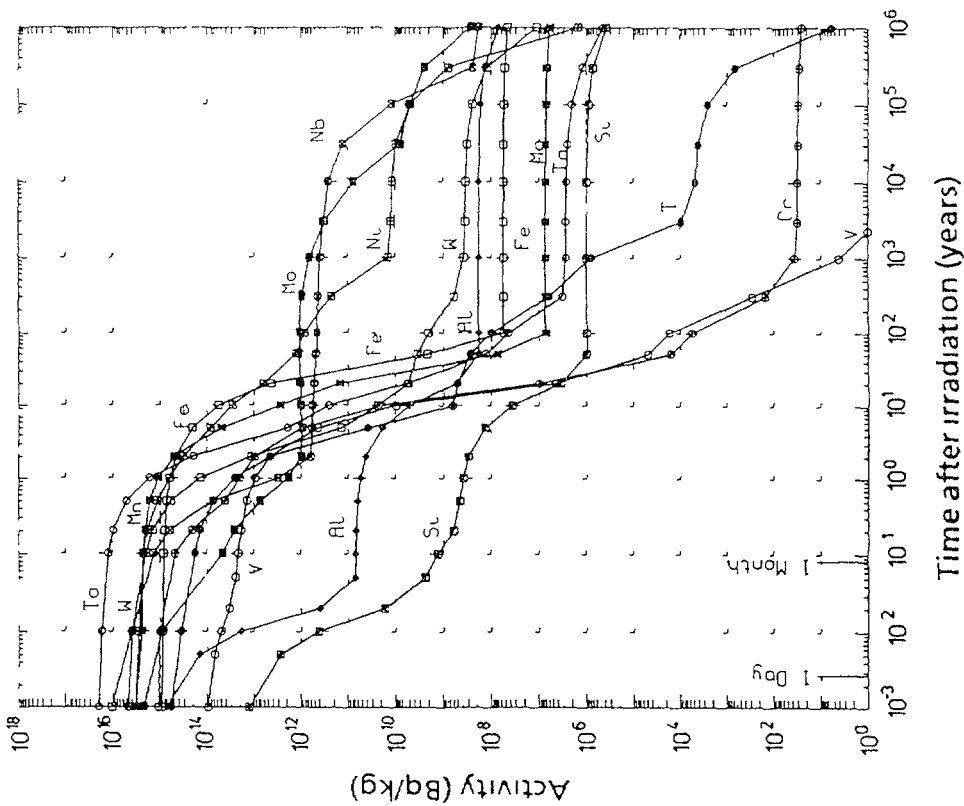
Fig 3

Calculated induced activities as a function of cooling time for twelve technologically important elements The results refer to neutron irradiation in the first wall of a DEMO fusion reactor [10] A wall loading of 5 MW m^{-2} for 2 5 years was assumed

58

A summary of the KfK work on sequential (x,n) reactions performed up to now [18] is given in Table II. This table lists the important radionuclides produced in element activation by sequential (x,n) reactions on Na, Mg, V, Cr and Fe. A comparison of the inventories achieved for calculations with and without (x,n) reactions is shown in the third and fourth columns. The numerical values given in these columns are total inventories which might have been produced by more than one sequential reaction or more than one neutron reaction chain, respectively. In the last column the type(s) of sequential (x,n) reaction(s) leading to the production of the corresponding radionuclides are indicated. For the elements Na, Mg, V and Cr, the additionally produced inventories drastically alter the integral element activities and/or the related dose rates and decay heats, while the additional activities for iron are masked in the integral quantities by other radionuclides with comparable half-lives. Already these limited results give a clear indication that sequential (x,n) reactions cannot be neglected in reliable activity calculations.

5. Nuclear Data Needs

5.1 General Requirements

The nuclear data base required for activation calculations in support of LAM development primarily concerns energy-dependent neutron activation cross sections and decay data for a very large number of stable and radioactive nuclides. The requirements and the status of these data have been recently reviewed by several authors [19-23]. In addition, other data such as Bremsstrahlung data (for predictions of dose rates and decay heats), double-differential charged-particle-emission cross sections or differential cross sections and stopping powers of charged particles (for estimates of (x,n)-induced activities) and CEDE factors (for calculations of biological hazards) are needed for calculations of all radiological properties. Concerning neutron data, the required data base can be divided into two main groups: 1) Data needed for the determination of space-dependent neutron fluxes in the various reactor components, and 2) data required for the estimate of radioactivities induced in potential "low-activation" fusion materials.

For flux and spectrum calculations the most important neutron data are total, double-differential neutron-emission and photon-production cross sections. These cross sections must be known for the entire energy range from thermal (threshold) to 15 MeV for the important structural, tritium-breeding, shielding and magnet materials e.g. Li, Be, O, Fe, Cr, Ni, V, Pb, Cu etc. Even though a large amount of data for this purpose are already available from previous work in fission reactor development, there is still a considerable demand of additional data more specific for fusion applications. Such demands have been reviewed in the past by some groups, e.g. [19,21,22]: A general observation was that data below 8 MeV and at 14 Mev are widely available, while data in the intermediate range from 8 to 14 MeV are scarce, and need further investigation.

The required data base for activity calculations is much broader. For an adequate assessment of potential "low-activation" materials and the effects of critical impurity elements on the radiological properties appropriate libraries must contain cross sections for all possible neutron-induced reactions and all potential target nuclei. A few of the presently existing

Table II. Important radioisotopes produced by sequential (x,n) reactions, but only very weakly produced by neutron-induced reactions

Element	Radio-Nuclide	Inventory after 2 5 y Irradiation with Sequential (x,n) Reactions (at /kg)	Inventory after 2 5 y Irradiation without Sequential (x,n) Reactions (at /kg)	Important Sequential Reactions
Na	^{26}Al	$5\ 2\times10^{18}$	2.9×10^{5}	^{23}Na$(a,n)^{26}$Al
Mg	^{26}Al	1.2×10^{18}	$3\ 7\times10^{16}$	^{26}Mg$(p,n)^{26}$Al ^{25}Mg$(d,n)^{26}$Al
V	^{53}Mn ^{54}Mn	$6\ 8\times10^{14}$ $8\ 3\times10^{16}$	2.2×10^{8} 6.3×10^{10}	^{50}V$(a,n)^{53}$Mn ^{51}V$(a,n)^{54}$Mn
Cr	^{53}Mn	1.5×10^{18}	$5\ 2\times10^{15}$	^{53}Cr$(p,n)^{53}$Mn ^{52}Cr$(d,n)^{53}$Mn ^{50}Cr$(a,n)^{53}$Mn ^{52}Cr$(a,n)^{55}$Fe
	^{55}Fe	$2\ 3\times10^{17}$	1.2×10^{16}	
Fe	^{56}Co ^{57}Co ^{59}Ni	$5\ 6\times10^{17}$ 1.9×10^{17} 2.7×10^{17}	$2\ 3\times10^{13}$ $2\ 1\times10^{15}$ 8.0×10^{12}	^{56}Fe$(p,n)^{56}$Co ^{56}Fe$(d,n)^{57}$Co ^{56}Fe$(a,n)^{59}$Ni

neutron data libraries used for activity calculations are listed in Table III. As can be seen from this table these libraries typically cover almost ten thousend reactions for many hundreds of target nuclei [12,24-26]. For instance, the UKACT1 library contains cross section data in the 100-group GAM-II format for all important reactions on 625 target nuclides. These include all stable isotopes and radionuclides with half-lives longer than 1 day with atomic numbers $\leq$ 84, including a large number of first and second isomers. All first three libraries of Table III are not independent of each other. They are all based on the early US activation library, REAC [27], which then has been largely extended and improved in the three laboratories, all of which are presently maintaining their own files. The listed versions of the files all contain contributions from each other. In recent years, exchanges of additions and improved parts of the files have been made on the basis of an inofficial collaboration. All currently released libraries were known to have still weaknesses, e.g. with respect to still lacking reaction data, unsatisfactory capture data, simple THRESH-code generated cross sections, and sometimes insufficient isomeric and ground state cross sections.

Table III. Presently available activation libraries for fusion reactor development

Name	Laboratory/ Country	Number of reactions	Responsible maintainer(s)/Ref
UKACT1	Harwell/UK	~8 700	R A Forrest [11]
REAC2	Hanford/LSA	~9 000	F M Mann/[25]
REAC-ECN-3	ECN-Petten/NL	~8 500	H. Gruppelaar '[24]
JENDL-3 *	JEARI,Jpn	~2 000	JAERI-NDC/[26]

* Activation file (not yet released)

Therefore, further improved versions are in progress, e.g. REAC-ECN-4 at Petten, UKACT2 at Harwell and USACT-88 at Hanford. After release of the new versions it is expected that the inofficial cooperation could continue to create a joint activation library for common use in Europe and the United States [28]. The present intent is to take the best parts from each of the three libraries, and to use a pointwise format similar to that of ENDF-IV. While in Europe and the United States the activation libraries for fusion applications have been separated from the general purpose files ENDF/B and JEF, the activation library in Japan is still part of JENDL-3. The JENDL-3 activation file presently contains only about 2.000 reactions, but it is expected that the number of reactions will be extended to ~ 4.000 by early 1991 [26]. The Japanese activation file will not be released before the general purpose file JENDL-3 has been finalized.

5.2 Needs for Additional and Improved Nuclear Data

In the past, work on activation cross section and decay data libraries has been mainly driven by the force of completeness rather than by the intent of achieving good accuracy in the first instance. At present, increasingly more attention is given to the improvement of the quality of the data contained in the interim libraries. Some types of data for which more and/or better-quality data are currently required are given in Table IV.

Table IV. Some present requirements and current activities for extended and/or improved nuclear data

Type of data	Institution, country	Current activity, status
Activation reactions leading to long-lived nuclei	IAEA/CRP, US	Measurements or evaluations in progress [21]
Activation cross sections for selected important reactions	EC, UK, US	Improvements by new evaluat. and model calculations [28]
Cross sections for inclusion of sequential (x,n) reactions $(\sigma_{nx}(E_n,E_x), \sigma_{xn}(E_x))$	KfK, EC, UK	Selection of important reactions subject to further systematic studies [18]
Decay data: halve-lives, spectral distributions	US, EC	Review of decay data underway at NNDC [19]

One particular type of data which has been first reviewed for completeness and accuracy concerned activation reactions leading to long-lived radionuclides with half-lives longer than 5 years [21]. Good quality data of this type are important to answer questions currently raised at the political level about the type and amount of waste expected from fusion reactors. Therefore, work was organized by initiative of IAEA, and in this context the corresponding activation cross sections were compiled and screened, and high-priority needs were identified. For improvement of this data base, measurements and new evaluations within a Coordinated Research Program (CRP) organized by the Nuclear Data Section of IAEA have been initiated.

A second type of data are cross sections for other important reactions. Although there is a general need for a tremendous number of activation cross sections, primarily only the most critical ones need major effort. On this basis Forrest [29] has recently released a list with high-priority needs. This compilation contains 256 reactions leading to the most important radionuclides produced in elements ranging from boron to bismuth. The important reactions were selected through sensitivity studies performed by means of a special sensivity option of the FISPACT code. In addition to selections made at Harwell, this list includes also important reactions selected by the groups at Ispra and at Hanford. (For details of this list see Appendix 2 of the Summary Report of Workshop 1 of this Meeting). Important improvements are expected to come mainly from two types of work: a) New evaluations and b) replacement of THRESH-code generated data by better estimates from more accurate nuclear models.

The necessary inclusion of sequential (x,n) reactions in activity calculations requires a completely new data base not yet contained in any of the present libraries. The three types of nuclear data needed for this purpose are : 1. Double differential neutron-induced charged-particle-emission cross sections for neutron energies between 0 to 15 MeV. 2. Differential charged-particle-induced neutron-emission cross sections for the range ~1-15 MeV. 3. Stopping powers for the involved charged particles and target elements. While charged particle stopping powers are readily available from various compilations, the first two types of data exist only for limited isotopes and incident particle energies. Especially, experimental double differential neutron data are only scarcely available. The few existing data sets refer almost completely to the energy range 14-15 MeV, so that adequate data must be taken from broad-scale systematics of model calculations. The situation is much better for charged-particle cross sections, where suitable measurement, compilations and systematics exist, e.g. the compilation of experimental results by Lange et al. [30]. There is, however, no sufficient information on the isotope dependence of such cross sections. In general, there is a need of more double differential neutron and differential charged-particle cross sections in the energy range between ~1 and 20 MeV. The existing data base is too scarce to establish suitable systematics over sufficiently large ranges of incident energies, target masses and relevant types of nuclear reactions. At this stage of the investigations on sequential (x,n) reactions, however, important data needs cannot be specified in more detail. Identification of individual critical cross sections will be subject to forthcoming sensitivity studies.

Further improvements are also needed for a large amount of decay data, particularly half-lives and spectral data [19,31]. For instance in the Harwell dacay data-library UKDECAY2 for 1314 nuclides [12] no spectral decay data for 420 radionuclides are included, since such information was not available, neither from the the European and the US main purpose files, nor from the handbook Table of Radioactive Isotopes [32]. Especially for the nuclides which contribute significantly to the total dose rates, more and/or better-quality spectral data are needed. In addition to spectral data, also the half-lives of long-lived radioisotopes need to be reviewed. As has been shown by Greenwood [31] these are often badly known. In a recent investigation this author showed that several measured activation cross sections were clearly deteriorated in accuracy due to large uncertainties (up to 20%) in the corresponding half-lives.

6. Summary

At present, low-activation materials promise to become an important means for the development of fusion as a safe and environmentally-acceptable energy source. Potential benefits are expected in various areas of utilization ranging from considerations of normal reactor operation to aspects of possible accidents and reactor decommissioning. In order to quantify the benefits to be gained from the use of low-activity materials in all reactor components, more complete and accurate predictions of the induced radioactivities and their related quantities such as surface γ-dose rates, decay heats and biological hazards are needed. This requires adequate activation codes and appropriate nuclear data libraries. Although there have been great advances in recent years in establishing appropriate computer codes and large activation libraries, further progress is still needed concerning completeness and accuracy. Currently major effort is put into improvements of the following types of important nuclear data: 1. Threshold and capture reactions leading to long-lived radionuclides. 2. Other important neutron-induced reactions producing the most critical activities in elements ranging from boron to bismuth. 3. Charged-particle emission spectra of neutron-induced reactions and charged-particle induced reactions needed to treat the important sequential (x,n) reactions. 4. Half-lives of long-lived radionuclides and lacking spectral information for the decay of nuclides contributing significantly to the total surface γ-dose rates. In addition to these activities, there is a stressing need for detailed error estimates of critical nuclear data, in order to specify the uncertainty levels of current predictions for the radiological properties of potential low-activation materials.

ACKNOWLEDGEMENTS

REFERENCES

[1] G J. Butterworth, "Low-activation Structural Materials for Fusion", 15th Symposium on Fusion Technology (SOFT), Utrecht NL, 1988, Fus Eng and Design 11, 231 (1989).

[2] O N Jarvis, "Low-activity Materials. Reuse and Disposal", Harwell Laboratory Report, AERE-R 10860, July 1983

[3] C Ponti, "Recycling and Shallow Land Burial as Goals for Fusion Reactor Materials Development", Fusion Technology 13, 157 (1988)

[4] C. Ponti, "Fusion Reactor Materials to Minimize Long-lived Radiocative Waste", Fusion Eng and Design 10, 243 (1989)

[5] E T. Cheng, "Radioactivity Aspects of Fusion Reactors", Fusion Eng and Design 10, 231 (1989).

[6] S Fetter, E T. Cheng and F.M. Mann, "Long-term Radioactivity in Fusion Reactors", Fusion Eng and Design 6, 123 (1988)

[7] Code of Federal Regulations, "Licensing Requirements for Land Disposal of Radioactive Waste, Title 10, Part 61", Nuclear Regulatory Commission, Washington, December 30, 1982

[8] Radioactive Waste, Vol I, First Report from the Environment Committee of the House of Commons, UK, Session 1985-86

[9] Council Directive of July 15, 1980, EUR Report, EUR-7330, European Atomic Energy Community (1980)

[10] P I H Cooke and P Reynolds et al A DEMO Tokamak Reactor Aspects of the Conceptual Design" Culham Laboratory Report, CLM R 254 , 1985

[11] R A Forrest and D A Endacott, "Activation Data for Some Elements Relevant to Fusion", Harwell Laboratory Report, ALRI R 13402, 1989

[12] Forrest, M G Sowerby, B H Patrick and D A J Endacott, "The Data Library UKACII and the Inventory Code FISPACI", Proc Intern Conf on Nuclear Data for Science and Technology, Mito, Japan, p 1061 (1988)

[13] C Ponti, Calculations of Radioactive Decay Chains Produced by Neutron Irradiations", I UR Report, EUR 9389 1984

[14] F M Mann, "Transmutations of Alloys in MFF Facilities as Calculated by REAC (A Computer Program for Activation and Transmutations)", HDL Report, HLDL 1ML 81-37, 1982

[15] S Cierjacks and Y Hino, "Study of Element Activation in Fusion Reactor Materials", KfK Report, KfK-4523, in preparation

[16] R A Forrest, D A J Endacott and A Khursheed, FISPACI - Programme Manual", Harwell Laboratory Report, ALRL M 3655, 1988

[17] S Cierjacks and Y Hino, "The Influence of Sequential (x n) Reactions on Total Element Activities J Nuclear Materials, in press

[18] S Cierjacks and Y Hino, "The Role of Sequential (x,n) Reactions on Element Activation of Fusion Materials and Related Nuclear Data Needs", NEANDC Specialists Meeting on Neutron Activation Cross Sections for Fission and Fusion Energy, Argonne, Sept 1989, Proceedings to be published

[19] E T Cheng, Review of the Nuclear Data Status and Requirements for Fusion Reactors", Proc Int Conf on Nuclear Data for Science and Technology Mito, June 1988, p 187, Japan Atomic Energy Research Institut, 1988

[20] E T Cheng, Nuclear Data Needs for Fusion Energy Development", Fusion Technology 8, 1423 (1985)

[21] V Goulo, "Report on the IAEA Advisory Group Meeting on Nuclear Data for Fusion Reactor Technology" Gaussig German Democratic Republic, December 1-5 1986, IAEA Report INDC/P (87) 3, 1987

[22] F M Mann, "Status of Dosimetry and Activation Data Proc Int Conf Nuclear Data for Science and Technology, Mito, June 1988, p 1013, Japan Atomic Energy Research Institut, 1988

[23] E T Cheng "Activation Cross Section for Safety and Environmental Assessments of Fusion Reactors", NEANDC Specialists Meeting on Neutron Activation Cross Sections for Fission and Fusion Energy Argonn Sept 1989 Proceedings to be published

[24] H Grupelaar, H A J Van der Kamp J Kopecki and D Nierop, "The REAC ECN 3 Data Library with Neutron Activation and Transmutation Cross Sections for Use in Fusion Reactor Technology" ECN Petten Report ECN 207, 1988

[25] J Ch Sublet, F M Mann and A F H Goodduad One group Averaged Cross Section s Benchmark Comparisons for Fusion Activation Studies", NEANDC Specialists Meeting on Neutron Activation Cross Sections for Fission and Fusion Energy, Argonne, Sept 1989, Proceedings to be published

[26] Y Nakajima et al , Present Status of the JENDL Activation File NEANDC Specialists Meeting on Neutron Activation Cross Sections for Fission and Fusion Energy Argonne Sept 1989, Proceedings to be published

[27] F M Mann, D L Lessor and J S Pintler, REAC Nuclear Data Libraries" Proc Int Conf Nuclear Data for Basic and Applied Science, Santa Fe, May 1985, p 207 (Gordon and Breich, 1986)

[28] J Kopecki and H Gruppelar, European Activation Library for Fusion Reactor Technology", NEANDC Specialists Meeting on Neutron Activation Cross Sections for Fission and Fusion Energy Argonne Sept 1989 Proceedings to be published

[29] R A Forrest Reactions Important for Activation", NEANDC Specialists Meeting on Neutron Activation Cross Sections for Fission and Fusion Energy Argonne, Sept 1989, Proceedings to be published

[30] J Lange, H Munzel, K A Keller and G Pfennig Excitation Functions for Charged Particle Induced Nuclear Reactions , in Landolt Bornstein New Series I, Vol 5, Part b, ed H Schopper, (Springer Verlag Berlin 1973)

[31] I R Greenwood and D I Bowers, "The Production of ^{49}V, ^{93}Mo, ^{93m}Nb and Other Long lived Isotopes in Fusion Materials with 14 MeV Neutrons", NEANDC Specialists Meeting on Neutron Activation Cross Sections for Fission and Fusion Energy, Argonne, Sept 1989 Proceedings to be published

[32] E Brown and R B Firestone, Table of Radioactive Isotopes, (John Wiley and Sons, New York 1986)

64

HIGH ENERGY NEUTRON DOSIMETRY
AND RADIATION DAMAGE CALCULATIONS

(Session II)

Chairman

R. DIERCKX
Commission of the European Communities

NEUTRON ACTIVATION DOSIMETRY IN EXPERIMENTS WITH MASSIVE TARGETS IRRADIATED WITH 1 GeV PROTONS

S.V. BAKHMUTKIN, A.I. BOGDANOV, V.G. BOGDANOV,
V.I. KUCHERYUK, A.A. NOSSOV, A.A. RIMSKI-KORSAKOV
V.G. Khlopin Institute,
Leningrad, Union of Soviet Socialist Republics

N.P. KOCHEROV
International Atomic Energy Agency,
Vienna

Abstract

Foil activation measurements on the surface of massive cylindrical metal targets irradiated with 1Gev protons along the cylinder axis are reported. The reaction rates for 13 dosimetry reactions are reported for aluminium, iron and composite aluminium–uranium targets. The activation on the surface is mainly produced by secondary neutrons generated in multiplication processes inside the massive targets, but effects of possible interference from secondary protons are also discussed.

The process of neutron multiplication in high energy proton bombardments of massive targets has recently received a considerable attention in literature. In this context the term "massive target" usually means that it is large enough for the proton beam striking the target to loose a considerable portion of its initial kinetic energy or slow down completely.

Recently some work with massive targets of lead, iron, aluminium + uranium was performed at the 1Gev proton accelerator of the Institute of Nuclear Physics in Gatchina (near Leningrad, USSR)(1,2,3). The reaction rates for production of several nuclides in the dosimetry material foils placed on the surface of the targets were measured. The aim of this work was to get experience in high energy neutron dosimetry and to produce benchmark data for testing calculational models of high energy particle transport in massive solid media.

The purpose of the present paper is to describe the results of the measurements of activation reaction rates in foils placed on the surface of aluminium, iron and composite aluminium–uranium targets. The geometry of the experiment is shown on Fig. 1a and 1b.

The targets were irradiated with a beam of 1Gev protons up to the integral flux of the order of 10^{16} protons. The range of 1Gev protons in lead and iron is less than the length of the target (60 cm in all cases), but in case of aluminium only part of kinetic energy is deposited in the target and the protons come through. The activation foils were placed on the surface of the cylindrical target as shown on Fig. 1a. To avoid possible shielding effects the foils were not mounted in stacks, but separately with the help of special plastic holders as shown on Fig. 1a.
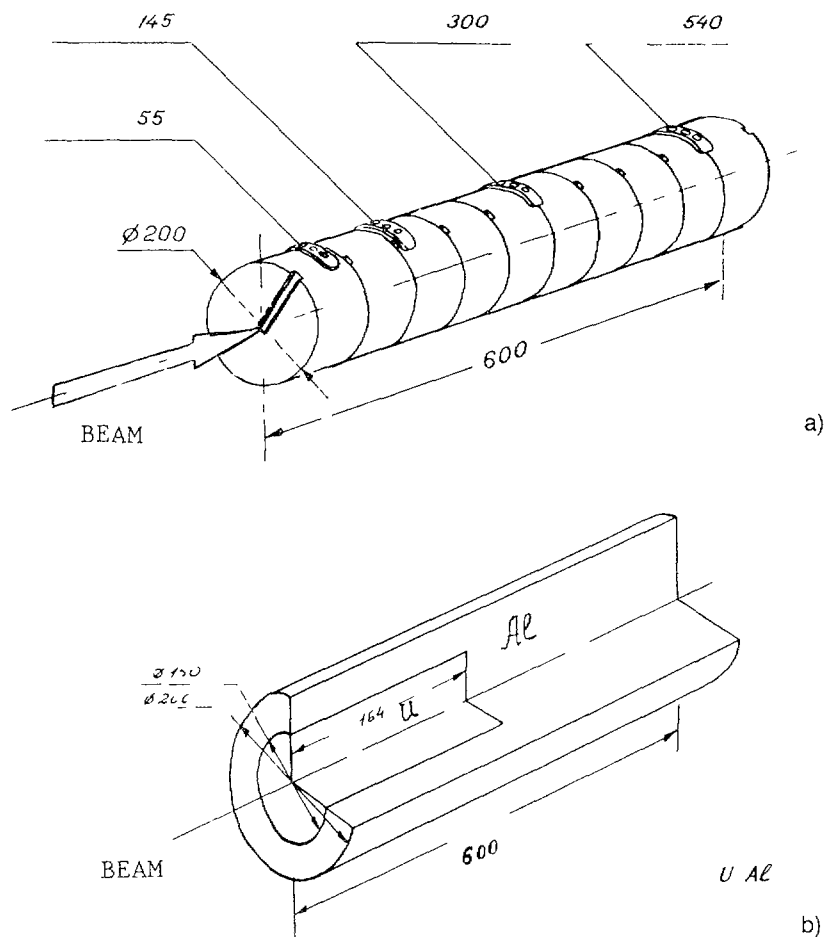
FIG 1 Geometry of massive targets used in experiments The dosimetry foil locations are also shown

The measurements of induced γ-activity in the foils were started 3 hours after irradiation and were done with two germanium spectrometers with 0.7 and 1.2 Kev resolution at 122 Kev. The detector efficiences were calibrated against the standard sources with accuracies ranging 0.6 - 1.5%. The errors quoted in the tables include uncertainties in efficiency and statistics but do not include uncertainties in branching ratios and monitor cross-section. All activities were recalculated to the moment when the irradiation was stopped and then the reaction rates were calculated taking into account the duration of the irradiation. The foils of 99.999 pure aluminium were used for monitoring the beam. The yield of ^{22}Na was measured, the reference cross-section of ^{27}Al(p,pnα) ^{22}Na was taken to be $12.6 \cdot 10^{-27}$ barn.

The results of the measurements are shown in Tables 1,2,3 and Figures 2 and 3. The effect of the presence of a uranium cylinder inside the aluminium target is clearly seen. In case of (n,γ) reactions the effect (increase of yields) is more pronounced, for other reactions the effect is significant only in the vicinity of the uranium material itself, the yields behind the uranium bloc can be seen to decrease in several cases.

Analysis of possible systamatic errors shows that the more likely sources of such errors are contributions to foil activation from protons, in those cases when they can lead to the same residual nuclides.

68

Table 1. Reaction rate data measured from activation foil detectors placed on the surface of aluminium massive target, exposure time 4.35 hrs.

Distance from entry, cm Reaction	Reaction rates* x 10^{-15} sec^{-1}			
	5.5	14	30	54
^{59}Co$(n,\alpha)^{56}$Mn	0.0136(1.5)	0.0297(1.5)	0.0328(1)	0.0237(1.5)
^{59}Co$(n,3n)^{57}$Co	0.0688(2)	0.162(1.5)	0.172(1.5)	0.138(2)
^{59}Co$(n,2n)$ ^{58}Co	0.216(1)	0.417(1)	0.434(1)	0.325(1)
^{59}Co(n,p) ^{59}Fe	0.0194(4)	0.0324(4)	0.032(4)	0.022(5)
^{59}Co$(n,\gamma)^{60}$Co	0.229(6)	0.327(7)	0.342(6)	0.519(5)
^{27}Al$(n,\alpha)^{24}$Na	0.040(2)	0.0624(1.5)	0.0627(1.5)	0.0443(2)
^{197}Au$(n,4n)^{194}$Au	0.188(2.5)	0.394(2.5)	0.417(2.5)	0.308(2.5)
^{197}Au$(n,2n)^{196}$Au	0.436(2)	0.774(2)	0.788(2)	0.558(2.5)
^{197}Au$(n,3n)^{195}$Au	0.367(7.5)	0.66(7)	0.703(7)	0.534(7)
^{117}Au$(n,\gamma)^{198}$Au	1.20(1.5)	2.139(1.5)	2.256(1)	2.879(1)
^{238}U$(n,\gamma)^{239}$U$\rightarrow^{239}$Np	0.430(4)	0.425(4)	0.425(5)	0.395(4)
^{238}U$(n,2n)^{237}$U	0.667(3.5)	0.934(3)	0.942(3)	0.723(3.5)
^{93}Nb$(n,2n)^{93}$Nb	0.116(3.5)	0.169(3)	0.163(3.5)	0.116(3.5)
* Standard	deviations	in % are	given	in brackets

Table 2. Reaction rate data measured from activation foil detectors placed
on the surface of iron massive target.
Time 8.567 hrs.

	Reaction	rates*		
Distance from entry, cm Reaction	5.5	14	30	54
$^{59}Co(n,\alpha)^{56}Mn$	0.027(2)	0.036(2.5)	0.024(3)	0.007(4)
$^{59}Co(n,3n)^{57}Co$	0.131(2)	0.169(1)	0.105(4)	0.034(2)
$^{59}Co(n,2n)$ ^{58}Co	0.419(1)	0.498(1)	0.295(1)	0.087(1)
$^{59}Co(n,p)$ ^{59}Fe	0.040(3)	0.045(2.5)	0.025(4)	0.007(5)
$^{59}Co(n,\gamma)^{60}Co$	0.214(7)	0.244(7)	0.194(7.5)	0.140(5)
$^{27}Al(n,\alpha)^{24}Na$	0.079(2.5)	0.091(2)	0.053(3)	0.016(3.5)
$^{197}Au(n,4n)^{194}Au$	0.432(3)	0.516(2.5)	0.310(2.5)	0.093(3.5)
$^{197}Au(n,2n)^{196}Au$	0.953(2)	1.035(2.5)	0.576(2.5)	0.160(3.5)
$^{197}Au(n,3n)^{195}Au$	0.626(6)	0.840(6)	0.508(7)	0.143(11)
$^{117}Au(n,\gamma)^{198}Au$	1.781(2)	1.932(1.5)	1.389(1.5)	0.809(1)
$^{238}U(n,\gamma)^{239}U \rightarrow ^{239}Np$	1.028(3)	1.155(3)	0.719(4.5)	0.331(3.5)
$^{238}U(n,2n)^{237}U$	1.157(3)	1.317(3)	0.755(3.5)	0.205(6)
$^{93}Nb(n,2n)^{93}Nb$	0.204(2.5)	0.208(2.5)	0.138(3)	0.040(2.5)

Table 3. Reaction rate data measured from activation foil detectors placed on the surface of aluminium-uranium massive target. Exposure time 6.083 hrs.

	Reaction		rates*		
Distance from entry, cm	5.5	14	30	54	
Reaction					
$^{59}Co(n,\alpha)^{56}Mn$		0.044(1.5)	0.024(2)		
$^{59}Co(n,3n)^{57}Co$		0.186(2.5)	0.113(3)		
$^{59}Co(n,2n)\ ^{58}Co$		0.647(2.0)	0.347(3)		
$^{59}Co(n,p)\ ^{59}Fe$		0.093(3.5)	0.041(5)		
$^{59}Co(n,\gamma)^{60}Co$		0.967(4.5)	1.844(5)		
$^{27}Al(n,\alpha)^{24}Na$			0.070(2)		
$^{197}Au(n,4n)^{194}Au$		0.581(3.5)	0.346(5)		
$^{197}Au(n,2n)^{196}Au$		1.663(2)	0.796(2.5)		
$^{197}Au(n,3n)^{195}Au$		1.391(7)	0.772(7)		
$^{117}Au(n,\gamma)^{198}Au$		11.643(1)	17.200(1)		
$^{238}U(n,\gamma)^{239}U \rightarrow ^{239}Np$		5.843(2)	3.803(2)		
$^{238}U(n,2n)^{237}U$		1.738(5)	0.894(5)		
$^{93}Nb(n,2n)^{93}Nb$		0.351(2)	0.166(3)		

71

Reaction rates for 59-Co(n,A)56-Mn

Reaction rates for 59-Co(n,3n)57-Co

Reaction rates for 59-Co(n,2n)58-Co

Reaction rates for 59-Co(n,G)60-Co

Reaction rates for 59-Co(n,p)59-Fe

Reaction rates for 27-Al(n,A)24-Na

Reaction rates for 93-Nb(n,n')92m-Nb

FIG. 2. Reaction rates multiplied by 10^{-15} for different activation reactions

Reaction rates for 197-Au(n,4n)194-Au

Reaction rates 10 -15

0.6-
0.5-
0.4-
0.3-
0.2-
0.1-

—▽— Al
□ Al+U

0 10 20 30 40 50 60
Distance, см

Reaction rates for 197-Au(n,3n)195-Au

Reaction rates 10 -15

1.5-
1.0-
0.5-
0.0-

—▽— Al
□ Al+U

0 10 20 30 40 50 60
Distance, см

Reaction rates for 197-Au(n,2n)196-Au

Reaction rates 10 -15

2.0-
1.5-
1.0-
0.5-
0.0-

—▽— Al
□ Al+U

0 10 20 30 40 50 60
Distance, см

Reaction rates for 197-Au(n,G)198-Au

Reaction rates 10 -15

20-
15-
10-
5-
0-

—▽— Al
□ Al+U

0 10 20 30 40 50 60
Distance, см

Reaction rates for 238-U(n,G)239-U - 239-Np

Reaction rates 10 -15

6-
4-
2-
0-

—▽— Al
□ Al+U

0 10 20 30 40 50 60
Distance, см

Reaction rates for 238-U(n,2n)237-U

Reaction rates 10 -15

2.0-
1.5-
1.0-
0.5-

—▽— Al
□ Al+U

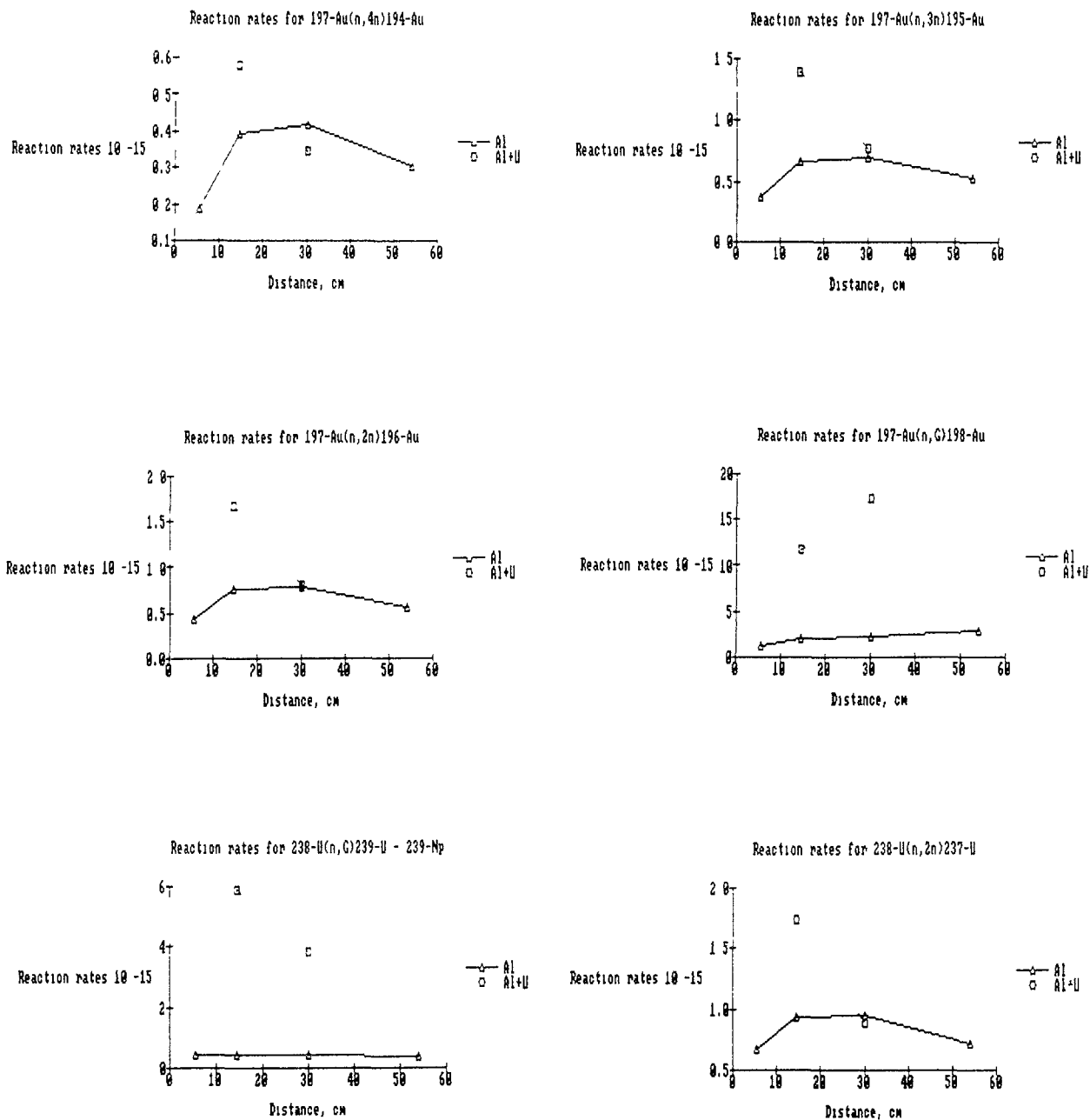0 10 20 30 40 50 60
Distance, см

FIG 3 Reaction rates multiplied by 10^{-15} for different activation reactions

To evaluate the contribution from protons an additional iron foil was placed and the yields of [55], [56], [57]Co were measured in it. Co isotopes could be produced in iron in the result of proton capture and subsequent emission of neutrons. Among all Co isotopes 56-Co has the largest production cross-section, but we could not detect it with any certainty above the background radiation. ^{54}Mn, which could be produced by both neutrons and protons through ^{56}Fe(p,2pn) and ^{54}Fe(n,p) was detected very easily. This enabled us to estimate the upper limit for proton flux on the surface of the cylinder as being very small, $Np/Nn < 0.005$. So the conclusion is that protons are not likely to contribute significantly to production of isotopes in our measurements.

ACKNOWLEDGEMENTS

REFERENCES

1. Bakhmutkin et al., Atomnaya Energia (in Russian) v. 62 p.59-61 (1987)

2. Yu. V. Alexandrov et al. Proc. of Nuclear Spectroscopy and Nuclear Structure Conference, Leningrad, 1989 p.536-537

3. Yu. V. Alexandrov et al., Ibid., Riga, 1988 p.544-545

74

DOSIMETRY AND RADIATION DAMAGE IN
HIGH-ENERGY NEUTRON FIELDS;
NUCLEAR DATA NEEDS

D.J. BOERMAN, R. DIERCKX, A. DUPASQUIER[1],
V. SANGIUST[1], P. TRINCHERINI
Joint Research Centre,
Commission of the European Communities,
Ispra Establishment,
Ispra

Abstract

Irradiation experiments at spallation neutron sources are of particular interest in view of the development of such a source for fusion simulated radiation damage experiments. Such an irradiation is executed in a spallation neutron spectrum at the beam stop of LAMPF, Los Alamos. This neutron spectrum is much harder than a fission spectrum, a few percent of the neutrons have energies above 10 MeV and up to some hundreds of MeV. Temperature during irradiation was 140°C. The neutron spectrum is monitored by monitor foils. From the foil activities the spectrum is deduced by unfolding codes. The irradiation has reached a fluence of 2.21×10^{19} n/cm^2. It is found that the spallation neutrons are accompanied by a few percent of high energy protons.

On some foils total He production and solid transmutation products are measured. On a Ni foil the radiation damage is measured by positron annihilation. Tensile-tests are executed on Al probes. Cross-section data needs are discussed.

---

1. INTRODUCTION

Radiation damage by fast (14 MeV) neutrons is expected to be a severe problem in future fusion reactors. The search for appropriate materials requires a high intensity neutron source which simulates the neutron spectrum and the radiation conditions at the first wall in a fusion reactor. For this purpose 14 MeV, deuteron-lithium and spallation neutron sources have been proposed /1/.

Before the beam stop area of LAMPF/LANL Los Alamos was rebuilt as a spallation neutron source of medium intensity for radiation damage experiments /2/, already in the old beam stop configuration, irradiations with spallation neutrons were possible. The experiment described here was carried out in the old beam stop configuration.

---

[1] Politecnico di Milano, 20133 Milano, Italy.

2. IRRADIATION

On the side of the beam stop of LAMPF (Los Alamos), a capsule was irradiated. During the irradiation the capsule (Fig.1) was cadmium-covered, sealed off hermetically and filled with helium gas. Thermocouples were placed inside the aluminium matrix. The channels numbered 0 till 12 were filled with samples for radiation damage effect measurements; the detector set positions are labelled C1 till C7. The fluence reached was 2.21×10^{19} n/cm^2 (detector set position 2), corresponding to about 0.04 dpa in iron. Temperature during irradiation was found to be 140°C.

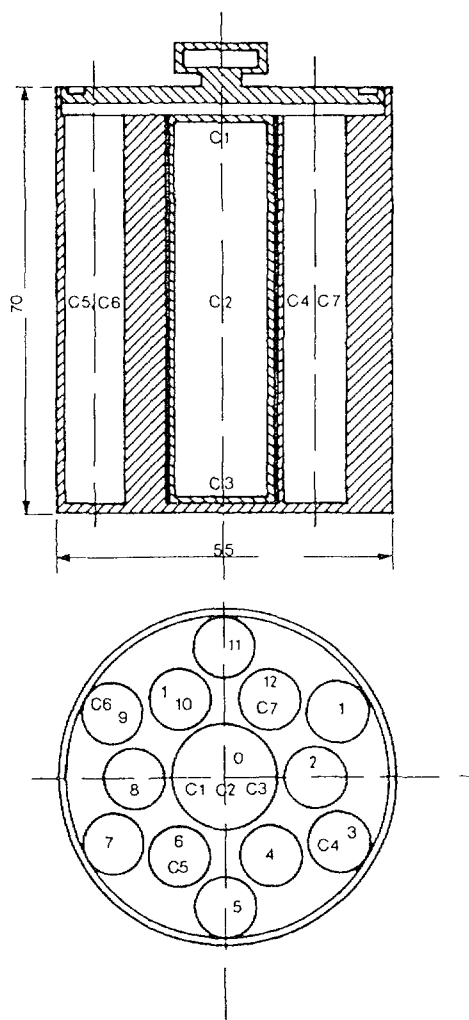Fig.1   Irradiation capsule. C1-C7   position of 7 detector sets. 0-12 radiation damage samples.

3. NEUTRON FLUENCE MONITORING /3/

Seven sets of detector foils were placed in the positions labelled C1-C7. Each set contained nine foils of the following detector materials: Co, Nb, Au, Ni and Ti. The measured reaction rates were used as input in the SAND II adjustment procedure. In Fig.2 the 5%-50%-95% response functions in the output spectrum for each reaction rate are shown. An adequate covering may be observed in the region between a few MeV and 200 MeV while in the low and very high energy range the information is clearly very scarce. In the two regions of scarce covering the adjustment is actually only a kind of normalization. In Table I the adjusted fluence rates are given in five
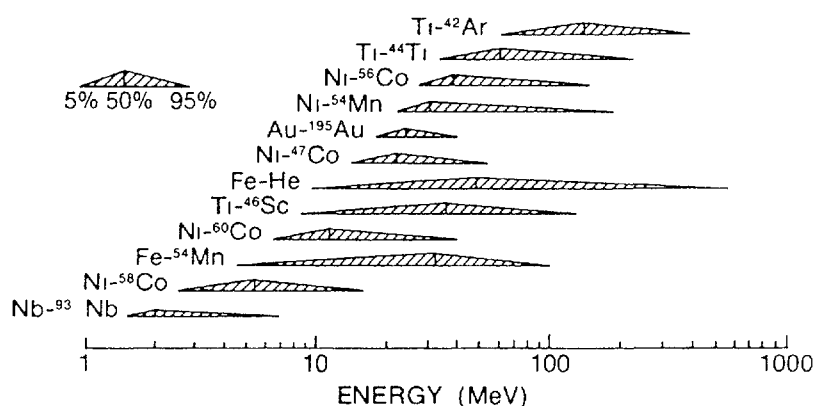
Fig.2   Response function of the detectors in adjusted spectrum of position 2 (centre of capsule).

TABLE I: Adjusted fluence rates for all detector positions in the capsule

Energy groups (upper limit)	Fluence rate per group					Total fluence rate
	I (1.3 eV)	II (0.1 MeV)	III (44 MeV)	IV (200 MeV)	V (800 MeV)	
Position 2 (n/cm^2.s.mA)	2.58×10^9	2.21×10^{12}	3.45×10^{12}	1.18×10^{10}	6.6×10^9	5.68×10^{12}
Ratio to pos.2						
Pos.1	.95	.97	.97	1.03	1.04	0.97
Pos.3	1.04	1.04	1.05	1.18	1.23	1.04
Pos.4	1.03	1.00	1.02	1.26	1.23	1.01
Pos.5	.93	.96	.96	1.00	1.02	0.97
Pos.6	1.02	.97	.96	1.06	1.08	0.97
Pos.7	.96	.89	.91	1.05	1.01	0.90

77

large energy groups in $n/cm^2.s.mA$ for position 2 and for the other positions the ratios of the fluence rate with respect to the one of detector set 2 (centre of capsule). The measured fluence above 44 MeV is surely due partly to protons which lose energy much faster than neutrons.

It has to be noted that the particle fluence above 50 MeV is responsible for 50% of the He production. The same effect is observed by F. Hegedus /4/. The high energy particles cause spallation reactions with the material leading to spallation products; this means nuclei with a smaller energy. These nuclei slow down and cause damage. It is expected that the small high energy particle fluence is responsible for a relatively great part of the damage.

4. CROSS-SECTION LIBRARY

A 100 group cross-section library was prepared using the energy grid and the weight spectrum given by Greenwood /5/. The energy grid from 10^{-10} to 800 MeV is detailed enough to make the derived group cross-sections relatively problem-independent. In the energy range of interest for fission reactors, data files exist to be used with confidence. At higher energy, however, the situation is much worse and most of the data come from calculations with scarce or no experimental validation.

For $Co(n,\gamma)$ and $Nb(n,\gamma)$ the ENDF B/V dosimetry file was used while for the $Nb(n,n')$ and Fe total He production the data of Hegedus /4/ and Greenwood /6/ were employed, respectively.

The calculations by ALICE code /7,8/ are the only data at our disposition for the other ten reactions. ALICE gives the cross-section for the formation of a nuclide considering the many paths through different particle (or combination of particles) emission; as a consequence our final cross-section data are the sum for all the

78

stable isotopes of a detector material, of a large number of (n,x) reactions. The upper energy limit of ALICE calculations is 200 MeV and we have arbitrarily extrapolated the data up to 800 MeV assuming an $E^{-1.5}$ dependence of the cross-section with energy. The calculated cross sections, which have a relative low energy maximum, show a cross-section decrease of approximately $E^{-1.5}$ up to 200 MeV. The rapid fall with energy of most of the cross-sections makes this assumption of little weight on the results with the exception for the $Ti(n,x)^{42}Ar$ reaction.

5. TOTAL HELIUM MEASUREMENTS /3/

Samples of Ni, Co, Fe (4 samples), Au, Ti and V were analyzed for total helium content at Rockwell International Corporation (USA) /9/. The Ni, Co, Fe, Ti and V samples were etched to remove approximately 0.025 mm of surface material. This was done to remove material which could have been affected by helium recoil either into or out of the samples during irradiation. The Au and Nb disks could not be etched because they were too thin. As already pointed out in section 3, more than half of the production is due to the small fraction of the neutron fluence above 40 MeV.

6. TRANSMUTATION PRODUCTS

One of the problems with high energy neutron sources, especially spallation sources, is the production of transmutation products. In the LAMPF irradiation, a series of pure samples were irradiated especially to measure which and how much of these products are formed. Some radioactive transmutation products due to spallation were determined /3/: $^{93}Nb(n,x)^{88}Zr(\rightarrow ^{88}Y)$, $Ni(n,x)^{54}Mn$, $Ti(n,x)^{42}Ar(\rightarrow ^{42}K)$ and $V(n,x)^{42}Ar(\rightarrow ^{42}K)$.

At the same time, samples of pure Ni and Au (2) were analysed for total impurities and transmutation products using an ICP-MS at JRC-Ispra (I).

The use of inductively coupled plasma mass spectrometer (ICP-MS) is quickly expanding because of its improvement in the detection limit of several elements (part per trillion, across essentially the entire Periodic Table) together with the additional possibility of measuring isotope ratios /15,16,17/.

The work described was carried out using a Plasma Quad ICP-MS (VG Elemental, Winsford, Cheshire, UK).

Analyses and data reported were obtained making use of the "Standard addition" method.

The samples (irradiated foils and matrix before irradiation) were accurately weighed, dissolved with redistilled $HCl-HNO_3$ before dilution, by weighing, with de-ionised water. Each standard addition analysis was performed running two different spiked solutions and sample solution together with a blank samples. The amount of the standard added should be roughly the same as the amount of unknown elements present in the sample solution.

Table IV shows preliminary results obtained on irradiated nickel foil. Differences in concentration measured for the transmutation products after irradiation are clearly reported. The results are expressed in part per million on the solid sample.

The standard deviation can be considered between 2-3% and the average accuracy of the final results should be contained within 5%. Precision and accuracy related with the isotope ratios measured can be compared with the uncertainty obtained measuring the "natural" ratios.

Using the same general criteria, Table V shows the results obtained for two different Au irradiated foils which give the opportunity to derive the internal reproducibility of the measurement.

80

TABLE II: Chemical composition (wt%) and metallurgical state of the two high purity aluminium alloys, placed in the irradiation capsule (see /13/)

ISML designation	Approximate USA correspondance	Metallurgical condition	Mg	Si	V	Fe	Cu	Zn	Mn	Ti
5188 or Al-Mg-V	5252	H112 as extruded	2.68	0.001	0.21	0.0013	0.0010	0.0002	0.0005	0.001
5153 or Al-Mg-Si	6063	T4 press quenched condition (not artificially aged)	0.72	0.34	–	0.0030	0.0026	0.0002	0.0002	0.001

TABLE III: Tensile tests on two irradiated high purity Al alloys (see ref./14/)

Alloy	Temp.	Condition	Spec.	S(0.2)(MPa)	mean	S(u)(MPa)	mean	e(pu)(%)	mean	e(pb)(%)	mean
		Non-irradiated	6	–		61.0	–	145.5	–	21.4	–	31.9
Al-Mg-V ISML-5188 (H112)	20°C	Irradiated	1	54.8	56.0	161.7	161.7	23.4	24.0	34.8	34.4
			4	57.3		161.7		24.5		34.0	
	150°C	Irradiated	3	62.4	62.7	147.7	145.4	20.5	20.4	37.5	36.9
			5	63.0		143.0		20.2		36.2	
		Non-irradiated	F	–		116.2	–	199.8	–	14.9	–	18.3
Al-Mg-Si ISML-5153 (T4)	20°C	Irradiated	A	220.2	220.9	272.5	274.0	10.8	10.9	16.9	15.8
			B	225.9		280.8		10.6		15.8	
			D	216.5		268.7		11.3		14.6	
	150°C	Irradiated	C	180.8	184.5	210.1	211.9	9.2	8.4	22.3	20.7
			E	188.1		213.7		7.5		19.1	

TABLE IV: Comparison between matrix before irradiation and an irradiated sample of nickel (Ni 7)

(a.m.u.) Isotopes measured n	[conc.] Matrix before irradiation Ni [ppm]	Ni bis	[conc.] Irradiated foils Ni 7 [ppm]	Ni 7bis	natural	Isotopic ratios before irradiation	after irradiation
^{65}Cu	7.4	7.8	15.8	13.7		$^{65}Cu/^{63}Cu$	
^{63}Cu	7.8	8.1	13.9	13.2	0.447	0.449	0.405
^{55}Mn	1.4	1.4	2.7	2.6			
^{53}Cr	1.5	1.5	2.2	2.0		$^{53}Cr/^{52}Cr$	
^{52}Cr	1.4	1.5	2.1	2.3	0.113	0.115	0.105
^{51}V	0.2	0.16	0.3	-			
^{48}Ti			1.8	-		$^{47}Ti/^{48}Ti$	
^{47}Ti	1.0	1.1	1.8	1.6	0.102	0.103	0.100

TABLE V: Comparison between matrix before irradiation and two samples (Au 2, Au 4) irradiated

(a.m.u) Isotopes measured n	[conc.] Matrix before [ppm]	Sample 2	[conc.] Irradiated foils Sample 2bis [ppm]	Sample 4	natural	Isotopic ratios before irradiation	after
^{195}Pt	1.7	2.5	2.4	2.2		$^{194}Pt/^{195}Pt$	
^{194}Pt	1.7	2.3	2.3	2.1	0.973	0.979	0.922
^{193}Ir	0.32	0.9	0.95	0.6		$^{191}Ir/^{193}Ir$	
^{191}Ir	0.30	0.8	1.1	0.7	0.597	0.620	0.606
^{186}W	0.5	0.6		0.6			

Experimental conditions and more details regarding the assessment of analyte matrices will be presently reported in a specialised analytical review.

7. POSITRON ANNIHILATION STUDIES /10/

Irradiated disks of high purity Ni were studied by positron annihilation techniques. The so-called "Doppler broadening" technique was applied, based on the measurement of the energy spectrum of the annihilation radiation. The shape parameter /11/ used in this work is the ratio S between the area of a central portion of the 511 keV peak and the total peak area. The energy window used to define the central portion of the line was chosen such that $S = 0.5$ for the reference samples of annealed Ni. Comparing regularly this reference with the measurements on the irradiated foils, we obtained full reproducibility of S values within a purely statistical fluctuation of 3×10^{-3}. A special problem in this measurement was the high gamma background level given by the active species (mainly ^{60}Co and ^{54}Mn) present in the irradiated samples. Therefore, a special experimental procedure was developed, keeping the disturbance at a constant level.

The evidence for any radiation damage caused in the irradiated sample, n, by the relatively low dose of neutrons in the presence of pre-existing structural disorder must come from a careful comparison with a non-irradiated sample, c. Fig.3 shows the dependence of the S parameter on the annealing temperature for both samples, with curves drawn through the experimental points as guides for the eye. The following features are evident:

1) in the initial state, both samples are characterized by an S parameter definitely larger than in bulk nickel, which is represented by the reference line at 0.5; sample c starts slightly above sample n;
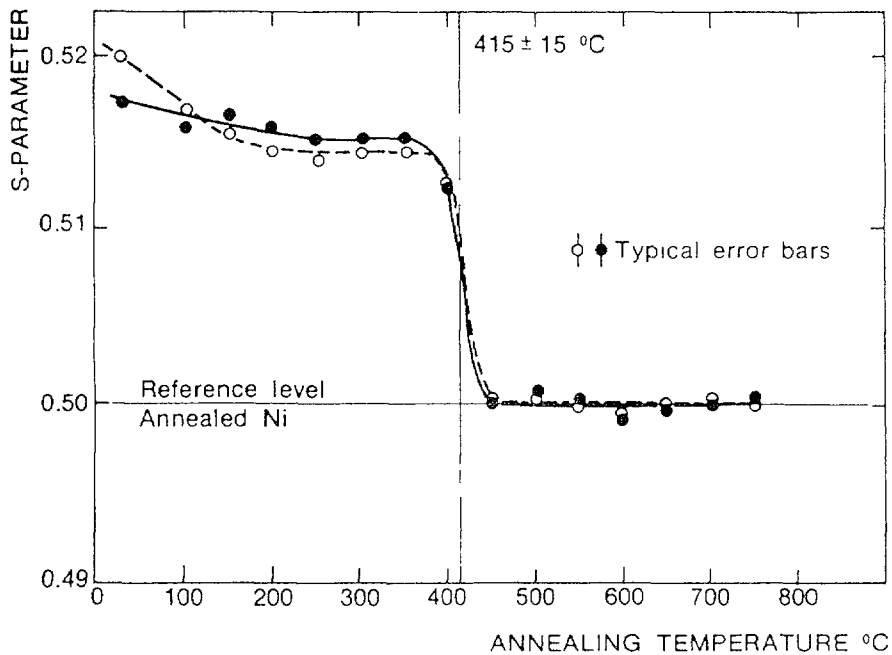
Fig.3   Isochronal   annealing of   Ni shown through the   dependence of
the   annihilation   peak   parameter   S   on   the   annealing
temperature (dots: sample n; circles: sample c).

2) the   two curves   cross at   100°C; from   150°C to 400°C both curves

display a plateau, with n-points now slightly above c-points;

3) a   sharp fall   of both   curves down   to the   reference occurs   above

400°C;   above 450°C   no further   variations occur (a shallow minimum

visible   around 600°C   certainly has no physical meaning, and is due

to   a small   alteration of the reference that we have removed with a

second anneal).

We   interpret the   experimental data   as follows.   Let us   discuss

sample c   first: the   high initial   value   of   S   comes   from   positron

trapping   at dislocations   and other   defects,   most   probably   vacancy

clusters   of various   size produced by the motion of dislocations under

mechanical   stresses. These   point defects   disappear at   a rather   low

temperature,   causing the   small decrease   in S   occurring below 150°C.

From   this   point   to   about   400°C   positrons   are   captured   only   by

dislocations: the plateau   in the   S curve   corresponds   to   saturated

trapping   at dislocations,   which gives   less narrow annihilation lines

84

than vacancy cluster trapping. Between 400°C and 450°C dislocations disappear, leaving the positron free to annihilate from a delocalized bulk state, corresponding to the lowest S value. Dislocation removal at a temperature below 40% of the melting point in K degrees is not unusual for a pure specimen /12/.

We have now a key to interpret sample n data. The dislocation density of this sample cannot be much different than the one of sample c. However, a three-month ageing, during irradiation, at a temperature of 140°C has certainly suppressed, or at least greatly reduced, the population of point defects which gives the initial high S of sample c, and that we have seen to disappear below 150°C. Sample n thus starts below sample c. However, in the plateau the order is reversed. This could be explained by a larger fraction of positrons trapped at dislocations in sample n than in sample c. Actually, even if both samples have the same origin, the dislocation network cannot be completely identical. We do not think, however, that this explanation is correct since most probably both samples contain a dislocation density more than sufficient to give saturation, i.e. 100% positron trapping, as it normally occurs for severely deformed metals. In our opinion, the different plateau level is due to the existence of another defect species corresponding to a higher value of S than dislocations, which trap positrons in competition with dislocations. The nature of this additional defect population, introduced in the sample by radiation damage, can only be conjectured until not positively identified by electron microscopy in a sample with a sufficiently high level of radiation damage. It seems reasonable to identify these defects with microvoids which do not anneal out below 150°C like small vacancy clusters, either because they have reached the critical size of a particularly stable configuration or because they are stabilized by the presence of He. In any case, they seem to

disappear above 400°C, when a major structural rearrangement occurs with the annealing of the dislocations.

Admittedly the experimental evidence on which we base our deductions is weak, as it comes only from small differences, barely above the statistical error margin.

8. TENSILE TESTS ON ALUMINIUM PROBES

In the capsule, several tensile test specimens were irradiated in the fluence of 2.2×10^{19} n/cm^2 corresponding to about 0.04 dpa.

The chemical composition and the metallurgical state of the two extended high purity aluminium alloys are given in Table II /13/. The first alloy (Al-Mg-V) is of the non heat-treatable type and one can only change the strain hardening during fabrication. The second alloy (Al-Mg-Si) is of age-hardenable type and after the press quenched condition (T4) one could effectuate a precipitation hardening treatment, for example 8 hrs at 160°C (T6 condition).

The results of the tensile tests are given in Table III /14/. The PIE results are very different for the two alloys. The Al-Mg-V alloy has an irradiation softening behaviour; only S(u), the ultimate tensile stress, increases, which was not expected. On the contrary the Al-Mg-Si alloy shows a significant hardening behaviour. However, a more precise analysis of all experimental circumstances. gives two concurrent causes:

a) irradiation damage;

b) dispersion hardening caused by the thermal treatment during irradiation; the specimen capsule was irregularly cycled according to the beam functioning, during 4 months between 20 and 140°C (measured on the outside wall of the capsule) and so the original T4 condition changed to the T6 condition!

To separate these two causes, more experiments are necessary.

9. DATA NEEDS FOR SPALLATION SOURCES

In order to interpret radiation damage experiments in spallation sources, the main problem is the cross-section knowledge above 20 MeV up to a few hundreds of MeV, depending on the reaction. All such cross-sections available up to now are calculated. Some calculations extend up to 40 MeV, others up to 200 MeV, and thereafter are extrapolated arbitrarily. Measurements as well as calculations up to 800 MeV are difficult and costly. The calculations have to be verified by differential measurements. Integral measurements may give some confidence in calculated cross-sections but not an absolute knowledge. This applies to dosimetry reactions, total He production, dpa calculation for structural materials and to transmutation product calculations. Apart from further theoretical calculations, at least a few differential measurements and integral measurements are necessary if a consistent cross-section file for energies up to some hundreds of MeV is to be constructed. The maximum energy depends on the primary proton beam energy envisaged in eventual future spallation source projects. It may be as high as 800 MeV, or even 1 GeV.

It would be desirable to construct a unique file which would have been discussed by and agreed upon by an international group of experts and used in Europe, Japan, USA, USSR and the rest of the world interested in this field. This holds not only for dosimetry reactions and cross-sections to determine radiation damage, but also for cross-sections and other nuclear data needed for the design of spallation sources, their shielding requirements and its applications.

REFERENCES

1. Dierckx R., IAEA Advisory Group Meeting on Properties of Neutron Sources, Leningrad, June 9-13, 1986, IAEA-TECDOC-410 (1987).

2. Wechsler M.S. and Sommer W.F., J. Nucl. Mat., Vol.123, p.1078 (1984).

3. Cesana A., Dierckx R., Sangiust V. and Terrani M., "Dosimetry for a radiation damage experiment in a spallation neutron source", in ASTM-STP 1001, Reactor Dosimetry Methods, Applications and Standardization (1989).

4. Hegedus F., Green W.V., Stiller P., Green S., Hernberger V., Steefel U. and Victoria M., EIR Bericht 579 (December 1985).

5. Davidson D.R.-, Greenwood L.R., Reedy R.C. and Sommer W.F., ASTM-STP 870, p.1199-1208 (1985).

6. Davidson D.R., Greenwood R.L., Sommer W.F. and Wechsler M.S., 12th Int. Symp. on Effects of Radiation Materials, Williamsburg (USA), June 18-20, 1984 (reprint LA-UR-84-1124).

7. Peiffer F., and Michel R., KCK-N-SIG84 Cross Section File, personal communication, University of Hannover (FRG).

8. Blann M. and Bisplinghoff J., UICD-19614 (1982).

9. Farrar H., McElroy W.N. and Lippincott E.P., Nucl. Technol., 25, 305 (1975).

10. Dierckx R., Dupasquier A., Brusa R.S., Grisenti R., Jang J., Oss S. and Zecca A., "Positron annihilation study of radiation damage in nickel irradiated in a spallation neutron source", Technical Note I.87.75, JRC-Ispra (1987).

11. Mackenzie I.K., in "Positron Solid State Physics", W. Brandt and A. Dupasquier (eds.), North Holland, Amsterdam, New York, Oxford 1983, p.198.

12. Petersen K., in "Positron Solid State Physics", W. Brandt and A. Dupasquier (eds.), North Holland, Amsterdam, New York, Oxford 1983, p.298.

13. Piatti G., Fiorini P. and Schiller P., "High purity aluminium alloys for experimental fusion reactors", Nuclear Engineering and Design/Fusion, Vol.1, N°2, April 1984.

14. Boerman D.J. and Piatti G., to be submitted to J. of Nuclear Materials.

15. Gray A.L. and Date A.R., Analyst, 108, 1033 (1983).

16. Gray A.L., Spectrochimica Acta, 41B, 151 (1986).

17. Luck J.H., Spectroscopy International, 1, 38 (1989).

DOSIMETRY OF MEDIUM ENERGY PROTONS AND NEUTRONS
IN RADIATION DAMAGE SIMULATION EXPERIMENTS
(Summary)

F. HEGEDÜS, S. GREEN, W.V. GREEN, M. VICTORIA
Paul Scherrer Institute,
Villigen, Switzerland

1. Introduction

In 1978 a program was started at the former Swiss Federal Institute for Reactor Research to study first wall material damage of fusion reactors. The program is focused on the "Proton Irradiation Experiment" (PIREX), however other studies, e.g. the usefulness of spallation sources for material damage simulation have also been performed.

The dosimetry associated to this program will be shortly described.

2. PIREX II

Thin (0.1 mm) material samples are irradiated with 590 MeV protons. The temperature of the sample is controlled. On the irradiated area, 30-50 mm^2, the typical current density is 0.4 mA/cm^2.

The planar dose distribution is determined by measuring an activity map of a strong gamma line of a long lived radioisotope (e.g. ^{22}Na in Al). This measurement is done by moving the sample in front of a lead collimator. On the rear side of the collimator there is a Ge gamma counter.

The helium concentration is measured by vacuum extraction inside a calibrated mass spectrograph.

The solid transmutational products are determined by two methods. One is by calculating the individual isotope yields by using the HETC code. The yield of some isotopes is measurable by gamma counting and the reliability of the calculated yields can be checked. Another method to measure the solid transmutational products is the mass spectrometry which has not provided up to now satisfactory and reproducible results.

In the near future a new method, the "Totally Reflected X-Ray Fluorescence" (TXRF), will be tested using a monoenergetic synchrotron radiation source. This method is well suited to measure the chemical yield of the solid transmutational products:

- By setting the primer X-ray energy just below the K shell binding energy of the target atom, the dominating effect of the target atom is eliminated.

- The sensitivity is 1-2 ppm, which is less than the 10-100 ppm yield of the transmutational products typically accumulated in the irradiated samples.

The principle of the TXRF method and the description of our spectrometer is given in Ref. 1 and 2.

3. **The Strength of the Spallation Neutron Flux of SINQ for Radiation Damage Fusion Technology**

The SINQ spallation neutron source was simulated and its source strength measured in terms of the radiation damage parameters:

Total flux of spallation neutrons with energy E > 1.0 MeV; spectral energy distribution; helium and displacement damage production rates; and their ratio. This simulation used the proton beam of the TRIUMF accelerator in Canada, and its molten lead beam stop as the source of spallation neutrons. The helium production per proton of beam was measured for several materials by vacuum extraction in a calibrated mass spectrograph; the spectrum, flux intensity, and the displacement radiation damage parameter were measured by multiple foil activation flux-unfolding combined with radiation damage calculations.

The helium to dpa ratio matches the fusion reactor first wall case; but the helium production in iron per mA*year at a radial distance of 15 cm is estimated to be 6 appm compared to 310 appm at the end of life in the first wall of NET.

Detailed description of this experiment is given in Ref. 3.

REFERENCES

1. H. Aiginger and P. Wobrauschek: Total Reflectance X Ray Spectrometry Advances in X-Ray Analysis, Vol. 30 (85-88)

2. F. Hegedüs et al., TXRF Spectrometer for Trace Element Detection Advances in X-Ray Analysis, Vol. 33 (to be published)

3. F. Hegedüs et al., J. Nucl. Mater. 141-143 (1986) 911

EVALUATION OF RADIATION EFFECTS
IN AMORPHOUS (-SOLID) MATTER

W. MATTHES
Joint Research Centre,
Commission of the European Communities,
Ispra Establishment,
Ispra

Abstract

A theoretical model of evaluation of radiation effects in solid matter is presented. At low radiation exposures changes in the atomic densities of the atoms in the media can be neglected and the equations become linear and are solved analytically. As an example damage production rates in ^{56}Fe were calculated in the energy range 7.0 to 40 MeV.

A) General Theoretical Model

The theoretical evaluation of radiation effects is based on the following model.

We consider different types of particles <u>moving</u> in the solid matrix and characterized by their corresponding fluxes $\phi_j(xvt)$ [$1/cm^2sec$], e.g.: neutrons, gammas, carbon atoms, oxygen atoms....etc. and different types of <u>stationary</u> atoms characterized by their corresponding atomic densities $N_\mu(xt)$ [$1/cm^3$], e.g.: iron-atoms, argon-atoms....etc.
We make the assumption, that moving particles collide only with stationary atoms and put the physics of the problem into the parameter.

$\sigma_{j\mu}(v/R)$ vhich is the microscopic cross-section for the reaction-event R in a collision between a moving particle of type j and velocity v (Lab.System) and a stationary atom of type μ .

The standard particle balance-argumentation then leads to the following coupled set of non-linear equations for the fluxes and the densities:

$$\frac{1}{v}\frac{\partial \phi_i}{\partial t} + \mu\frac{\partial \phi_i}{\partial x} + \phi_i \sum_\lambda N_\lambda \sigma_{i\lambda}(v/T) = Q_i + \sum_{j\lambda}\int dv' \phi_j(v')N_\lambda \sigma_{j\lambda}(v'/iv) + \frac{\partial}{\partial v}(S\cdot\phi_i) \quad (1)$$

$$\frac{\partial N_{\mu}}{\partial t} = \sum_{\lambda} P_{\mu\lambda} N_{\lambda} - D_{\mu} N_{\mu} \tag{2}$$

The quantities introduced in these equations in more detail are:

$\sigma_{j\mu}(v/T)$ total microscopic cross-section for a collision between a moving particle of type j with velocity v and a stationary atom of type μ.

$\sigma_{j\mu}(v'/iv)$ microscopic cross-section for a collision between {j,v'} and μ leading to a particle of type i leaving the collision with velocity v.

$$P_{\mu\lambda} = \sum_{j} \int dv' \phi_{j}(v') \sigma_{j\lambda}(v'/\overline{\mu})$$

$$D_{\mu} = \sum_{j} \int dv' \phi_{j}(v') \sigma_{j\lambda}(v'/\mu)$$

$\sigma_{j\lambda}(v/\mu)$ microscopic cross section for a collision between {j,v} and λ leaving <u>one</u> μ atom at the collision point

$\sigma_{j\lambda}(v/\overline{\mu})$ microscopic cross-section for a collision between {j,v} and λ leaving <u>no</u> μ atom at the collision point.

Interesting physical quantities (e.g. vacancy - interstitial - heat - ionization etc. production for radiation damage evaluations) may then be calculated by expression like:

$$D = \sum_{j} \int \phi_{j} R_{j} \, dx dv dt \tag{3}$$

where the function $R_{j}(xvt)$ has to be chosen according to the damage type of interest.

A fully numerical procedure for solving the coupled set of equations (1) and (2), based on the Monte Carlo methods, is realized for example in the code TRIDYN written by W.Möller et al.[1].

94

B) Linearized Model

Under low irradiations we may neglect the change in the atomic
densities of the stationary atoms and need only to solve the
linear (Boltzmann-) equations for the fluxes of the moving
particles. In this (linearized!) case the definition of an
"adjoint Boltzmann equation" makes sense and we may put the
quantities D in the form:

$$D = \sum_j \int Q_j \; D_j \; dxdvdt \tag{4}$$

where

$D_j(xvt)$ is obviously the total effect produced by one
source particle of type j injected into the system
at x and at time t with velocity v.

This function D_j may be obtained directly as the solution of the
adjoint (or backward-) transport equation.

$$-\frac{1}{v}\frac{\partial D_j}{\partial t} - \mu\frac{\partial D_j}{\partial x} + \int \frac{\partial D_j}{\partial v} + D_j \sum_\lambda N \, \sigma_{j\lambda}(v/r) = H_j + \sum_\lambda N \int \sigma_{j\tau}(v/R) D(R) \, dR \tag{5}$$

where the source H_j has to be constructed individually for each
damage type under investigation.

The symbol R for the reaction-event indicates in this case the
set $\{i_1 1v_1, \; i_2 v_2, \ldots i_M v_M\}$ of particles of types $\{i_1 i_2 \ldots i_M\}$
produced in the collision (between the incoming particle $\{jv\}$
and λ) and leaving the collision point with their corresponding
velocities $\{v_1 v_2 \ldots v_m\}$.

$$D(R) = \sum_m{}' \alpha_m \; D_{im} \; (x \; v_m \; t)$$

characterizes the total radiation effect (e.g. damage) due to the
particles $\{i_1 i_2 \ldots i_M\}$ (generated in a collision and) injected
into the system at the (collision-) point x at time t.

The quantities α_m are defined by

$$\alpha_m = \begin{cases} 0 & \text{if the particle } i_m \text{ does not leave the collision point} \\ 1 & \text{if the particle } i_m \text{ leaves the collision point} \end{cases}$$

95

Their choice depends on the detailed collision (or damage-) model.

The integration $\int dR$ indicates an integration over all the velocities $\{v_1 v_2 \ldots v_M\}$ and a summation over all possible reaction events R.

We simplify the adjoint equation (5) further by

a) neglecting space and time dependence, and
b) allowing for two particles only to leave a collision.

The adjoint equation becomes (we may use the energy variable T):

$$ S \cdot \frac{\partial D_j}{\partial \tau} + D_j \sum_\lambda N_\lambda \, \sigma_{j\lambda}(\tau) = H_j + \sum_\lambda N_\lambda \int \sigma_{j\lambda}(\tau/R)\, D(R)\, dR \qquad (6) $$

where the R-integral is now explicitly:

$$ \sum_{k\ell} \int dT_k \, dT_\ell \; \sigma_{j\lambda}(\tau/T_k T_\ell) \left\{ \alpha_k D_k(T_k) + \alpha_\ell D_\ell(T_\ell) \right\} $$

The production <u>rate</u> per cm^3 for the quantity D (eq.4) is then given by

$$ D = \sum_j \int Q_j(T) D_j(T)\, dT \qquad (7) $$

where

$Q_j(T)dT$ is the (mean) number of j type particles produced (by an external source) per cm^3 per sec and

$D_j(T)$ is the total effect produced by a particle of type j injected into the system with energy T.

Further comments on the linearized Forward - and Backward Boltzmann-equations in the context of radiation damage, dealing also with analytical solutions, may be found in the article written by M.M.R.Williams [2].

C) Radiation Damage Cross-Section

As an example we apply equations (6) and (7) for the damage production rate (vacancy production) in iron ^{56}Fe (in a

stationary neutron field $\phi(E)$) in the energy range from 7.0 to 40.0 MeV. The external source of ions of different types j (production rate Q_j of moving particles) is given by

$$Q_j(T) = \int dE\ \phi(E)\ \Sigma_j(T/E) \tag{8}$$

where

$\Sigma_j(T/E)$ is the macroscopic cross-section (for neutrons of energy E) for the production of j-type atoms with recoil energy T.

The damage production rate (7) becomes:

$$D = \int \phi(E)\ \Sigma_D(E)\ dE \tag{9}$$

where we have introduced

$$\Sigma_D(E) = \int dT\ \Sigma_j(T/E)\ D_j(T) \tag{10}$$

as the macroscopic "radiation damage cross-section".

Eventually we arrive at a number of steps for the "EVALUATION OF RADIATION DAMAGE CROSS-SECTIONS FOR (HOMOGENEOUS) AMORPHOUS STRUCTURE MATERIALS".

PEOBLEM:

The damage produced in a neutron field may be calculated by:

$$D(\phi) = \int \phi(E)\ \Sigma_D(E)dE \tag{11}$$

We construct a method for a fast calculation of the radiation damage cross-section $\Sigma_D(E)$ and evaluate $\Sigma_D(E)$ for vacancy production in IRON.

THE RADIATION DAMAGE CROSS SECTION $\Sigma_D(E)$

is decomposed in the following form:

$$\Sigma_D(E) = \int dT \underset{\substack{\text{nuclear} \\ \text{model}}}{\Sigma_j(T/E)} \cdot \underset{\substack{\text{Damage} \\ \text{model}}}{D_j(T)} \tag{12}$$

where

$\Sigma_j(T/E)$ is the production cross-section for reaction
products of type j with recoil energy T, and

$D_j(T)$ is the damage produced by a projectile j
injected with energy T into the medium.

The summation over j goes over all reaction products.

The "RECOIL PRODUCTION CROSS SECTION $\Sigma_j(T/E)$"

may be split in the form:

$$\Sigma_j(T/E) = \sum_{\mu} N_\mu \cdot \sigma_{o\mu}(E) \cdot y_{i\mu}(E) \cdot f_{i\mu}(T/E)$$

where

N_μ number of atoms of type μ per cm^3

$\sigma_{o\mu}(E)$ (neutron) non-elastic differential cross section for
nuclei of type μ

$y_{i\mu}(E)$ yield of i-type residual (or transmutation) nuclei in a
neutron reaction with a nucleus of type μ

$f_{i\mu}(T/E)$ normalized recoil spectrum of the i-type nuclei produced
in a (neutron-) reaction with a μ-type nucleus.

The possible recoil nuclei produced in neutron reactions with Fe-
nuclei in the considered energy range (7.0-40.0 MeV) are given in
Table 1. Fig. 1 and 2 give some examples of the differential-
production cross-sections of residual nuclei and their recoil
spectra.

Table 1:Light particles emitted and residual nuclei produced
in reactions between neutrons (in the energy range
7.0 [MeV] to 40.0 [MeV] and ^{56}Fe as target nuclei

TARGET NUCLEI ^{56}Fe

Emitted Particles γ, n, p, α

Residual Nuclei:

^{48}Ti	^{51}V	^{50}Cr	^{53}Mn	^{53}Fe
^{49}Ti	^{52}V	^{51}Cr	^{54}Mn	^{54}Fe
		^{52}Cr	^{55}Mn	^{55}Fe
		^{53}Cr	^{56}Mn	^{56}Fe
		^{54}Cr		^{57}Fe
		^{55}Cr		
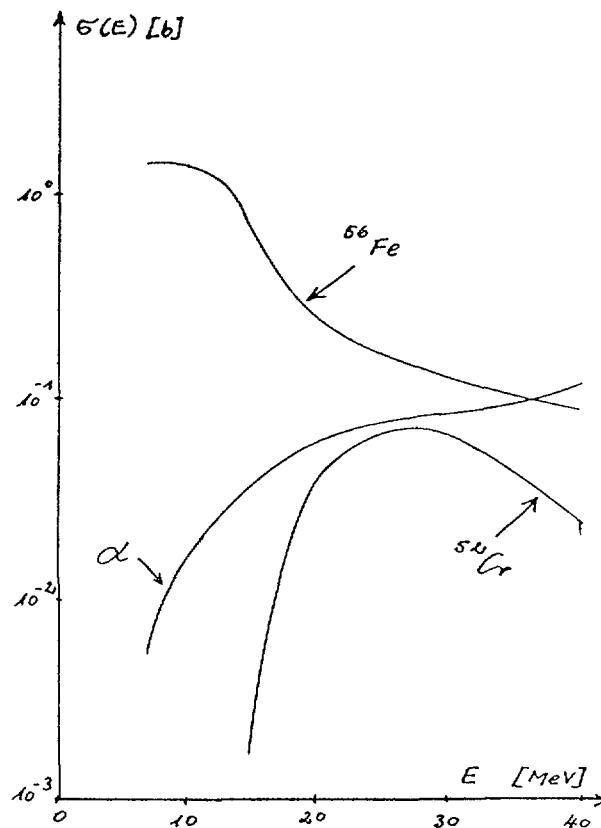
FIG. 1. Differential production cross-sections for some reaction products
(^{56}Fe, ^{52}Cr and He) in neutron reactions with iron. (For ^{56}Fe only the
inelastic production cross-section is given).

$f(T/E)$

$E = 3.2 [MeV]$

$E = 20.0 [MeV]$

$T [MeV]$
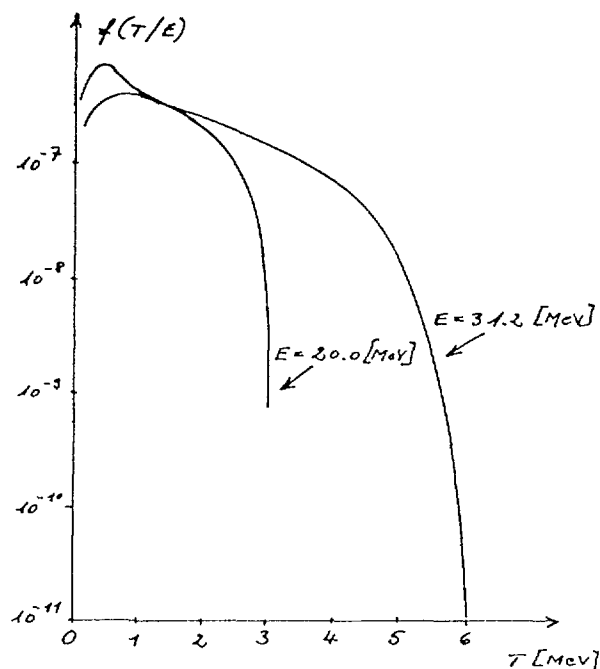
FIG. 2. Examples of (normalized) recoil spectra for the reaction product ^{49}Ti for two (neutron-) input energies.

THE DAMAGE FUNCTIONS D(T)

were found by numerically solving the integro-differential equation for D(T) which has the general structure

$$D(T) + A(T)\frac{\partial D}{\partial T} = Q(T) + \int B(T,T')\phi(T')dT' \qquad (13)$$

where

A(T)   is a function of the electronic stopping power and the total cross-section for ion transport in the medium

Q(T)   is a source term depending on the damage type considered

B(T;T') is essentially the scattering kernel for atom-atom scattering

ϕ(T')   is a linear combination of D(T') and D(T-T').

Fig. 3   shows examples of damage functions where we take $D_j(T)$

to be the number of vacancies produced (by different

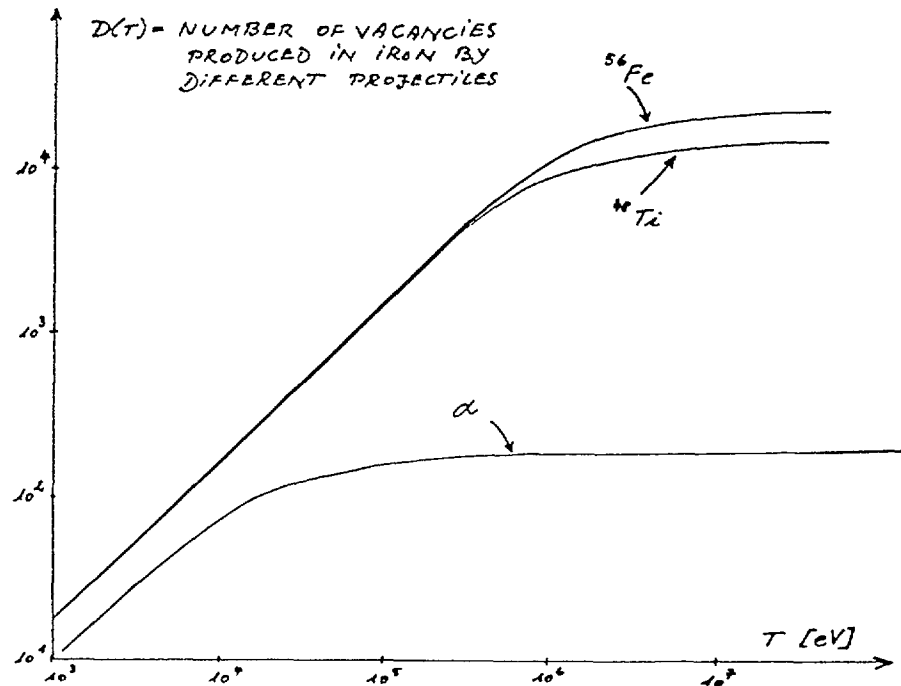projectiles j then injected with energy T into the

medium).

FIG. 3. Damage functions D(T) giving the number of vacancies produced by
different projectiles (^{56}Fe, ^{48}Ti, α) when injected with energy T into iron.

MACROSCOPIC DAMAGE CROSS SECTION

Combining now

- the recoil production cross-sections $\Sigma_j(T/E)$ as evaluated by
nuclear model codes and

- the damage functions $D_j(T)$ as evaluated by damage model codes

according to prescription (12), we obtain, see Fig. 4, the

macroscopic damage cross section for vacancy production for iron.
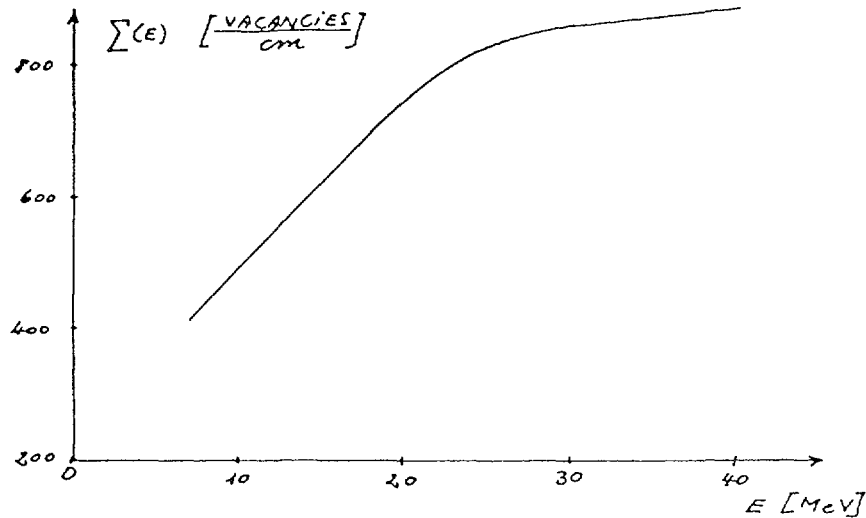
FIG. 4. Macroscopic damage cross-section for vacancy production in iron.

Details on the numerical solution of the integro differential equation (13) are described by W.Matthes [3]. The production cross sections for the residual nuclei and their recoil spectra were evaluated by M.Uhl [4] from the Institut für Radiumforschung at the University of Vienna with the nuclear model code MAURINA.

For the evaluation of the electronic stopping power $S_i(E)$ and the atom-atom reaction cross-sections $\sigma_{j\mu}(v/R)$ we used the subroutines developed by BIERSACK [5] on this purpose in his TRIM - Monte Carlo Programme.

REFERENCES

[1] Möller, W.,TRIDYN - Binary Collision Simulation of atomic Collisions and Dynamic Composition Changes in Solids. Computer Physics Communications 51 (1988) . 355-368

[2] WILLIAMS, M.M.R., The Role of the Boltzmann Transport Equation in Radiation Damage Calculations. Progress in Nuclear Energy, Vol.2 (1979) 1-65

[3] MATTHES, W., Evaluation of Global Radiation Damage Data for (homogeneous) amorphous Structure Materials. Am. Nucl. Energy, Vol. 14 (1987) 257-262

[4] UHL, M., Final Report on Contract No. 2795-85-10 EDISPA Dec.(1986) between the European Community (EURATOM) and the Institute für Radiumforschung und Kernphysik at the University of Vienna. Private Communication

[5] BIERSACK, J.P. and L.G.HAGGMARK, Nucl. Instrum. Methods. Vol. 174 (1980) 257

102

RADIATION DAMAGE CALCULATIONS
FOR COMPOUND MATERIALS

L.R. GREENWOOD
Argonne National Laboratory,
Argonne, Illinois,
United States of America

Abstract

Displacement damage calculations can be performed for 40 elements in the energy range up to 20 MeV with the SPECTER computer code. A recent addition to the code, called SPECOMP, can intermix atomic recoil energy distributions for any four elements to calculate the proper displacement damage for compound materials. The calculations take advantage of the atomic recoil data in the SPECTER libraries, which were determined by the DISCS computer code, using evaluated neutron cross section and angular distribution data in ENDF/B-V. Resultant damage cross sections for any compound can be added to the SPECTER libraries for the routine calculation of displacements in any given neutron field. Users do not require access to neutron cross section files. Results are presented for a variety of fusion materials and a new ceramic superconductor material. Future plans and nuclear data needs are discussed.

Introduction

Fundamental radiation damage calculations involve the determination of atomic recoil distributions induced by neutron irradiations. These primary knock-out (pka) energy distributions depend on the neutron cross sections and angular distributions as a function of neutron energy. We perform such calculations using the DISCS[1] computer code and using evaluated neutron data from the ENDF/B-V file.[2] DISCS results for yttrium are shown in figure 1, where the relative contributions from each reaction channel are displayed. The further calculation of total atomic displacements requires a model for the partition of recoil atom energy into nuclear and electronic energy loss events and a model for the production of secondary displacements caused by nuclear collisions and reactions. We have assumed the Lindhard[3] model, with modifications suggested by Robinson.[4] The DISCS code calculates the recoil atom energy distributions for each nuclear reaction given in ENDF. Angular distribution data is always given explicitly for elastic scattering and an evaporation model is assumed for other reactions, except for the (n,xn) reactions where a Monte Carlo calculation is needed to determine the proper recoil distributions. For charged particle emission, the evaporation model is centered on the coulomb barrier. Displacements are also included for (n,γ) reactions and for beta decay. It should be noted that our calculations of the displacements per atom (dpa) only describe the fundamental nuclear interactions and hence are useful as an exposure index which is independent of the neutron spectrum. However, dpa may not be necessarily related to materials property changes since many of the displacements may recombine with holes in the lattice and additional molecular dynamic calculations are needed to determine stable defects.

The calculated displacement damage cross sections and recoil energy atom distributions are stored in master libraries. The SPECTER computer code[5] is then used to calculate displacements and recoil distributions for any given neutron spectra. SPECTER also contains libraries for gas production[6] and
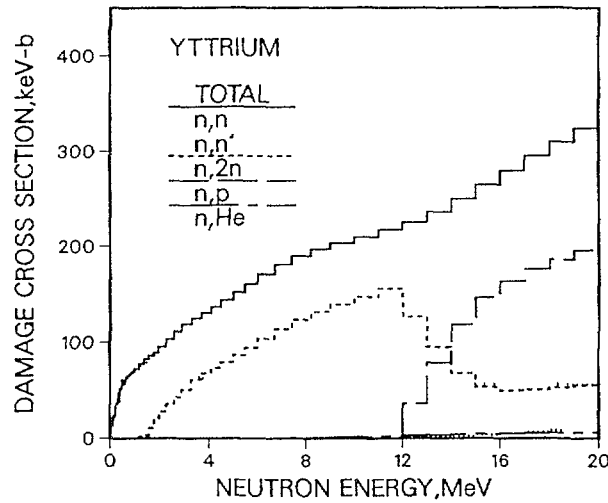
FIGURE 1

Illustration of DISCS displacement damage calculation for yttrium
where the contribution from each major reaction is shown separately.

total energy deposition. Hence, users will obtain a comprehensive set of
damage parameters for 40 different elements for any specified neutron
irradiation and they only need to specify the neutron spectra and length of
irradiation.

SPECOMP Calculations

The calculations from SPECTER only consider pure elements. In order to
calculate displacements from compound materials, the procedures must be
modified to include all combinations of recoiling atoms and matrix atoms. For
example, if we consider Li_2O, then we must calculate the probabilities that Li
atoms will displace O atoms as well as Li atoms and that O atoms will displace
both Li and O atoms. The relative contribution from each of these
combinations is shown in figure 2. These probabilities are determined by the
Lindhard equations[3] which are usually only seen in the reduced self-ion form.
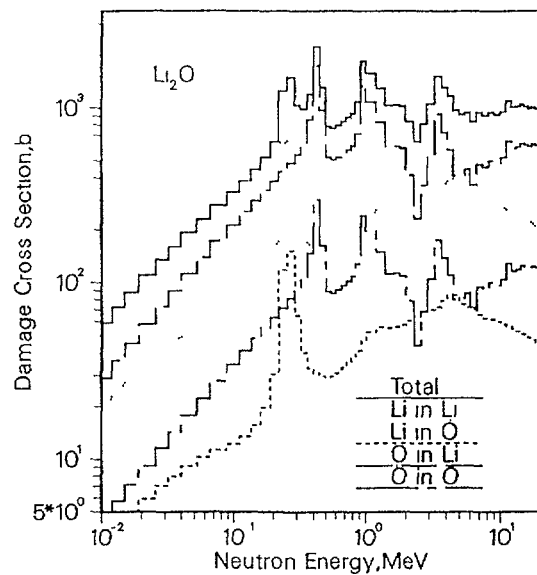These effects have been discussed by Parkin and Coulter.[7]

FIGURE 2

Displacement damage cross sections from SPECOMP are shown for Li_2O.
Each combination of recoiling atom and matrix atom is shown separately.

104

When considering damage in compounds, it is important to consider the possible atomic distribution of elements. In a true chemical compound, the probability that a recoiling atom will interact with a given species simply depends on the atomic abundance and this is the approximation which we have assumed in SPECOMP. However, if an alloy contains clumps or segregation of elements, then the present calculations are not necessarily appropriate and it might be better to sum the damage for the individual elements or to look at local damage by region in the material.

Secondary displacements are taken to be zero if the recoil energy is below a threshold energy, one from threshold up to twice that energy, and equal to the damage energy divided by twice the threshold at higher energies. For self-ion damage, appropriate threshold energies are recommended by the ASTM.[8] Unfortunately, there is no such agreement as to suitable values for the threshold energies for compound materials. This presents us with a serious problem since SPECOMP calculations are found to be very sensitive to our choice of threshold energies. When considering self-ion damage, the threshold can be changed after the calculations by simply renormalizing the results. This is not the case in compound calculations and it becomes meaningless to report damage energy cross sections in units such as keV-barns. Thus, a new calculation must be performed for each choice of threshold energy. The threshold for a given element will also differ according to the compound since the value really depends on the interatomic potentials for a given chemical species.

SPECOMP calculations can be performed rather quickly since they take advantage of the recoil atom energy distributions stored in the SPECTER libraries. These pka distributions only depend on the interaction of neutrons with a given element and hence do not have to be recalculated for different compounds. The pka data are stored in a 100 group energy structure at each of 100 incident neutron energies. Hence, there are 10,000 entries for each element. The SPECOMP code integrates over the allowable range of recoil energies at each of the 100 neutron energies for each combination of recoil and matrix atom. The results are then normalized by atomic abundances in each compound and summed to produce a singe displacement cross section value at each neutron energy.

Results

Displacement cross sections calculated with SPECOMP are usually added to a library in SPECTER for routine use, as described previously. SPECOMP also lists secondary displacement calculations and separate displacement cross sections for each element in the compound. This may be important to the user since the net dpa cross section conveys no information regarding the type of atoms which are being displaced. SPECOMP does not need to list pka recoil energy spectra since this information is already available for each element in SPECTER.

SPECOMP calculations have been completed for fusion breeder materials, such as Li_2O and $LiAlO_2$; insulators, such as Al_2O_3, SiO_2, and TaO; engineering alloys, such as 316 stainless steel, $NbTi$, and $V-15Cr-5Ti$; research materials, such as Cu_3Au; and the new ceramic superconductor $Y_1Ba_2Cu_3O_7$. In lieu of accurate knowledge of appropriate threshold values, we simply used the same thresholds for the compounds as we normally use for the pure elements. This has the advantage of facilitating comparisons with previous approximations of damage in compounds which simply sum elemental dpa values weighted by atomic abundances. Calculations for several compounds are listed in Table I and compared with elemental calculations in figures 3-5.

Table I: DPA Ratio (SPECOMP/SPECTER)

Compound	Fission[a]	14 MeV	STARFIRE[b]	HFIR[c]	FFTF[d]
Li_2O	1.43	1.43	1.31	1.04	1.47
$LiAlO_2$	1.26	1.23	1.25	1.07	1.28
Al_2O_3	0.99	0.98	0.99	1.00	1.00
SiO_2	0.99	0.96	0.99	1.00	1.00
V-15Cr-5Ti	1.00	1.00	1.00	1.00	1.00
316 SS	1.00	1.00	1.00	1.00	1.00
Cu_3Au	0.98	0.98	0.98	0.99	0.99
Nb-Ti	0.99	1.00	0.99	0.99	0.99
TaO	0.89	1.16	0.96	0.86	0 80

[a] ^{235}U fission spectrum
[b] STARFIRE, first wall spectrum (Ref. 9)
[c] High Flux Isotopes Reactor, PTP, midplane (Ref. 10)
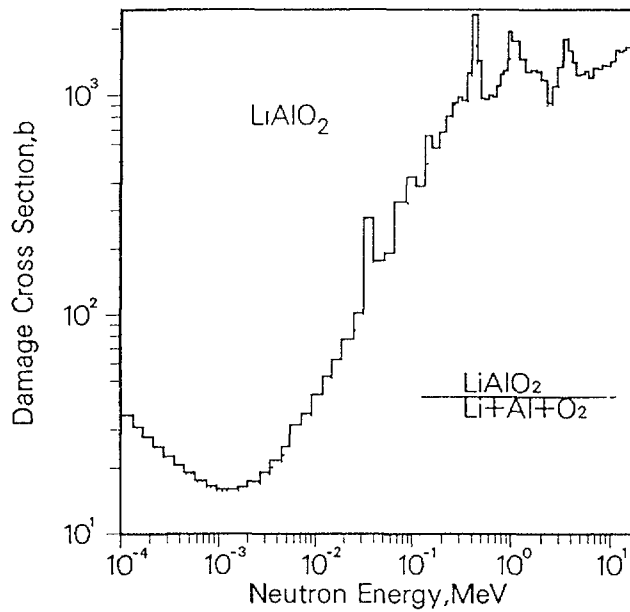[d] Fast Flux Test Facility, mota, midplane (Ref. 11)

FIGURE 3

Comparison of dpa cross sections for $LiAlO_2$ calculated by SPECOMP (solid line) with a weighted sum of elemental damage (dotted line).
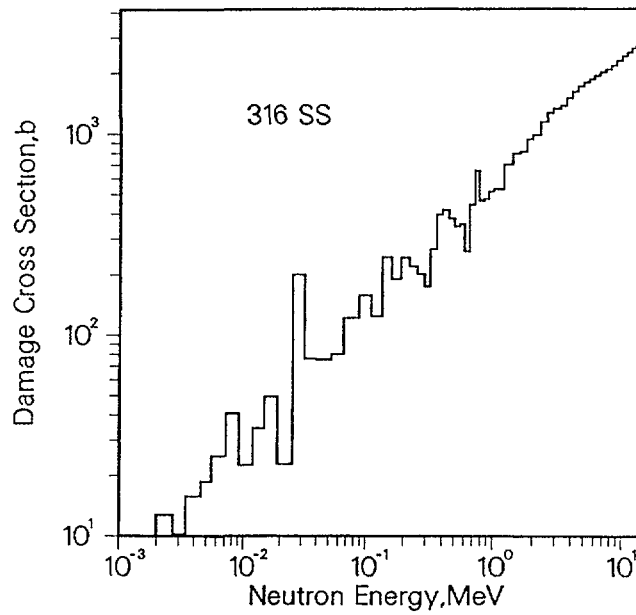
FIGURE 4

Calculated damage cross sections for 316 stainless steel. In this case there is no difference with the weighted sum of elemental damage.
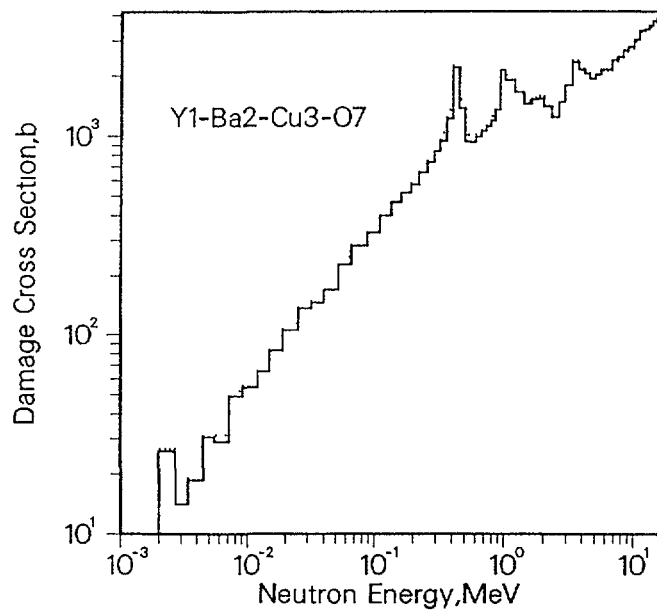

FIGURE 5

Calculated damage cross sections for the new ceramic superconductor Y1-Ba2-Cu3-O7. SPECOMP results (solid line) are compared with the weighted sum of elemental damage (dotted line).

As can be seen in Table I and figures 3-5, there may be sizable differences (eg - LiO2, LiAlO2, and TaO) between the SPECOMP calculations and damage calculated from a weighted elemental sum. This is shown more clearly in figure 6 which displays the ratio of the damage calculated with SPECOMP divided by a weighted sum of elemental damage. In some cases, such as stainless steel and the vanadium alloy, the results of both calculations are nearly identical. Three factors appear to be important in determining whether or not SPECOMP results differ substantially from elemental sums, namely, differences in atomic mass, differences in threshold energies, and differences in cross sections. These effects can be seen in figure 2 which shows that more displacements result when Li is the secondary atom rather than O; O displaces more Li atoms than when Li displaces O atoms; and the effect of the 250 keV resonance in the ^6Li cross section is clearly seen. As a general rule, SPECOMP calculations show increasingly larger effects as differences in mass, threshold energy, and cross sections increase between the elements in the compound.
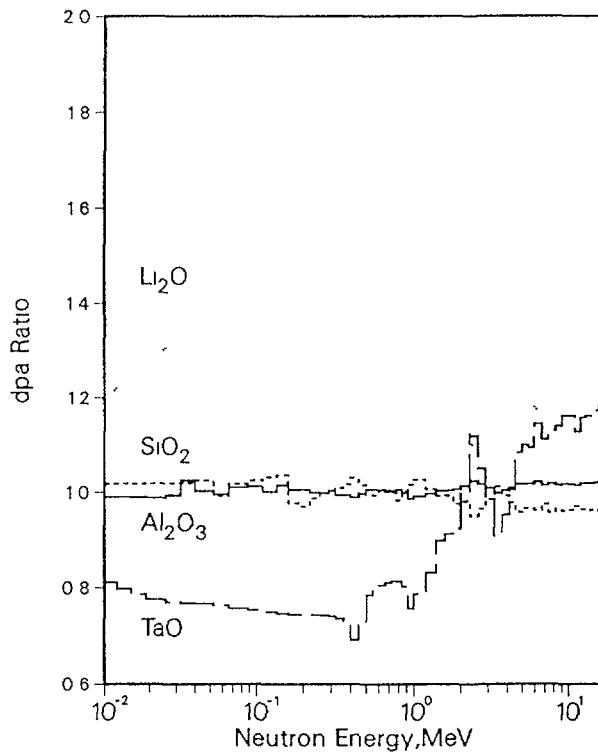

FIGURE 6

Ratios of damage calculated with SPECOMP divided by the weighted sum of elemental damage are shown for various compounds.

Future Work

SPECOMP is available to SPECTER users and can be easily added to the computer code package. Calculations can be run for any combinations of four elements from the 40 elements now contained in SPECTER. Compounds with more than four elements would require expansion of the matrices in SPECOMP. Calculations with other elements require DISCS calculations and additions to the SPECTER libraries prior to running SPECOMP.

Calculations are now being run for a variety of compounds and recommended dpa cross sections will be added to SPECTER. In this case, users need not run SPECOMP directly unless they wish to change the threshold energies. Of

course, the largest uncertainties in such calculations remain the assignment of appropriate threshold energies and further work is needed in this area.

Evaluated nuclear data is now becoming available for ENDF/B-VI. Data formats will be different from ENDF/B-V and recoil atom energy distributions may be given explicitly. Consequently, existing damage codes must be revised to accept the new data prior to recalculating with version VI. There is also a need to extend the calculations to additional elements and to higher neutron energies, especially for accelerator-based neutron sources.

REFERENCES

1. G.R. Odette and D.R. Dorian, Nucl. Technol. 29 (1976) 346.

2. Evaluated Neutron Data File, Version V, Part B, National Neutron Cross Section Center, Brookhaven National Laboratory (1979).

3. J. Lindhard, V. Nielsen, M. Scharff, and P.V. Thomsen, Mat. Phys. Medd. Dar. V. D. Selk., 22 (1963) 10.

4. M. Robinson, AEC Symp. Ser. 26 (1971) 397.

5. L.R. Greenwood and R.K. Smither, ANL/FPP/TM-197 (1985).

6. ENDF/B-V Gas Production File 533, National Neutron Cross Section Center, Brookhaven National Laboratory (1979).

7. D.M. Parkin and C.A. Coulter, J. Nucl. Mater. 103 (1981) 1315.

8. Standard Practice for Neutron Radiation Damage Simulation by Charged Particle Irradiation, E521-83, Annual Book of ASTM Standards (1988)168.

9. STARFIRE Commercial Tokamak Fusion Power Plant Study,ANL/FPP-80-1 (1980).

10. L.R. Greenwood, Damage Analysis and Fundamental Studies Quarterly Progress Report, DOE/ER-0046/13 (1983) 13.

11. R.L. Simons, Damage Analysis and Fundamental Studies Quarterly Progress Report, DOE/ER-0046/21 (1985) 10.

THE EFFECT OF NUCLEAR TRANSMUTATIONS UNDER NEUTRON IRRADIATION ON MECHANICAL PROPERTIES OF REACTOR STRUCTURAL MATERIALS

A.I. RYAZANOV, V.A. BORODIN, V.M. MANICHEV
I.V. Kurchatov Institute of Atomic Energy,
Moscow,
Union of Soviet Socialist Republics

Abstract

The paper presents a short review of the principal nuclear transmutations in irradiated reactor structural materials and the effect of transmutant accumulation on irradiation stability of these materials, in particular, on swelling, irradiation creep, and high temperature embrittlement.

1. INTRODUCTION

The service of structural materials in fission and fusion reactors is characterized by the irradiation of these materials with intensive neutron fluxes in the wide energy range (up to several MeV). Nuclear reactions of neutrons with the constituent elements of irradiated materials result in compositional modification of material and can influence its irradiation stability, in particular - such effects as swelling, irradiation creep and high-temperature irradiation embrittlement [1]. Here we present a short review of the modern knowledge concerning the effect of nuclear transmutations under neutron irradiation on irradiation effects in fusion and fission reactor structural materials.

2. NUCLEAR TRANSMUTATIONS IN IRRADIATED STRUCTURAL MATERIALS

Let us suppose that an alloy consists of N elements with the corresponding atomic concentrations C_n^i ($1 \leq n \leq N$; $1 \leq i \leq i_n$, where i denotes the isotope and i_n is determined by the total number of isotopes of the n-th element). The variation of the element concentrations with the neutron exposure Φ can be described with the set of linear first-order differential equations:

$$\frac{dC_n^i}{d\Phi} = \sum_{k=1}^{N} \sum_{j=1}^{i_k}{}' A_{nk}^{ij} C_k^j - (\sum_{k=1}^{N} \sum_{j=1}^{i_k}{}' A_{kn}^{ji}) C_n^i \qquad (2.1)$$

where the primed summation sign denotes the summation without the term for which $k = n$ and $j = i$. A_{nk}^{ij} is the reactor spectrum ($\Psi(E)$) averaged cross-section of nuclear transmutation of the k-th element into the n-th one with the corresponding isotope numbers

$$A_{nk}^{ij} = \int_{E_{min}}^{E_{max}} \sigma_{nk}^{ij}(E)\Psi(E)dE ,\qquad (2.2)$$

where $\sigma_{nk}^{ij}(E)$ is the corresponding energy-dependent cross-section, E_{max} are E_{min} are the upper and the lower edges of the reactor energy spectrum. Thus, the effective transmutation cross-sections depend on both the neutron cross-sections and the spectrum of each particular reactor.

Fig. 1 demonstrates typical neutron spectra for fast reactors (EBR-II), mixed-spectrum reactors (HFIR), and for a conceptual TOKAMAK fusion reactor (CCTR)[2]. It is seen that the spectra differ considerably, although all of them have a part of neutrons with high energy (up to 5+8 MeV in fission reactor and a spike at ~14 MeV in fusion reactors), which is over the threshold for many nuclear reactions. Also, thermal neutrons effectively produced in mixed-spectrum reactors can interact with some important constituents of stainless steels, in particular with nickel and boron.
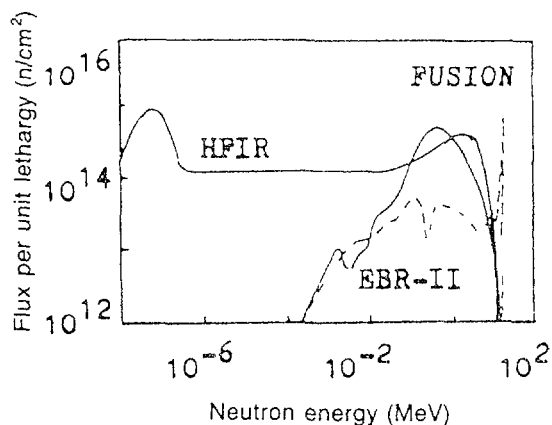

Fig. 1. Typical spectra for different reactors: fast reactor (EBR-II), mixed-spectrum reactor (HFIR), and conceptual TOKAMAK-type reactor (CCTR). After [2].

Solution of the set (1.1) is straightforward, though for practical manycomponent materials (structural steels) it can be somewhat cumbersome and so numerical calculations are necessary. At present there exist special computer codes to facilitate such calculations and a typical result can be found in Fig. 2 (owned from [3]).
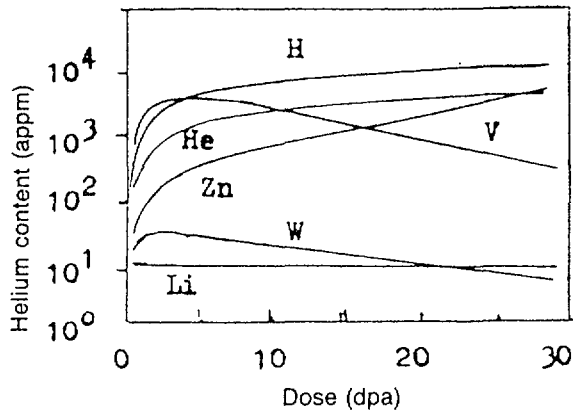
112

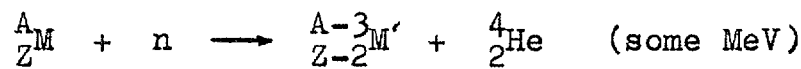Fig. 2. Build up of nuclear product concentrations in AISI 316 stainless steel irradiated in HFIR. After [3].

As far as the modification of mechanical properties of irradiated materials is concerned, the most important reactions are thought to be (n,α) - reactions that lead to accumulation of helium and the reactions resulting in the build up or burn out of some principal and impurity components of structural alloys, such as Fe, Ni, Cr, Mn, V, B, etc.
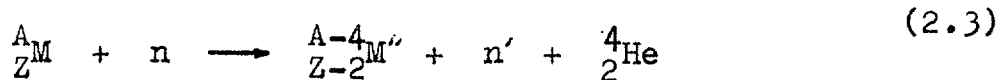
2.1. (n,α)-reactions

The main types of He producing reactions may be summarized as follows [4]:

a. Reactions with fast neutrons $(E_n \gtrsim 0.1$ MeV$)$

Fast neutrons interact with metal atoms according to such reactions as

$$^A_Z M + n \longrightarrow ^{A-3}_{Z-2}M' + ^4_2He \quad (\text{some MeV})$$

and

$$^A_Z M + n \longrightarrow ^{A-4}_{Z-2}M'' + n' + ^4_2He \quad (2.3)$$

Some charactristic (n,α) cross sections are presented in Fig. 3.
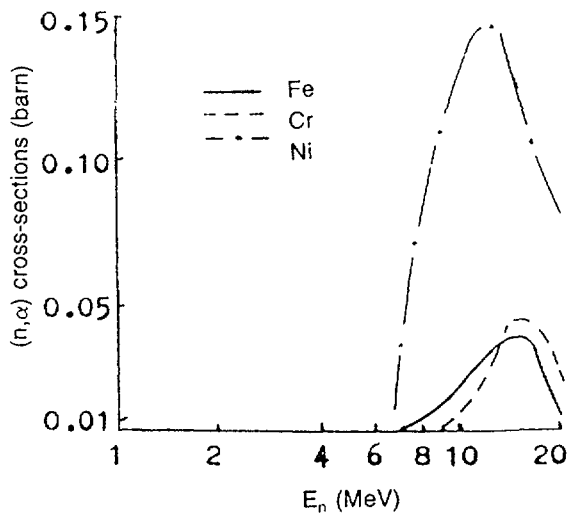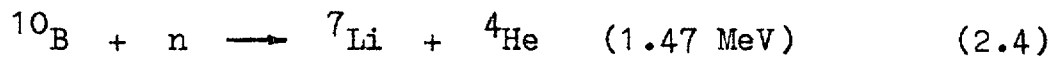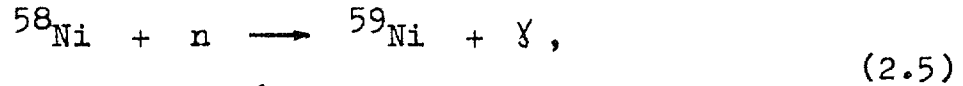

Fig. 3. Cross sections fo (n,α) reactions with prin cipal components of struc tural stainless steels. After [2].

113

b. Reactions with thermal neutrons ($E_n \le 0.025$ MeV)

The most important reactions in this energy range are the reaction with boron ($\mathfrak{G}_{2200}$ = 4010 b)

$$^{10}B + n \longrightarrow {}^{7}Li + {}^{4}He \quad (1.47 \text{ MeV}) \tag{2.4}$$

and the two stage reaction with nickel

$$^{58}Ni + n \longrightarrow {}^{59}Ni + \gamma ,$$
$$^{59}Ni + n \longrightarrow {}^{56}Fe + {}^{4}He \quad (4.76 \text{ MeV}) . \tag{2.5}$$

The energy dependent cross sections for these reactions are presented in Fig. 4 a,b.

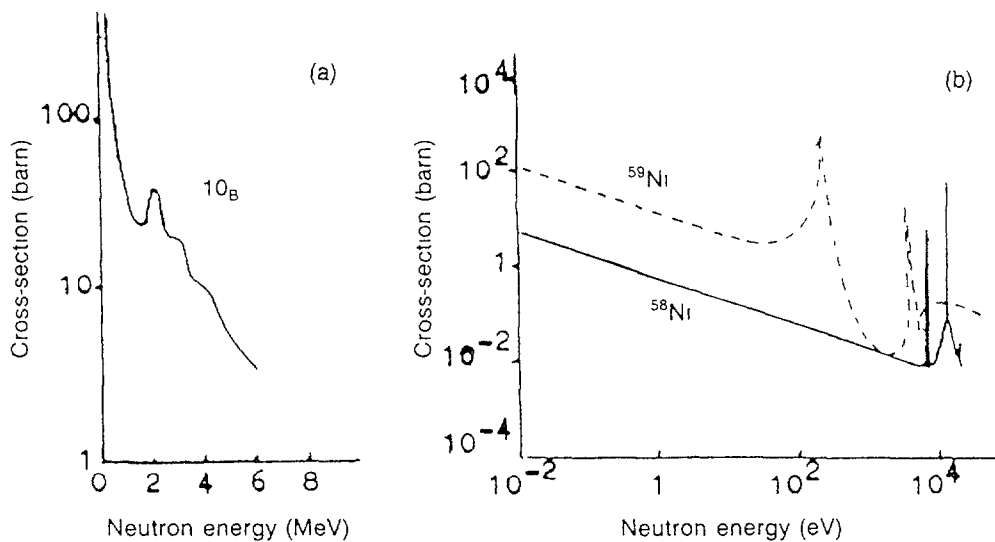Fig. 4. Cross-sections for (n,α) reactions with ^{10}B (a, after [5]) and with nickel (b, after [6])

The quantity of accumulated helium, its accumulation rate and relative importance of that or another reaction depend on both the initial composition of material and the reactor neutron spectrum. As an example, Fig. 5 presents the calculated results of He accumulation in steels with nominal composition of AISI 316 (17Cr-12Ni) and DIN 1.4914 (11Cr-1Ni-9Mo) irradiated by neutrons with energy spectra of HFIR and of CCTR [3]. Not only the rates of He accumulation in these two reactors are quite different, but the principal sources of helium are in each case different as well (see Table 1). Namely, in the fusion reactor He is supplied mainly through the reactions of
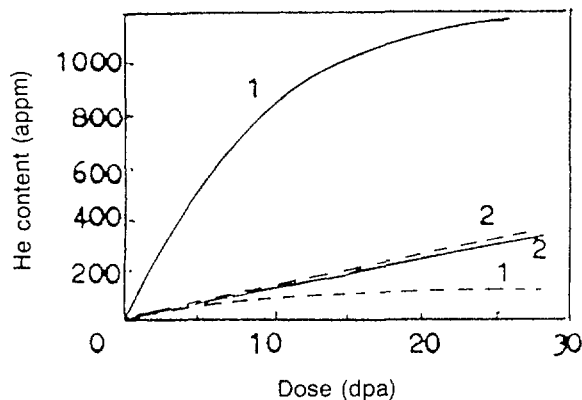
Fig. 5. Calculated helium accumulation in AISI 316 (———) and DIN 1.4914 (– – –) stainless steels being irradiated in HFIR (1) and CCTR (2). After [3].

Table 1

Percentage of He produced in different elements in AISI 316 and DIN 1.4914 stainless steels irradiated in CCTR and HFIR (according to [3])

Reactor	Element Steel	Fe	Ni	Cr	C	B
CCTR	316	64%	23%	8%		
	1.4914	81%		5%	11%	
HFIR	316		99%			
	1.4914	5-10%	80-90%			2%

neutrons with Fe, whereas in the mixed-spectrum reactor He is produced almost exclusively in Ni.

As a rule, the rates of He production in austenitic stainless steel equal ~0.1 appm/dpa in fast reactors, ~10 appm/dpa for fusion reactors, and ~50 appm/dpa for mixed-spectrum reactors (see also Fig. 6).
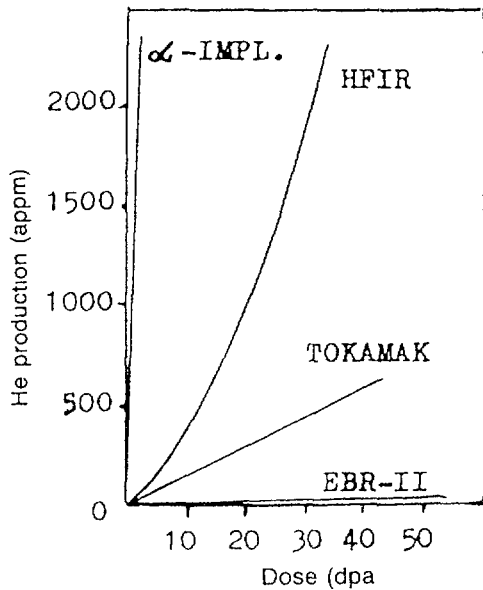
115

Fig. 6. The rates of He accumulation in austenitic stainless steels for different reactors and for α-implantation (after [4])

2.2. "Solid-state" transmutation products

Mechanical properties of irradiated structural materials can be influenced, as well, by the production of small quantities of some impurity elements. The most interesting from this point of view are the production of vanadium through the reaction $^{50}Cr(n,\gamma)^{51}Cr \longrightarrow ^{51}V$ (with 28 days half-life of ^{51}Cr) and a possible modification of manganese content (e.g. by the reaction $^{55}Mn(n,\gamma)^{56}Mn \longrightarrow ^{56}Fe$ with 3 hrs half-life of ^{56}Mn). Fig. 7 demonstrates that V is produced most effectively in mixed-spectrum reactors (reaching ~1% at 50 dpa in 316 stainless steel). At the same time, the content of Mn in HFIR demonstrates ~60-70% decrease at 50 dpa, whereas in TOKAMAK it grows (mainly through different (n,p) and (n,2n) reactions), see Fig. 8.
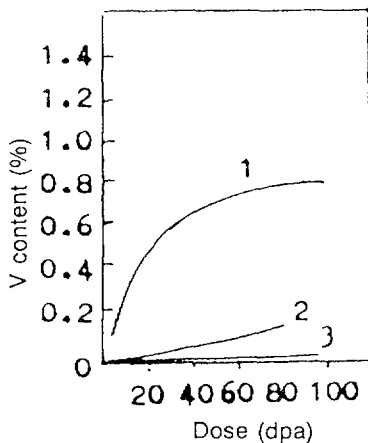

Fig. 7. Calculated accumulation of vanadium in 316 SS irradiated in HFIR (1), UWMAK (tokamak) (2), and EBR-II (3). After [7].
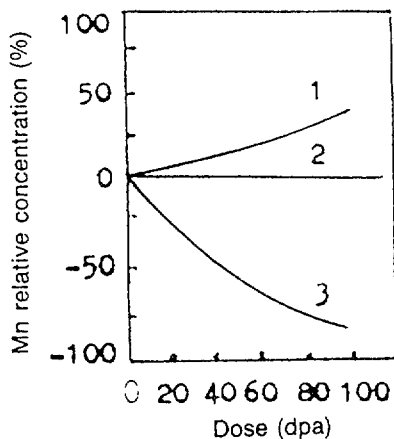
Fig. 8. Percentage of Mo content (initial content = 1.65 at.%) in 316 SS during irradiation in reactors UWMAK (1), EBR-II (2), and HFIR (3). After [7].

3. THE EFFECT OF TRANSMUTATION PRODUCTS ON SWELLING

Variations in impurity quantities and composition can have a considerable influence on the swelling of irradiated materials. Since the accumulation of gaseous and solid transmutation products influences swelling in different ways, we shall discuss their influence separately.

3.1. The effect of helium

Helium is the most important gaseous impurity with regard to its effect on swelling. The production of hydrogen through (n,p) reactions is far less important, although it can be generated even more effectively than He (see Fig. 2). However, the high diffusivity of hydrogen and its too weak binding to the principal point defect sinks (grain boundaries, dislocations, second-phase particles) [8] prevent hydrogen accumulation in material. On the contrary, He atoms are effectively captured by various sinks and, besides, promote nucleation of small helium bubbles, thus leading to swelling and facilitating the further development of vacancy voids.

To date there exist two principal experimental approaches to study the effect of helium on swelling of materials:

1. preirradiation saturation of materials with helium by implantation or through the "tritium trick", and

2. simultaneous defect production and helium introduction either in reactors (by (n,α) reactions), or on accelerators (by dual irradiation with heavy ions and alpha-particles).

Here we shall be interested only in the second case, where He production and point defect generation proceed simultaneously.

The effect of helium production is manifested usually at high enough temperatures, where vacancy supersaturations are too low for development of the usual bias-driven swelling. At the same time, the gas-driven swelling is highly sensitive to the ratio of helium production rate G_H to point defect generation rate G, the swelling either increasing, or decreasing depending on G_H/G.

The characteristic pattern of experimentally observed material microstructure evolution during simultaneous effect of irradiation and helium production can be described as follows [9]. At the first stage of irradiation helium accumulates approximately proportional to irradiation dose. However, as the concentration of helium increases, the process of helium diffusion to various sinks becomes of growing importance and, at the same time, diffusing helium atoms can collide, nucleating small helium-vacancy clusters, that develop further into gas bubbles. With the increase of their concentration, N_B, these bubbles become more and more effective sinks for free helium atoms, so that helium concentration in the matrix will reach some "steady-state" value C_H and the formation of new bubbles will be strongly suppressed. This picture is presented qualitatively in Fig. 9.
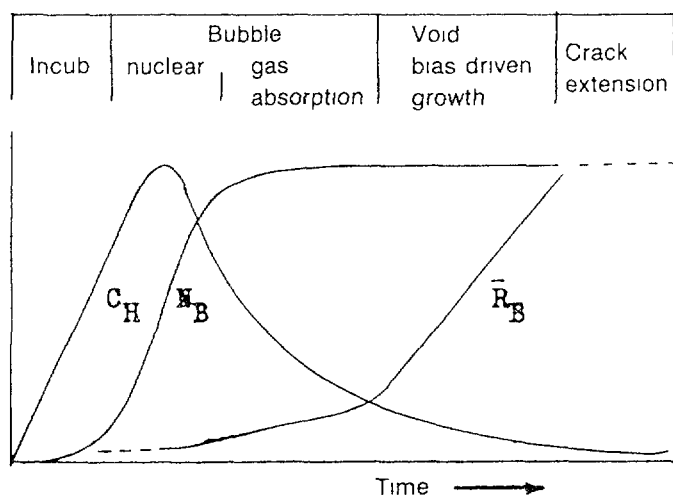

Fig. 9. Schematic evolution of helium concentration C_H, cavity density N_B and cavity average radius R_B defining characteristic stages of cavity evolution for in-beam creep tests. After [10].

118

Based on this picture of helium bubble evolution, one can obtain a simple estimate of the total helium bubble concentration as a function of helium production rate [10]. Indeed, the bubble nucleation rate is at maximum when the density of bubbles N_B^* is such that a free helium atom can be captured by a bubble or by another free helium atom with approximately equal probability, that is when $N_B^* \approx C_H^*/\omega$, where C_H^* is the corresponding atomic concentration of free helium atoms and ω is the atomic volume. Since, evidently, $N_B^* \approx N_B/2$, $C_H^* \approx C_H/2$, and C_H is related to G_H as

$$G_H = 4\pi R_B D_H C_H N_B , \qquad (3.1)$$

where R_B is the average bubble radius and D_H is helium diffusivity, then we obtain

$$N_B = \left(\frac{G_H}{4\pi R_B D_H \omega}\right)^{1/2} \propto G_H^{1/2} \qquad (3.2)$$

The square root dependence of N_B on G_H can be obtained also by the computer modelling [11] and is usually observed (e.g. see Fig.10), though sometimes the power index can differ from ½ and be equal to ¼, 1 or 2.
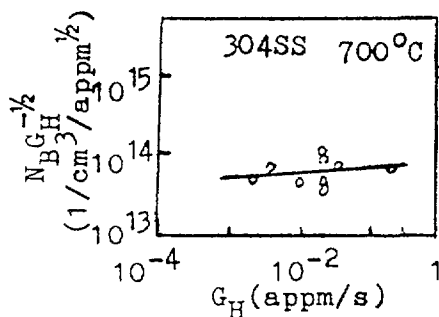
Fig. 10. Gas bubble density N_B versus helium accumulation rate in 304 SS at 700°C. After [12].

The further growth of gas bubbles is also dependent on the relation between G and G_H. The key role in the theoretical description of bubble ensemble evolution should be ascribed to the concept of critical radius (discussed in detail in [13]). At the early stages of bubble growth the average volume concentrations of irradiation-produced vacancies and interstitials, C_v and C_i, are determined by their absorption at dislocations and/or by mutual recombination:

$$G - Z_\alpha \rho_d D_\alpha (C_\alpha - C_{\alpha o}) - K C_v C_i = 0 , \qquad (3.3)$$

where D_α is the diffusion coefficient for α-type point defects ($\alpha = i,v$), Z_α is the corresponding bias factor, ρ_d is the dislocation density, K is the recombination coefficient, C_{vo} is the equilibrium concentration of vacancies and $C_{io} = 0$. On the other hand, the rate of growth of an individual bubble with the radius R is

$$\dot{R} = \frac{1}{R}\left[D_v(C_v - C_{vo}\exp(-\frac{\sigma\omega}{T})) - D_iC_i\right] , \qquad (3.4)$$

where $\sigma = P - 2\gamma/R$, γ is the surface energy, T is the tempe - rature (in units of energy) and P is the inside pressure that is related to the number of gas atoms in the bubble (for the ideal gas law) as

$$\frac{4\pi}{3}PR^3 = nT , \qquad (3.5)$$

Dependence of $\dot{R}$ on R for different n is depicted qualitatively in Fig. 11. If n is small enough, then the right-hand side of the equation (3.4) have two positive roots. The smaller root corresponds to equilibrium size of the bubble stabilized with inner gas pressure, whereas the larger one gives the value of critical radius, R_c, such that at $R > R_c$ no additional gas is necessary for the bubble to grow further in a void-like manner. It is evident, however, that at early stages of bubble growth their radii are maintained at equilibrium values, since the intrinsic point defects diffuse usually much faster than helium atoms.
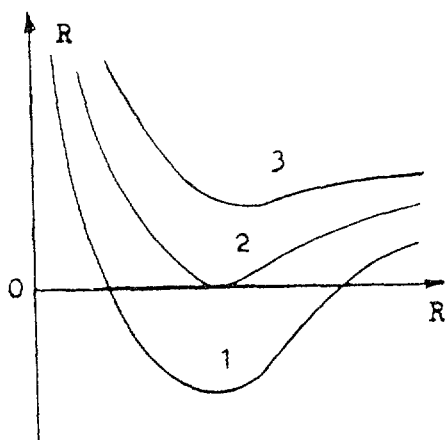

Fig. 11. Gas bubble growth rate versus bubble radius R at diffe- rent numbers of helium atoms in the bubble: 1. $n < n^*$; 2. $n = n^*$; 3. $n > n^*$

Let us suppose for some time that all bubbles are of the same size. As the number of gas atoms in bubbles increases, their radii also increase and R_c decreases until at some criti-

cal n* they coincide. When n becomes larger than n*, no additional gas is necessary for the bubble to grow.

The values of n* and the corresponding critical radius R_c^* are given by

$$R^* = \frac{4 \gamma \omega}{3T} \ln^{-1}\left(1 + \Delta Z \frac{C_v - C_{vo}}{C_{vo}}\right) , \qquad (3.6)$$

$$n^* = \frac{8\pi\gamma}{9T} (R_c^*)^2 , \qquad (3.7)$$

where $\Delta Z = (Z_i - Z_v)/Z_i$. For large enough G and/or low enough temperatures the value of R_c^* can be less than the interatomic distance α and so the swelling will be bias-driven from the beginning. Equating $R_c^* = \alpha$, we can find the limiting value of G (in function of temperature) such that at higher generation rates the swelling is weakly sensitive to the presence of helium (mainly through N_B). The expression for the limiting generation rate can be obtained in quite a simple form. Indeed, at characteristic values of $\gamma = 1.25 \cdot 10^{11} \, \text{eV/cm}^2$, $\omega = 2 \cdot 10^{-8} \text{cm}$ [11] and $T \gtrsim 300$ K we have $\gamma\alpha^2/T \ll 1$, so that the logarithm in the right-hand side of (3.6) can be expanded to the first order in $\Delta Z \ll 1$. Also, as it can be checked, the recombination term in (3.3) can be neglected (see also Fig.12). With these simplifications in mind, we easily obtain

$$G = \frac{4 Z_v \gamma \alpha^2 \rho_d D_{vo}}{3\Delta Z} \frac{\exp(-E_s/T)}{T} . \qquad (3.8)$$
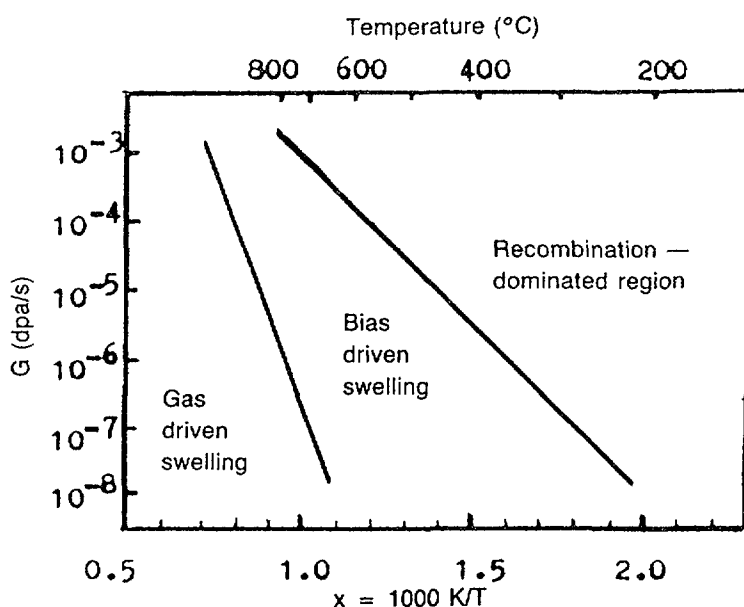

Fig. 12. Temperature regions of gas-driven swelling, of bias-driven swelling and of swelling suppression by point-defect recombination

This temperature dependence is presented in Fig. 12. The influence of helium is manifested only at high temperatures, in accordance with the predictions of computer modelling [11].

The size of equilibrium gas bubble is determined by the number of gas atoms in the bubble n, which grows according to the relation

$$\dot{n} = \frac{4\pi R}{\omega} D_H C_H \approx \frac{G_H}{N_B \omega} \, , \qquad (3.9)$$

so that the characteristic time to achive n* is

$$\tau_n = \frac{N_B n^* \omega}{G_H} \propto G_H^{-1/2} G^{-2} \, . \qquad (3.10)$$

It is seen that τ_n depend not on the ratio G_H/G, but on each of these parameters in quite different fashion (cf. Fig. 13 a and b).
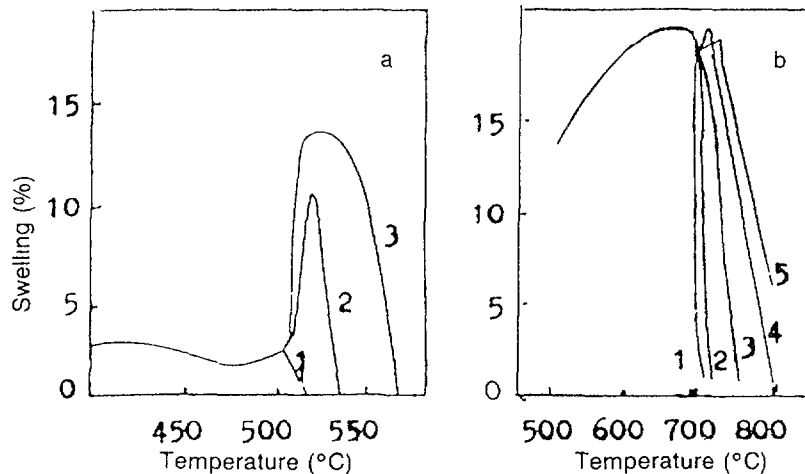
Fig. 13. Calculated swelling of 316 stainless steel at 40 dpa
(after [11]):
   a: $G = 10^{-6}$dpa/s; $G_H = 0$ (1), 10^{-13} (2), 10^{-12} (3) appm/s
   b: $G = 5\ 10^{-3}$dpa/s; $G_H = 0$ (1), 10^{-12} (2), 10^{-11} (3),
      10^{-10}(4), 10^{-9} (5) appm/s

The physical meaning of τ_n is transparent. Indeed, since after the accumulation of the critical quantity of gas in the bubble the latter grows as a usual void , then τ_n is the in - cubation time for void swelling of material.

As the rate of helium accumulation increases the value of τ_n decreases. Therefore the transition from bubbles to vois can be observed at reasonable (not too long and not too short)

fluences only in the very restricted range of G_H/G. This is illustrated in Fig. 14, where the results of computer simulation of bubble growth are presented [11].
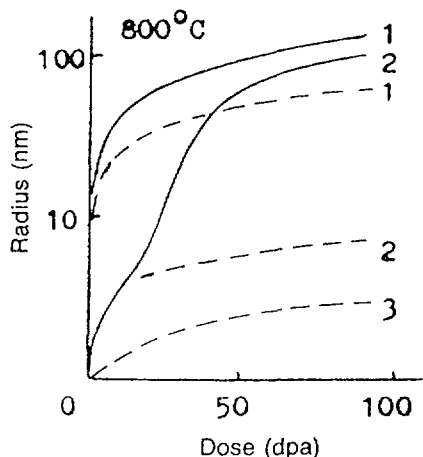
Fig. 14. Helium bubble growth kinetics with (———) and without (— — —) account of "bubble-void" transition for $G = 5 \cdot 10^{-3}$ dpa/s and $G_H = 10^{-m}$ appm/s, where m = 7 (1), 16 (2), 11 (3). After [11].

In real materials the nucleation of bubbles needs certain time and some distribution of bubbles in sizes is produced by the end of the nucleation period. Therefore, the critical radius will be reached first by the largest bubbles. These bubbles will grow further as voids. As the number of voids grows the concentration of vacancies in the material falls, leading to the increase of R_c^* for the rest of bubbles (in accordance with (3.6)). A bimodal distribution of cavities will arise as a result, where large growing voids and "frozen" in size gas bubbles can be simultaneously observed (see e.g. Fig. 15).
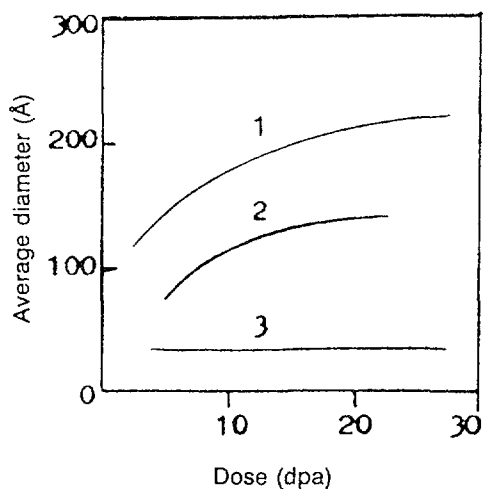
Fig. 15. Average diameter of voids and gas bubbles versus dose in 316 stainless steel at $625^{\circ}C$ and $G = 3 \cdot 10^{-3}$dpa/s:
1. Voids, 5 appm/dpa
2. Voids, 50 appm/dpa
3. Gas bubbles

Thus, the rate of helium accumulation in irradiated material can substantially influence the swelling behaviour. As a general trend one may observe that large quantities of helium suppress swelling, whereas small quantities of helium enhance

it [12]. In this connection a possibility arises of swelling monitoring through the appropriate variation of G_H/G either by the alloying of material with isotopes of its main components (e.g. ^{58}Ni, ^{59}Ni), or by spectrum tailoring with absorbers and moderators of neutrons [15].

3.2. Solid-state transmutation products

Variation of swelling kinetics due to nuclear transmutations that result in production or burn out of solid elements is investigated to much less extent than in the case of helium accumulation. Production of V and Mn in mixed-spectrum fusion and in fission reactors seems to be most important here. It is known that the presence of Mn favours swelling suppression (see Fig. 16), though deviation of Mn concentration from the optimum one (in either direction) weakens the effect. Vanadium can influence swelling behaviour of stainless steels by promoting carbide formation, though experimental data concerning this effect are far from comlete.
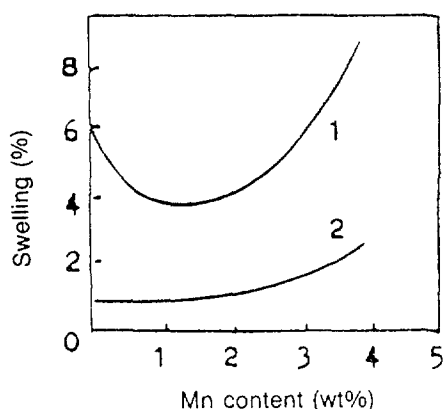
Fig. 16. The effect of Mn addition on the swelling of 316 stainless steel (after [7]):
1. 61.5 dpa, $620^\circ C$
2. 45.5 dpa, $510^\circ C$

4. THE EFFECT OF HELIUM ACCUMULATION ON IRRADIATION CREEP

The data about irradiation creep modification in response to impurity additions are rather scarce. Usually their effect is not too pronounced, though sometimes some atomic percent of impurity can vary irradiation creep rate of material up to 10-30 times. In particular, the creep rate of 316 stainless steel at $330-600^\circ C$ in the reactor with the helium production rate of 12 appm/dpa was 3-10 times higher than in the analogous reactor with $G_H = 0.28$ appm/dpa, see Fig. 17 [16]. No reasonable explanation of the effect have been presented by now.
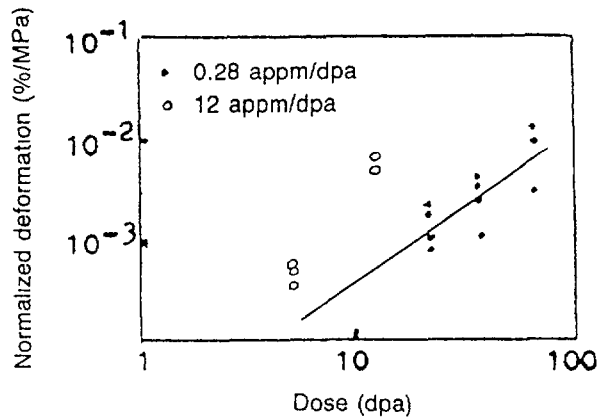
Fig. 17. The effect of G_H/G ratio on irradiation creep rate of PCA (25% CW) at 500°C. After [16].

5. THE EFFECT OF HELIUM ACCUMULATION ON HIGH TEMPERATURE IRRADIATION EMBRITTLEMENT

One of the most detrimental results of helium accumulation is the unrecoverable degradation of mechanical properties of irradiated materials at temperatures exceeding ~0.5 of the melting temperature, see Fig. 18. Both the principal cause and the possible mechanism of this phenomenon were first proposed in [17], where it has been postulated that high temperature embrittlement of irradiated materials is due to helium generated by (n,α) reactions. In particular, the assumption that He accumulates in grain boundaries was confirmed by further investigations. Also, it has been found that fracture becomes
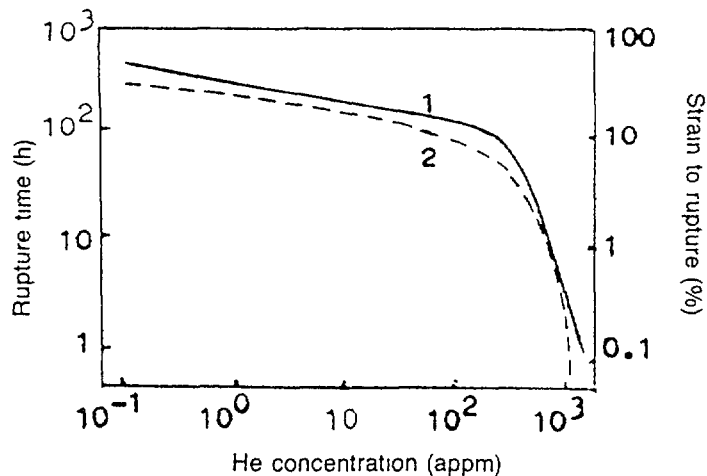
Fig. 18. Rupture time (1) and strain to rupture (2) as functions of the accumulated He concentration in AISI 316 stainless steel preirradiated with He and tested at 750°C. G_H = 100 appm/h. After [4].

125

brittle and intergranular, that no effect can be observed in monocrystals, and that the onset of embrittlement takes place after some incubation fluence.

Qualitative picture of high-temperature embrittlement can be presented as follows [4]. Helium atoms, that have been introduced into the material by implantation or by nuclear reactions, diffuse to point defect sinks (dislocations, grain boundaries, etc.) and form clusters both in the volume of material and on the sinks. Later on these clusters evolve into helium bubbles. As a rule, the bubbles on sinks, especially on grain boundaries, grow appreciably faster than the bubbles in the volume of material [18]. This effect is due to supplementary currents of helium captured by sinks. The growing cavities affect the mechanical properties of material in two ways. Relatively small bubbles in the grain interior act as obstacles for dislocation motion, thus leading to grain hardening and to degradation of material plasticity. On the other hand, the grain boundary-associated cavities weaken the bounderies by decreasing their area and also deteriorate plasticity by preventing grain boundary sliding. The arising disbalance between the strength of grain boundaries and grain matrix results in the transition to brittle and intergranular mode of fracture of material.

The existing models of high temperature embrittlement deal usually with investigation of bubble growth kinetics, without consideration of processes of crack development that directly lead to the rupture of material. In this connection we should mention the paper [19], where gas accumulation in cracks was investigated in detail. It has been shown that the evolution of gas-filled crack closely resembles that of gas bubble. In particular, the inner gas pressure stabilizes crack size and with the accumulation of gas the crack progressively develops until it attains some critical length at which its stability is lost. However, unlike the case of gas bubbles, further the crack propagates practically instantly, leading to destruction of material.

Although the phenomenon of high temperature embrittlement can be described qualitatively in relatively simple manner, it is extreamly difficult to compare the predictions of vari-

126

ous theoretical models with experimental results, despite of the very extensive experimental data accumulated by now. This is due to the fact that the overwhelming majority of the existing data is application-oriented and is of little use where the comparisons with theory predictions are necessary. It concerns both the methods of parameter measurement and the parameters themselves.

The most appropriate approach to investigations of high temperature embrittlement seems to be the creep-rupture testing directly under irradiation, but only negligible part of existing information is obtained in this way. Usually materials are tested after the termination of preliminary irradiation. Here short-term strength determination tests are preferable for comparison with theory predictions, since in this case the results reflect to some extent the "snapshot" of defect microstructure formed in the material by the end of irradiation. The long-time strength tests of preirradiated materials are the most wide-spread and, at the same time, the least informative, because irradiation effects get "smeared" by postirradiation changes in defect microstructure. The interpretation of experimental results for preirradiated materials becomes even more uncertain when long time pass between the termination of irradiation and the beginning of testing and/or when the test temperature differs from the irradiation one.

The parameters measured in high temperature embrittlement studies may be divided into three groups, namely, those characterizing either plasticity ($\sigma_{0,2}$, σ_y - various tensile strengths), or strength (t_R - rupture time, σ_f - short-term strength), or both (ε_R - strain to rupture). One or several of these parameters are measured in particular experiments. It should be clearly understood, however, that from the microscopic point of view plasticity and strength are determined by different components of defect structure of material. The processes related to dislocation motion and to grain boundary sliding are responsible for the changes of plastic properties of materials, whereas the strength properties are determined by nucleation and growth of cracks and grain-boundary-associated bubbles. Certainly, these components of microstructure

interact with each other and in most cases decrease in plasticity is accompanied by decreasing strength, but this correlation is indirect and sometimes does not hold. That is why the plasticity parameters are nearly useless for physical simulation of high temperature embrittlement, while the use of mixed parameters is restricted and needs extra information. For example, variations of ε_R may be due either to plasticity loss without strength loss, or to a drastic strength fall (decrease of t_R) with unchanged plasticity. Fig. 19 demonstrates an example of the latter behaviour.
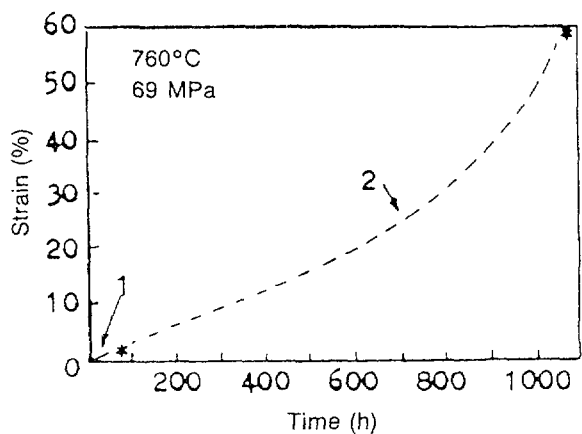
Fig. 19. Creep curves for unirradiated (1) and preirradiated (14 dpa, 8.5 ppm He) (2) samples of AISI 316 stainless steel (after [20])

With all this in mind, the limited results concerning the effect of He generation rate on various measured parameters (see e.g. Fig. 20) can not be described in any unequivocal way. It means that the theory of high temperature embrittlement needs further development.
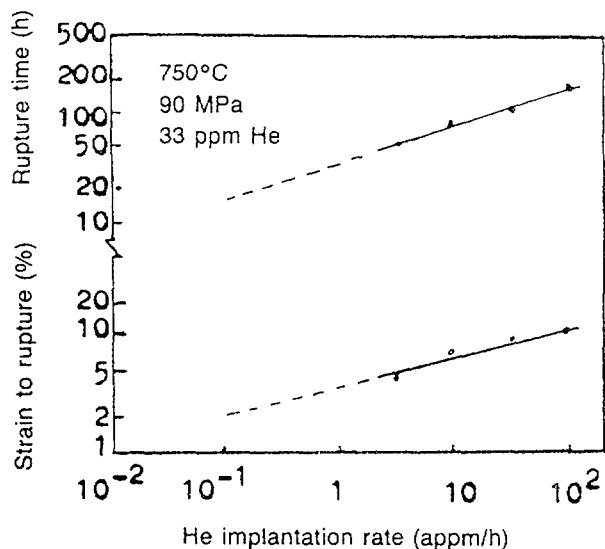
Fig. 20. Rupture time and strain to rupture as a function of He implantation rate in AISI 316 stainless steel. After [4].

REFERENCES

1. Zelensky V.F. et al. Some physical problems of irradiation damage in materials. - Kiev: Naukova Dumka, 1979. - 240 p. (in Russian)

2. Mansur L.K., Grossbeck M.L. - Journal of Nuclear Materials, 1988, v. 155-157, p. 130

3. Sanz J., De la Fuente R., Perlado J.M. - Journal of Nuclear Materials, 1988, v. 155-157, p. 592

4. Ullmaier H. - Nuclear Fusion, 1984, v. 24, p. 1039

5. Tables of physical values (I.K. Kikoin, Ed.). - Moscow: Atomizdat, 1976. - 1006 p. (in Russian)

6. Greenwood L.K., Kneff D.W., Skowronski R.P. - Journal of Nuclear Materials, 1984, v. 122-123, p. 1002

7. Bates J.F., Garner F.A., Mann F.M. - Journal of Nuclear Materials, 1981, v. 103-104, p. 999

8. Baskes M.I., Vitek V. - Metallurgical Transactions, 1985, v. A16, p. 1625

9. Odette G.R. - Journal of Nuclear Materials, 1979, v. 85-86, p. 533

10. Trinkaus H. - Radiation Effects, 1987, v. 101, p. 91

11. Bullough R., Hayns M.R., Wood M.H., Journal of Nuclear Materials, 1979, v. 85-86, p. 559

12. Odette G.R., Maziasz P.J., Spitznagel J.A. - Journal of Nuclear Materials, 1981, v. 103-104, p. 1289

13. Mansur L.K., Coghlan W.A. - Journal of Nuclear Materials, 1983, v. 119, p. 1

14. Ayrault G., Hoft H.A., Nolfi F.V., Turner A.P.L. - Journal of Nuclear Materials, 1981, v. 103-104, p. 1035

15. Odette G.R. - Radiation Effects, 1987, v. 101, p. 55

16. Grossbeck M.L., Horak J.A.,- Journal of Nuclear Materials, 1988,v. 155-157, p. 1001

17. Barnes R.S. - Nature, 1965, v. 206, p. 1307

18. Ryazanov A.I. et al., Atomnaya Energiya, 1985, v. 59, p.35

19. Borodin V.A., Manichev V.M., Ryazanov A.I. - IAE-4616/11, 1988

20. Lovell A.J. -Nuclear Technology, 1972, v. 16, p. 323

REAL-88 RESULTS AND PROSPECTS

(Session III)

Chairman

H.J. NOLTHENIUS
Netherlands

THE ROLE OF THE REAL-88 EXERCISE IN
THE RADIATION DAMAGE CHARACTERIZATION
OF NUCLEAR FACILITIES

E.M. ZSOLNAY*, H.J. NOLTHENIUS**, E.J. SZONDI*

* Institute of Nuclear Techniques,
  Technical University of Budapest,
  Budapest, Hungary

** Netherlands Energy Research Foundation (ECN),
  Petten, Netherlands

Abstract

In frame of the REAL-88 project a reference file will be produced for neutron metrology use containing the best available input-output information for 6 typical neutron spectrum cases, furthermore, cross section processing codes and several utility programs. A number of reactions cannot be incorporated because no adequate cross section data are available. Discrepant cross section values furthermore clearly imperfect cross section uncertainty data were found in the IRDF-85 for several reactions.

---

1. INTRODUCTION

The IAEA Nuclear Data Section has organized a series of international interlaboratory exercises (called REAL-80, REAL-84 and REAL-88) in order to improve the life-time prediction of nuclear facilities. The emphasis was concentrated on radiation damage (exposure) parameters for reactor pressure vessels and related technology.

The aim of the REAL-80 exercise [1] was to determine the state-of-art of neutron spectrum adjustment and subsequent prediction of the number of displacements in irradiated steel specimens, performed by different laboratories. Based on the experiences of this interlaboratory exercise a next step, REAL-84 [2] was organized with the purpose of improving the uncertainty assessment of the radiation damage parameters. The results of the REAL-84 program have shown the need of establishing standard metrology procedures and recommended nuclear data for use in neutron spectrum adjustment and damage parameter calculations. Therefore, according to the recommendations of an IAEA Specialists' Meeting (held in Jackson Hole, from May 31 to June 5 1987) [3] the REAL-88 program has been started. In frame of this program a reference file will be produced for neutron metrology use. This file will contain the best available input-output information for some typical neutron spectrum cases [4], furthermore, cross section processing codes and several utility programs. The aim of such a reference data set is to provide a tool for testing neutron spectrum adjustment codes and radiation damage calculation procedures for an unambiguous test case. IAEA should then distribute the reference file upon request to all experienced or new-coming laboratories interested in the neutron metrology work.

2. FIRST RESULTS OF THE REAL-88 PROJECT

In frame of the REAL-88 project 6 different neutron spectra (which were already investigated in the REAL-84 exercise) were considered:
- 3 neutron spectra for thermal reactors,
- 1 fusion spectrum,
- 1 ^{235}U fission neutron spectrum,
- 1 fast reactor spectrum.

A working group of experts from different institutes and laboratories [5] has undertaken the task to prepare consistent and reliable input data resulting in reference files for the above mentioned spectrum cases. The input sets and accompanying utility programs were then checked also by some volunteering laboratories - others than the compilers - using their own adjustment codes, calculation methods and procedures. The outputs of the calculations were intercompared and improvement in the data - where it was necessary and possible - was introduced. A large effort was made by the working group to remove the inconsistencies and find the best available data and methods. Repeated adjustment runs with the new data sets were then performed to arrive in interactive way at the best results attainable in the present circumstances.

The first results of the REAL-88 exercise [6] were discussed by an IAEA Consultants Meeting [7], where nuclear data needs, applicable methods and procedures, furthermore, special physics and mathematics problems of the neutron spectrum adjustment and related radiation damage calculations were also overviewed. A large - unexpected and sometimes unjustified - spread in the spectrum characteristic integral data and especially in the related uncertainty values was detected [6].

During the evaluation it has turned out that several inconsistencies and problems encountered in the neutron spectrum adjustment and reported earlier [2,8-10] were still present. Some of them originated from the different normalization procedures and/or incorrect algorythms (eg in the uncertainty propagation), unsatisfactory energy grids, etc, applied, but the majority of the difficulties was due to the non-satisfactory availability of nuclear data and/or shortcomings of the neutron transport calculations. These two latter important factors, which strongly influence the results of the neutron spectrum adjustment and related damage estimates will be discussed here shortly again, in hope, that the participants of this meeting can contribute to the solution of the problems.

3. SHORTCOMINGS OF NUCLEAR DATA AND NEUTRON TRANSPORT CALCULATIONS

3.1. Reaction cross sections and their uncertainties

The reaction cross section data for the exercise were derived from the best available compilations (dosimetry and gas production file of ENDF/B-V [11], and IRDF-85 [12]). Nevertheless, during the preparation of the input data sets a number of reactions - for which measured activities were available - could not be incorporated because no adequate cross section data were available. The reactions with lacking cross section uncertainty information were: ^{45}Sc(n,2n), ^{52}Cr(n,p), ^{54}Fe(n,α), ^{59}Co(n,p), ^{64}Zn(n,g), ^{89}Y(n,2n), ^{93}Nb(n,g), ^{93}Nb(n,2n), ^{107}Ag(n,g),

^{169}Tm(n,2n), ^{197}Au(n,2n) and ^{238}U(n,2n). The majority of these reactions is of special interest for fusion neutron metrology. For a number of these reactions evaluations are available which are not yet incorporated in the metrology cross section libraries.

Discrepant cross section values were found for a number of reactions, eg ^{47}Ti(n,p), ^{56}Fe(n,g), ^{58}Ni(n,2n) and ^{127}I(n,2n), furthermore, the ^{115}In(n,g)^{116m}In reaction cross section is not present in the ENDF/B-V Version 2 dosimetry file, only the total (n,g) reaction cross section data are given.

Clearly imperfect cross section uncertainty data were found in the IRDF-85 for the following reactions: ^{32}S(n,p), ^{47}Ti(n,p), ^{63}Cu(n,α), ^{232}Th(n,f), ^{237}Np(n,f).

For these reactions it occurs that in neutron energy regions where the cross section values are different from zero in the file #3 of the IRDF-85 library, no uncertainty data are given in the file #33. As a result, for the corresponding cross section uncertainty values zero or any "random number" - depending on the energy group structure applied by the user - can be obtained (eg in our case different values between zero and 2500 % were found). Improvement of these inconsistencies is necessary.

Similar problems could be observed at the reactions ^{58}Ni(n,p), ^{238}U(n,f) and ^{238}U(n,g).

For several reactions the uncertainties calculated from the IRDF-85 library were so large that they resulted in a negligible statistical weight for the reaction of interest in the adjustment procedure.

Also the too coarse original group structure of the uncertainty information with large jumps in the uncertainty values seems to be unrealistic (eg in case of ^{197}Au(n,g)). In the groups structure of interest in the exercise the cross section covariance matrices were found to be singular within computer accuracy.

3.2. Input spectrum covariance information

No positive definite input spectrum covariance matrices in the group structure of interest were available for the spectra considered, only semidefinite ones. Calculations have shown that all the matrices were singular within computer accuracy [2,7]. To improve the situation, the neutron transport calculations should be accompanied by sensitivity analysis investigations. At the same time, for a number of materials of interest nuclear data (cross sections and related uncertainty information) are lacking.

3.3. Input spectrum group structure

The group structure of the input neutron spectra derived from transport calculations was in most cases not satisfactory [2,13]. In the low neutron energy region a too broad group structure was used, and sometimes no spectrum information was available below about 1 eV. Similar problems (ie too broad energy groups in the input spectrum) could be encountered also in other - especially in the higher - energy

ranges of the spectra. The shortcomings of the input spectrum informa-
tion gave difficulties in the adjustment and in the calculation of the
characteristic integral spectrum- and damage parameters. To solve the
problems, the transport calculations should be performed in a finer
energy group structure. At the same time, this type of calculations
require a more detailed uncertainty information than the one available
presently. Therefore, improvement is needed also in this field.

4. CONCLUSIONS

1. The reference data file for neutron spectrum adjustment and radiation
   damage calculations, being under preparation in frame of the REAL-88
   project, will be a useful tool in improving the uncertaintly assess-
   ment of radiation damage predictions in nuclear facilities by
     - giving the possibility for testing the abilities of the
       adjustment codes (algorythms) and calculational pro-
       cedures used by the neutron metrologists;
     - supplying tested up-to-date nuclear data and neutron
       spectrum information to the radiation damage calcula-
       tions;
     - supplying tested cross section and related uncertaintly
       processing codes, furthermore, several utility programs
       to the users.
   As a result, the neutron metrology work in the different laboratories
   will be striven towards the use of uniform nuclear data and calcula-
   tional procedures.

2. A considerable contribution from the nuclear data evaluating and com-
   piling experts is required in order to reach a significant improve-
   ment in the results of the radiation calculations.

3. Continuous up-dating of the reference file will be needed in order
   the most recent data and procedures should always be incorporated.

REFERENCES

[1] W. L. Zijp, é. M. Zsolnay, H. J. Nolthenius, E. J. Szondi, G. C.
    H. M. Verhaag, D. E. Cullen, C. Ertek: Final report on the REAL-80
    exercise. Report ECN-128, INDC(NED)-7, BME-TR-RES-6/82. Netherlands
    Energy Research Foundation, Petten, February 1983.
[2] W. L. Zijp, é. M. Zsolnay, H. J. Nolthenius, E. J. Szondi: Final
    report on the REAL-84 exercise. Report ECN-212, BME-TR-RES-18/88,
    IAEA-NDS-212. Netherlands Energy Research Foundation, Petten, Nov.
    1988.
[3] International Atomic Energy Agency: Analysis of the REAL-84 inter-
    comparison exercise. Summary of specialists' meeting, Jackson Hole,
    USA, 27-29 May 1987. Report INDC(NDS)-198. International Atomic
    Energy Agency, Vienna, October 1987.
[4] H. J. Nolthenius: Information for the REAL-88 exercise. Report for
    restricted distribution, ECN-88-023. Netherlands Energy Research
    Foundation, Petten, January 1988.

[5] Working group on the REAL-88 project: H. J. Nolthenius from ECN, Petten; M. Matzke from PTB Braunschweig; L. Greenwood from ANL, Argonne; F. Stallmann from ORNL, Oak Ridge; and É. M. Zsolnay - E. J. Szondi from BTU, Budapest.

[6] H. J. Nolthenius: Results of the REAL-88 exercise. Report for restricted distribution ECN-89-095. Netherlands Energy Research Foundation, Petten, June 1989.

[7] Proceedings of the IAEA Consultants' Meeting on the REAL-88 Exercise, Petten, October 24-26, 1988. To be published.

[8] H. J. Nolthenius, É. M. Zsolnay, W. L. Zijp, E. J. Szondi: Nuclear data aspects encountered in the REAL80 and REAL84 intercomparisons. = V. Piksaikin (Ed.): Nuclear data for radiation damage estimates for reactor structural materials. Proceedings of an IAEA Consultants' Meeting, Santa Fe, NM, USA, 20-22 May 1985. Report INDC(NDS)-179/G. p. 95-105. International Atomic Energy Agency, Vienna, June 1986.

[9] É. M. Zsolnay, H. J. Nolthenius: Proceedings of the IAEA Consultants' Meeting on the assesment of the results of the REAL-84 exercise. Report INDC(NDS)-190/G+F+R. IAEA, Vienna, March 1987.

[10] W. L. Zijp, É. M. Zsolnay, H. J. Nolthenius, E. J. Szondi: On the uncertainty involved in activation spectrometry and subsequent radiation damage predictions. Publication in progress in the Proceedings of the 6th ASTM-Euratom Symposium on Reactor Dosimetry, Jackson Hole, WY, May 31 - June 5, 1987.

[11] Guidebook for the ENDF/B-V nuclear data file. Report EPRI-NP-2510, BNL-NCS-31451, ENDF-328. Electric Power Research Institute, Palo Alto, CA, July 1982.

[12] D. E. Cullen, P. K. McLaughlin: The international reactor dosimetry file (IRDF-85). Report IAEA-NDS-41, Rev. 1. IAEA NDS, Vienna, April 1985.

[13] H. J. Nolthenius: Influence of the weighting spectrum in calculations with a coarse group structure. Report for restricted distribution ECN 89-079. Netherlands Energy Research Foundation, Petten, May 1989.

PHYSICALLY BASED WEIGHTING SPECTRUM GENERATION
FOR CROSS SECTION CALCULATIONS

E.J. SZONDI
Institute of Nuclear Techniques,
Technical University of Budapest

A.P. BOSZNAY
Department of Mathematics,
Technical University of Budapest

Budapest, Hungary

Abstract

For collapsing the cross section data into a coarse group structure one needs a continuous weighting neutron spectrum. This spectrum is known in the coarse structure. The newly developed procedure for converting the spectrum into the 640 group SAND II structure takes into account the few-group spectrum, a semi-analitically described model spectrum and the user's experience. The IBM PC/AT program "BLOW UP" will be distributed by the IAEA NDS among the utility programs of the REAL-88 neutron spectrum adjustment reference file.

The neutronics calculations, eg criticality investigations, neutron transport (shielding &c) analyses, neutron spectrum adjustment are usually made in the "group" principle. It means, that – neglecting the continuity of those – the cross sections and neutron flux density between the points of the selected energy grid are assumed being constant. The calculations can then be performed using matrix operations (eg summation can be made instead of integration).

Most of the important cross sections are described more detailly than the energy structures commonly used. For collapsing them one needs a weighting spectrum, to calculate the group averaged cross sections:

$$\langle \sigma \rangle_i = \frac{\displaystyle\int_{E_i}^{E_{i+1}} \sigma(E)\Phi(E)dE}{\displaystyle\int_{E_i}^{E_{i+1}} \Phi(E)dE} = \frac{\displaystyle\int_{u_i}^{u_{i+1}} \sigma(u)\Phi(u)du}{\displaystyle\int_{u_i}^{u_{i+1}} \Phi(u)du} \qquad i=1(1)m \qquad (1)$$

where:

E   neutron energy
E_i lower limit of the i-th energy group
m   number of the energy groups
u   lethargy [usually at 1 MeV u=0, ie u=-ln(E)]
u_i lover limit of the i-th lethargy group
Φ neutron flux density (continuous function), as weighting spectrum
σ cross section (continuous function)
$\langle \sigma \rangle_i$ average cross section in the i-th energy group

There are several computer programs to perform this calculation. Two codes have to be mentioned separately: the GROUPIE [1] and the UNC33 [2] have been widely used in frame of the REAL-84 and REAL-88 projects of the IAEA Nuclear Data Section [3,4]. Both of these codes process the IRDF-85 cross section library [5], the cross sections of which have been the basic data for the REAL-84 and REAL-88 neutron spectrum adjustment tasks. The IRDF-85G version comprises cross section data in the extended SAND II energy structure [1,6]: 45 groups in each decade from 10^{-10} MeV to 1 MeV, and 190 groups of 0.1 MeV width from 1 to 20 MeV. The total number of groups is 640, much more than the number of groups used in the neutron spectrum adjustment jobs. Therefore, this 640 group structure is suitable to describe the weighting spectrum, and Eq (1) becomes in the form:

$$\langle\sigma\rangle_i = \frac{\displaystyle\sum_{j=J_i}^{J_{i+1}} \sigma_j \Phi_j \delta E_j}{\displaystyle\sum_{j=J_i}^{J_{i+1}} \Phi_j \delta E_j} = \frac{\displaystyle\sum_{j=J_i}^{J_{i+1}} \sigma_j \Phi_j \delta u_j}{\displaystyle\sum_{j=J_i}^{J_{i+1}} \Phi_j \delta u_j} \qquad i=1(1)m \qquad (2)$$

where:

j   group serial number in the SAND II structure
J_i lower limit in the SAND II grid of the i-th energy group
m   number of the energy groups
δE_j energy width of the j-th group in the SAND II grid
δu_j lethargy width of the j-th group in the SAND II grid
Φ_j neutron flux density in the SAND II grid, as weighting spectrum
σ_j cross section in the SAND II grid
$\langle\sigma\rangle_i$ average cross section in the i-th energy group

Nevertheless, the $\Phi(E)$ or $\Phi(u)$ spectrum usually are not known in the SAND II structure. The most detailed neutron spectrum calculations by the one-dimensional neutron transport code ANISN [7] supply the weighting spectrum in 171 groups of the VITAMIN-C energy grid [8], but only for the intermediate and fast region. In the two- and three-dimensional cases the number of energy groups is much less due to the computer limits. One has to make the energy grid of the available weighting spectra finer.

In this paper, a physically based method for "blowing up" the weighting spectrum is described.

The information content of the spectrum to be blown up is the vector of the group fluxes (m values), and, of course, the energy grid (m+1 values). This information must be saved in the conversion process.

On the other side, the structure of the neutron spectrum is determined by the components of the environment (eg reactor core). This can be described in general with a low number of parameters, like the neutron gas temperature, the energy of the joining point of the Maxwell-Boltzmann and Fermi spectra, &c. This additional information has to be incorporated into the output spectrum.

Furthermore, the experience of the researcher should be taken into consideration. It cannot be formulated for computing yet, therefore the conversion process has to give possibility to the manual control.

140

The program BLOW UP solves all of these problems. The code re-
quires a model spectrum in analytical form with arbitrary parameters
(max. 15). As sample model spectrum, a general LWR spectrum is sup-
plied with the following parameters:

- integral flux over the whole SAND II energy region (10^{-10} to 20 MeV),
- neutron gas temperature
- energy of the joining point of the Maxwell-Boltzmann and Fermi
  spectra,
- the α value for the Fermi spectrum (the usual assumption is used:
  $\Phi(E) \approx const/E^{1+\alpha}$),
- energy of the joining point of the Fermi and fission spectra,
- fission temperature.

Three peaks and/or valleys may be present in the spectrum due to realis-
tic physical background, eg the oxygen-valley. The parameters of these
are energy, the ratio of the local extremum to the smooth environmental
flux density and the FWHM.

The program minimizes the average squared relative difference of
the group fluxes fixed by the input spectrum and the calculated ones,
modifying the values of the parameters.

$$\frac{1}{m} \sum_{i=1}^{m} \left[\frac{\Phi_{gi}}{\sum_{j=j_i}^{j_{i+1}} \Phi_j \delta u_j} - 1 \right]^2 =====> min! \qquad (3)$$

where:

j group serial number in the SAND II structure
j_i lower limit in the SAND II grid of the i-th energy group
m number of the energy groups
δu_j lethargy width of the j-th group in the SAND II grid
Φ_{gi} group flux in the i-th energy group of the input
Φ_j neutron flux density in the SAND II grid, to be fitted

The minimization is made by the direct numerical algorithm called
"flexibile polyeder method" [9], therefore, there is no need to develop
the gradient vector to the Eq (3), even if one exchanges the semi-ana-
lytical formula describing the spectrum. Like to any other method to
fit a multiparameter function, this algorithm is sensitive to the in-
itial data (eventually the convergence may be too slow, due to numerical
problems). Nevertheless, one should not forget, that a thermal reactor
spectrum can be described with IF ... THEN ... ELSE structures, so the
formula cannot be derived: there is no possibility for generating the
gradient vector.

In the next step, correction factors are calculated to save the
values of the group fluxes:

$$s_i = \frac{\sum_{j=j_i}^{j_{i+1}} \Phi_j \delta u_j}{\Phi_{gi}} \qquad i=1(1)m \qquad (4)$$

where the notation of Eq (3) is used; s_i is the correction factor for
the i-th coarse energy group.

The best approximation of the i-th energy group is calculated as

$$\Phi_{out}(u) = \Phi_m(p_1, p_2, p_3, \ldots, u)/s_i \qquad u_i \leq u < u_{i+1} \qquad (5)$$

where:

p_i fitted value of the i-th physically defined spectrum-parameter,
s_i correction factor for the i-th coarse energy group.
u   lethargy
u_i lower limit of the i-th lethargy group
Φ_m semi-analytical formula for the model spectrum
Φ_{out} output spectrum of the blowing up procedure

Part of a neutron spectrum is shown in Fig 1. Curve $\underline{a}$ is the coarse group spectrum, curve $\underline{b}$ is the fitted one, and curve $\underline{c}$ refers to the output spectrum defined by Eq (5). It is seen that breaks may be present in the generated output spectrum, therefore it may not be used as weighting spectrum in Eq (2). The program BLOW UP offers the possibility to the experienced user for manual control of the weighting spectrum calculation: the code accepts an input value as cut-off ratio to eliminate the corners from the output spectrum, as it is shown in Fig 2.
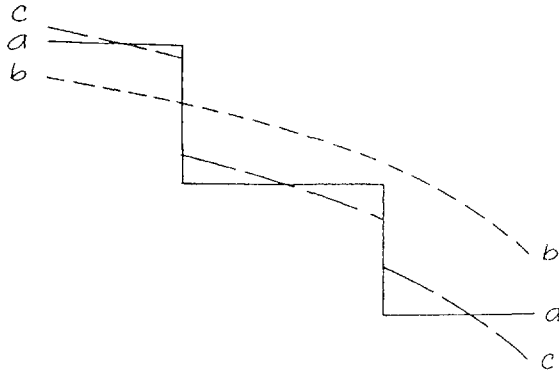

FIG. 1.
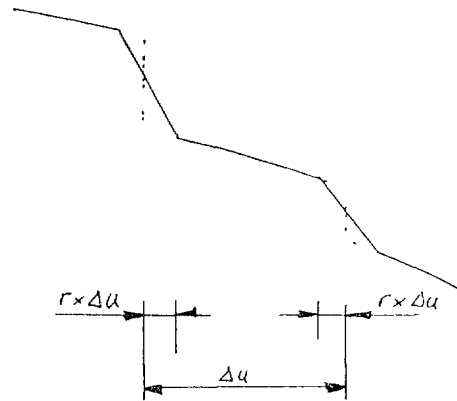
FIG. 2.

The program displays continuously the plots of the I/O spectra, to make easier the user's decisions. Fig 3 shows these for the the PS1 task of the REAL-84 and REAL-88 exercises. This picture illustrates the shortcomings of the selected group structure: one group covers the whole thermal spectrum, therefore it is not possibile to get proper weighting spectrum without the model spectrum.

The program runs on an IBM PC/AT or compatible computer. An EGA (occasionally CGA) display or/and HP 7475A plotter, and the mathematical coprocessor are required. The running time strongly depends on the number of parameters of the model spectrum and their initial values, but usually does not exceed 8-10 minutes. The basic concept of program development was to make it "user friendly". (Eg it does not omit to inform the user on the progress in curve fitting, that is very important in case of "bad" input or/and complicated model spectrum.)

The program will be distributed by the IAEA Nuclear Data Section among the utility programs of the REAL-88 neutron spectrum adjustment reference file.
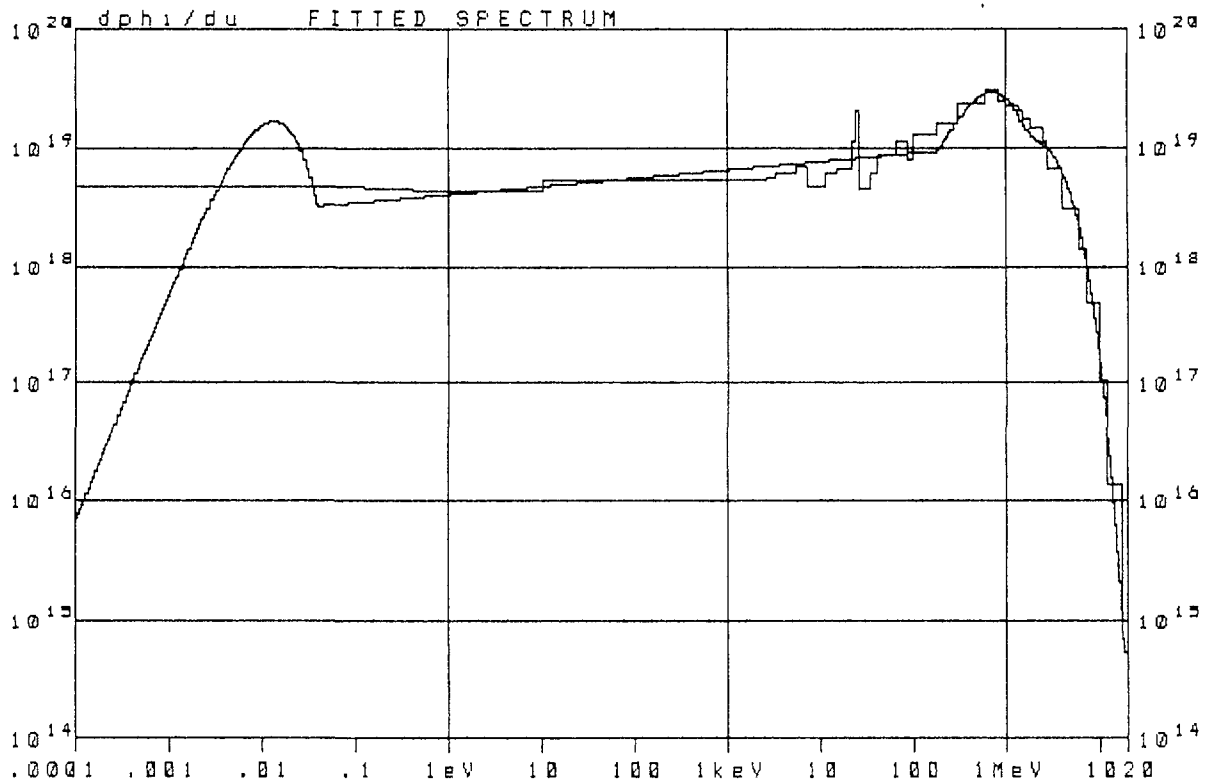
FIG. 3.

ACKNOWLEDGEMENT

REFERENCES

[1] D. E. Cullen: Frogram GROUPIE (version 79-1). Report UCRL-50400, Vol. 17, Part D. Lawrence Livermore Laboratory, July 1979.

[2] H. J. Nolthenius: Computer programs for calculating group cross-section covariances from uncertainty parameters in the ENDF/B-V format - UNC 32/33. Report ECN-202. Netherlands Energy Research Foundation, Petten, Oct. 1987.

[3] W. L. Zijp, É. M. Zsolnay, H. J. Nolthenius, E. J. Szondi: Final report on the REAL-84 exercise. Report ECN-212, BME-TR-RES-18/88, IAEA-NDS-212. Netherlands Energy Research Foundation, Petten, Nov. 1988.

[4] É. M. Zsolnay, H. J. Nolthenius: Proceedings of the IAEA Consultants' Meeting on the assesment of the results of the REAL-84 exercise. Report INDC(NDS)-190/G+F+R. IAEA, Vienna, March 1987.

[5] D. E. Cullen, P. K. McLaughlin: The international reactor dosimetry file (IRDF-85). Report IAEA-NDS-41, Rev. 1. IAEA NDS, Vienna, April 1985.

[6] W. N. McElroy et al: SAND II. Neutron flux spoectra determination by multiple foil activation iterative method. RSIC Computer Code Collection, CCC-112. Oak Ridge National Laboratory, Radiation Shielding Information Center, May 1969.

[7] W. W. Engle et al: ANISN. A one dimensional discrete ordinates transport code. RSIC Computer Code Collection, CCC-82. Oak Ridge National Laboratory, Radiation Shielding Information Center, March 1967.

[8] R. W. Roussin et al: VITAMIN-C. 171 neutron, 36 gamma-ray group cross sections in AMPX and CCCC interface formats for fusion and LMFBR neutronics. RSIC Data Library Collection, DLC-41. Oak Ridge National Laboratory, Radiation Shielding Information Center, July 1979.

[9] Ugray L.: Tobbváltozós fuggvény feltétel nélkuli lokális minimumá-nak meghatározása flexibilis poliéder módszerrel. (Determination of the local minimum of a multivariable function by the the flexibile polyeder method, in Hungarian). ESZK Tájékoztató 12 (1974) p. 108-116.

144

RESULTS OF CJD CALCULATIONS
ON THE REAL-88 PROJECT

K.I. ZOLOTAREV, A.B. PASHCHENKO, V.G. PRONYAEV
Institute of Physics and Power Engineering,
Obninsk, Union of Soviet Socialist Republics

Abstract

Calculation results of the rates of radiation damage in iron for the ANO, U-235, CFRMF, PS1 and PS2 neutron spectra unfolded by the measured reaction rates by means of the STAYSL code are presented. The cross-section files ZACRSS and BOSPOR, being developed in the USSR for neutron metrology are discussed. In the ENDF/B format the results of new evaluation of neutron radiation capture cross-sections for the ^{23}Na, ^{37}Cl, ^{55}Mn, ^{63}Cu, ^{139}La and ^{186}W isotopes are presented.

---

1. Adjustment of the REAL-88 Exercises with the STAYSL Adjustment Procedure.

Calculation within the frame of the REAL-88 investigation programme was carried out by means of the ES-1061 computer. Neutron spectra were unfolded by the given rates of reactions by means of the STAYSL [1] code. As for the rates of atomic displacement generation and helium and hydrogen production, they were calculated by the RDC code.

Microscopic cross-sections of the activation reactions were obtained from the IRDF-85 [2] and BOSPOR-86 [3] libraries.

Group cross-sections and covariance matrices of the reaction cross-section uncertainties used for neutron spectra unfolding were prepared by means of the UNC-33 code [4]

Preparation of group cross-sections to compute the rate of radiation damage generation in iron was performed by means of the FITOCO code [5] based on the multigroup data from the IRDF-85 library.

Table 1 shows calculation results of the rates of atomic displacement generation (R_{DPA}) and the rates of hydrogen (R_H) and helium (R_{He}) production in iron being irradiated in various neutron spectra. In the same table the χ^2 values are given which reflect the degree of agreement between the reaction rate values calculated in the unfolded spectrum and obtained experimentally.

Table 1.

Rates of radiation damage generation in iron
for neutron spectra of various facilities.

Spectrum type	Integral neutron flux, $n \cdot m^{-2} \cdot sec^{-1}$	χ^2	R_{DPA}, sec^{-1}	R_H, sec^{-1}	R_{He}, sec^{-1}
ANO	4.259E+13	2.03	7.571E-13	1.115E-18	1.162E-19
U-235 A	9.765E+20	140.98	8.537E-05	5.779E-10	3.230E-11
U-235 B	9.888E+20	138.89	8.636E-05	5.832E-10	3.250E-11
U-235 C	9.773E+20	52.75	8.511E-05	5.691E-10	3.126E-11
PS1	1.675E+14	28.96	3.917E-12	1.181E-17	6.438E-19
PS2	2.203E+14	190.78	4.256E-12	8.326E-18	5.584E-19
CFRMF A	8.783E+20	275.39	3.500E-05	1.217E-10	7.204E-12
CFRMF B	8.912E+20	232.14	3.566E-05	1.240E-10	7.240E-12

Calculations for the ANO, PS1 and PS2 spectra were performed using reaction cross-sections data only from the IRDF-85 library. When processing the data on PS1 we assumed that all the nine detectors were irradiated in the gadolinium filter of 0,5 mm in thickness $(1,523 \cdot 10^{-3}$ atoms/barn), with the neutron flux being isotropic. The PS2 neutron spectrum unfolding was performed on assuming that all the 6 detectors were irradiated without any filter.

It is necessary to point out that the great value of χ^2 for the PS1 spectrum is define mainly by the ^{58}Fe$(n,\gamma)^{59}$Fe detector.

For CFRMF two versions of calculation were prepared, where:

a) for all the 23 reactions the cross-section values from IRDF-85 were used;

b) the cross-section of the ^{47}Ti$(n,p)^{47}$Sc reaction was obtained from the BOSPOR-86 library and the data on the rest 22 reactions were taken from IRDF-85.

When determining the rates of radiation damage in iron irradiation in the U-235 fission spectrum, three versions of calculation were performed: A, B and C. In two versions (A and B) for neutron spectra to be unfolded the experimental data were specified for all the detectors, that is the information on the rates of 22 reactions was used. In the case in the A version the data on cross-sections of all the reactions were taken from the IRDF-85 library. In the B version the ^{47}Ti$(n,p)^{47}$Sc reaction cross-section was specified from the BOSPOR library, as for the cross-section values of the rest of the reactions, they were obtained from IRDF-85. From Table 1 it is clearly seen that application of the evaluated cross-section data for the ^{47}Ti$(n,p)^{47}$Sc reaction from the BOSPOR-86 library results in reducing the χ^2 value both when unfolding the CFRMF neutron spectrum and when determining the U-235 fission spectrum.

The first two calculation versions of unfolding the U-235 fission spectrum reveal a relatively great discrepancy between the ^{58}Ni$(n,2n)^{57}$Ni reaction data and the data on other high-threshold reactions. Calculations (version C) performed with the reaction cross-section data identical to those used in version B but without application of any information on the ^{58}Ni$(n,2n)^{57}$Ni reaction present a much lower value of χ^2 (see Table 1).

The discrepancy mentioned above evidently results from the fact that the data on the (n,2n) reaction cross-section for the ^{58}Ni isotope, contained in the IRDF-85 file need correction. It should be pointed out that the comparison

between the calculated values of the average reaction cross-sections in the Cf-252 spontaneous fission neutron spectrum and the evaluated experimental data for this spectrum [12] indicates that the (n,2n) reaction cross-section data for the ^{127}I and ^{55}Mn isotopes, contained in the IRDF-85 library, as well as the $^{58}Ni(n,2n)^{57}Ni$ reaction data require revaluation.

Figures 1-5 in their group presentation show a trial spectrum and a spectrum unfolded by means of the STAYSL code by the given reaction rates for five various facilities: ANO, U-235 (version C), PS1, PS2 and CFRMF (version B). All the values of the $E \cdot \varphi(E)$ function are given in absolute units. The trial spectra being used are presented normalized. Normalizing factors for initial trial spectra are determined from the equation:

$$K = \sum_{i=1}^{n} (R_i^c/R_i^m) / \sum_{i=1}^{n} (R_i^c/R_i^m)^2 ,$$

where R_i^c and R_i^m are the i-reaction rate values calculated in the initial trial spectrum and measured, respectively, n is the number of reactions used for neutron spectrum unfolding.

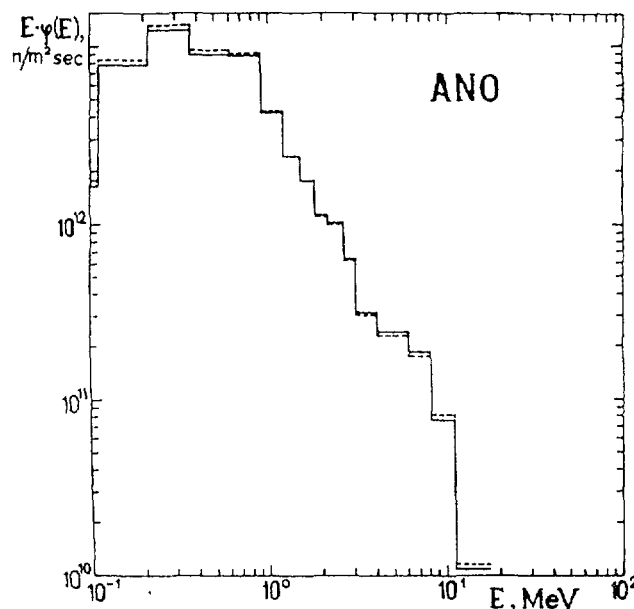
Fig.1. Prior (------) and unfolded by measured reaction
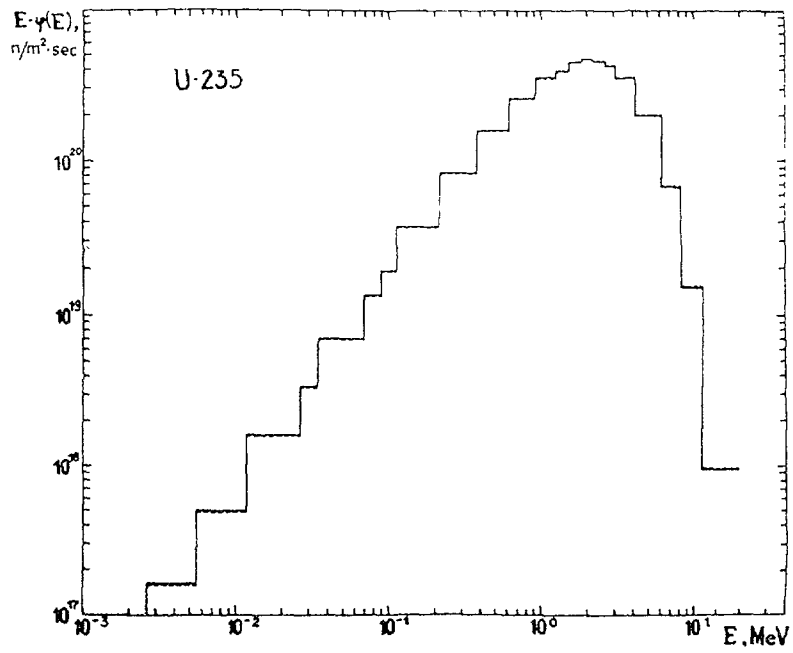rates neutron spectrum (--------) for ANO facility.
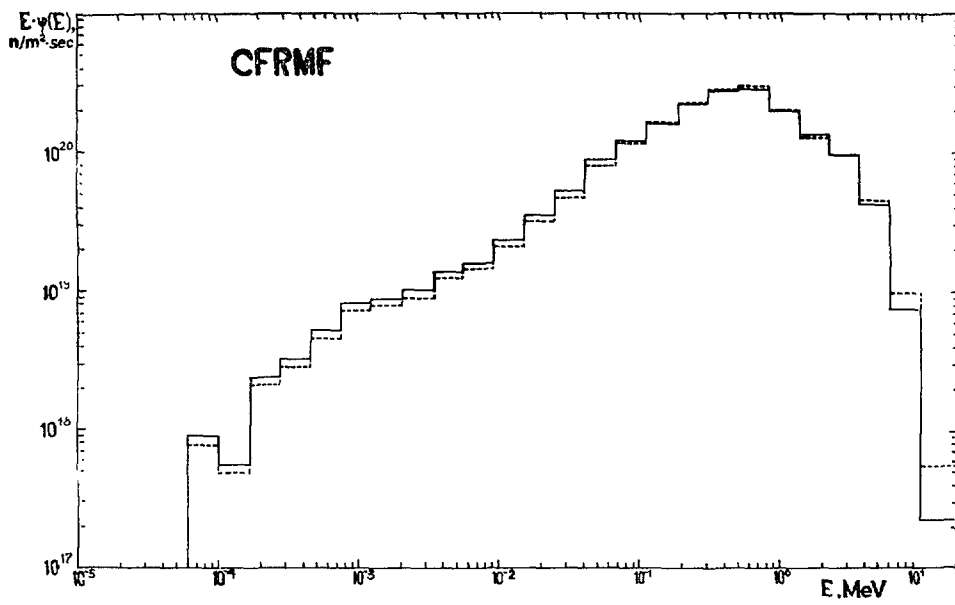
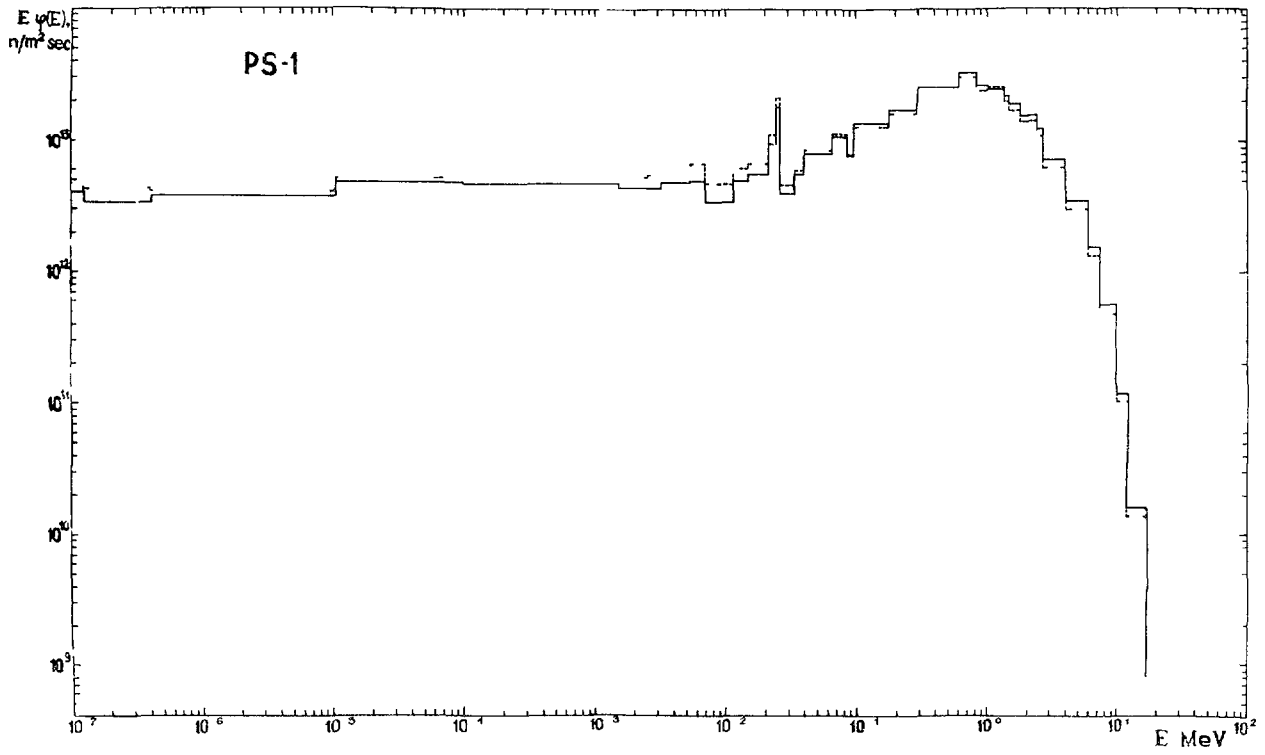Fig.2. The same for U-235.
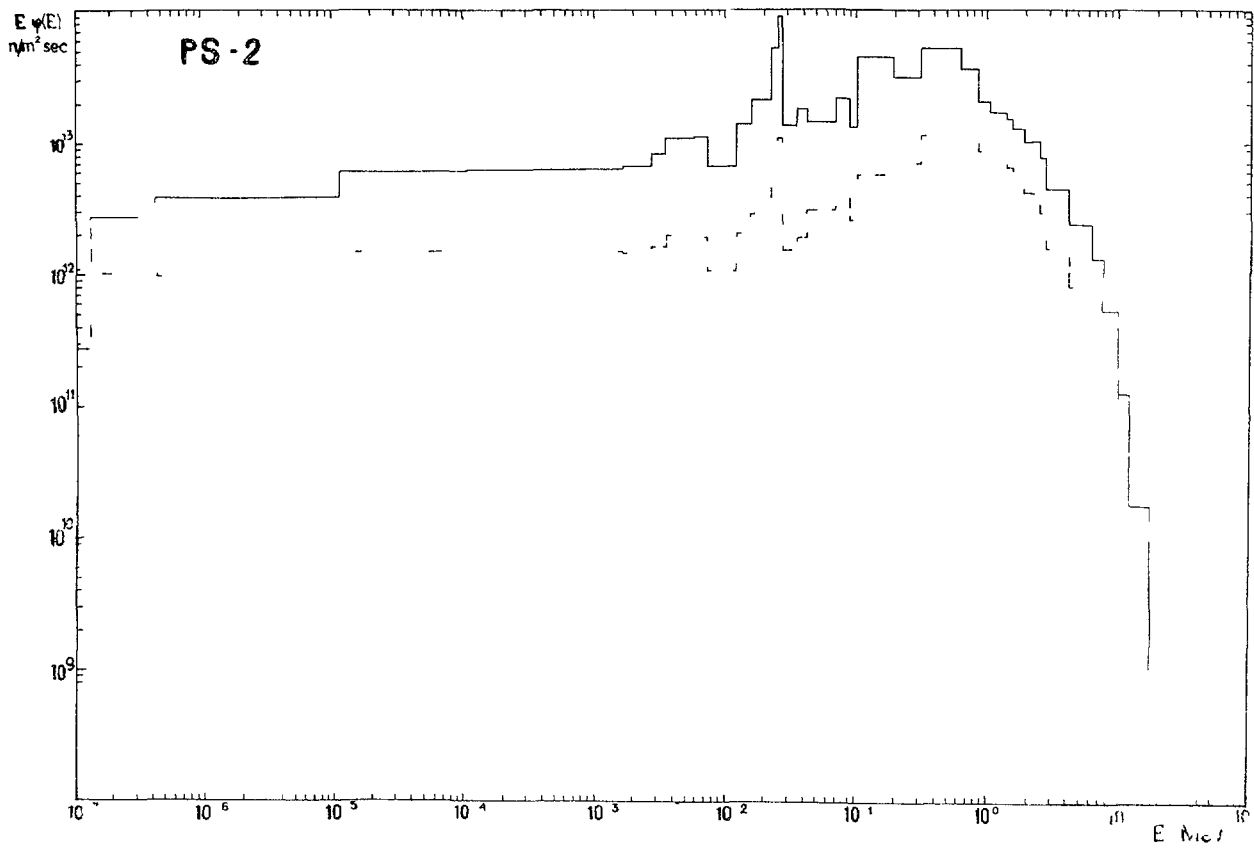

Fig.3. The same for CFRMF.

Fig.4. The same for PS1.

Fig.5. The same for PS2.

150

As it was mentioned earlier, for unfolding U-235 and CFRMF neutron spectra the $^{47}Ti(n,p)^{47}Sc$ reaction cross-section data were taken from the BOSPOR-86 library. The status of this file will be discussed in more detail in the next section.

2. Cross-section files being developed in the USSR for neutron metrology.

In the USSR two libraries of the evaluated cross-sections for reactor dosimetry have been prepared, they are ZACRSS [6] and BOSPOR [7].

ZACRSS was developed in 1975 by Lapenas A. et al. in the Latvian Institute of Physics. It includes excitation functions of 24 threshold activation reactions, most frequently used for neutron spectra unfolding by the measured reaction rates. Cross-section evaluation for ZACRSS was based on processing the available experimental data by the method of least squares.

BOSPOR, which means the library of evaluated threshold reaction cross-sections, was organized in 1980 in Nuclear Data Center by Bychkov V. et al. It contains 142 recommended excitation functions of the (n,p), (n,α) and (n,2n) reactions for 99 stable isotopes of 59 elements.

Evaluation of activation reaction cross-sections was based on the prepared compilation of experimental data [8] using calculations on the basis of theoretical models of nuclear reaction.

Critical analysis of all the experimental data results in choosing, from our point of view, the most significant values of the cross-sections measured. It means that the preference was given to the investigations performed with application of enriched isotopes and semiconductor detectors, their results being in agreement within the error limits of the experiment. The data significantly different from the other authors results being in good agreement, were not considered.

To obtain the cross-sections recommended the excitation functions of all reactions under analysis and the competing reactions were calculated within the frame of the optico-

statistical approach with taking into account of the reaction non-equilibrium mechanism contribution. Figures 6 and 7 show as an example calculation results [9] of α-particle emission spectra on the ^{50,52}Cr, ^{90}Zr and ^{93}Nb isotopes.

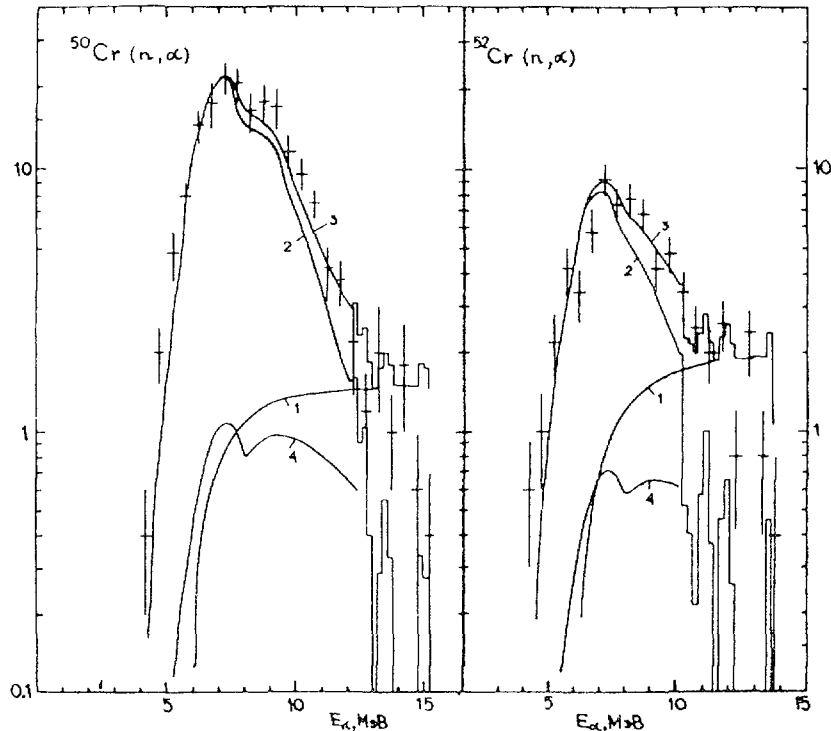Fig.6. The calculation results of α-particle emission spectra for chromium isotopes in comparison with the experimental data for ~15 MeV incident neutron energy. The spectrum contributions of different nuclear reaction mechanisms are shown by different lines.

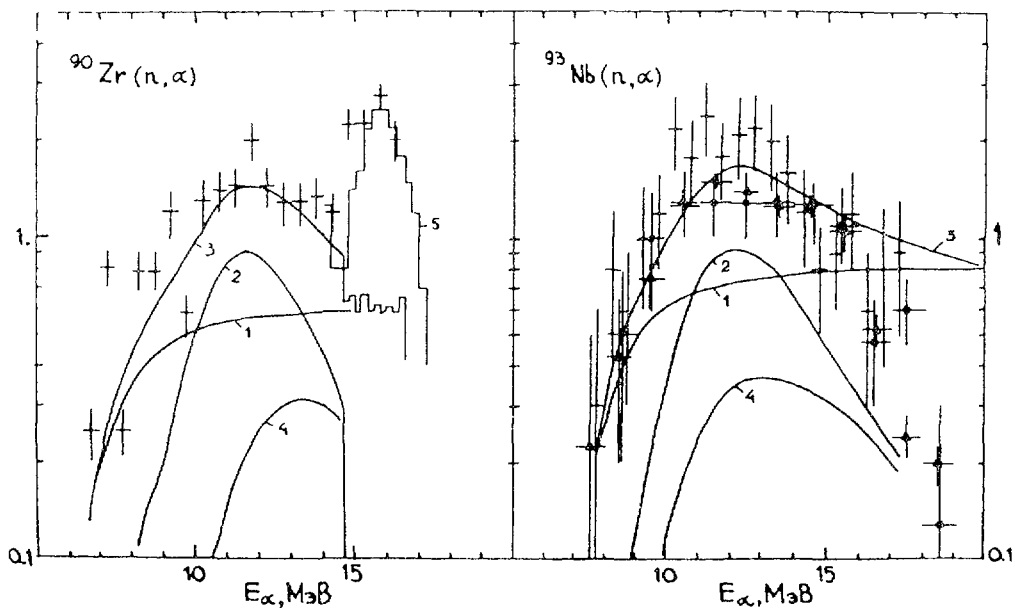Fig.7. The same for ^{90}Zr and ^{93}Nb.

The main reason for developing and applying such a method of evaluation of threshold reaction excitation functions consists in the fact that the experimental information is obviously insufficient for reliable cross-section evaluation within the energy interval up to 20MeV. Moreover, the data of various authors often differ much greater than the measurement errors presented.

Microscopic cross-section analysis with some calculations in frame of the theoretical nuclear reaction models makes it possible to compare the results of the experiments carried out at various energies and at various resolutions. The analysis enables to use all additional information, extracted from a more broad range of nuclear data, for evaluation of a certain cross-section with the help of some known theoretical relatioships. It results, firstly, to exclude obviously incorrect data from all the nuclear data compilation available, and, secondly, to evaluate the reaction cross-sections for those ranges of incident-particle energies and target nuclei mass numbers, where we have no experimental data.

When evaluating the threshold reaction excitation functions, the point with the incident-neutron energy of 14-15 Mev was considered to be very important. Almost always either the (n,p), (n,α) and (n,2n) reaction cross-sections were measured at this energy, or the experimental data for this point were much more numerous than for all the rest of the energy intervals. Systematizing a large body of experimental material some tendencies can be seen and dependences can be found in the behavior of the 14-MeV-neutron reaction cross-sections. In the papers [8] the following investigations were carried out:

a) based on the model of sequential particle emission with taking into account of non-equilibrium neutron emission in the first step of the reaction, as well as on the Weizsäckers' formula for nuclear binding energy we got a simple dependence of the (n,2n) reaction cross-section on the number of protons and neutrons in the nucleus at the incident neutron energy of ~14,5 MeV. The isotopic cross-section dependence is shown to be connected with the

dependence of nuclear neutron binding energy on the (N-Z)/A parameter;

b) based on the usual statistical correlations for a nuclear reaction cross-section and the Weizsäckers' formula for nuclear binding energy we got a simple dependence of the (n,p) reaction cross-section on the number of neutrons and protons in the nucleus at the incident-neutron energy of ~14,5 MeV. The observed dependence of the (n,p) reaction cross-section on the (N-Z)/A parameter is shown to result from the exponential dependence of the reaction cross-section on the proton binding energy in the nucleus;

c) we carried out a statistical analysis of cross-section prediction reliability and evaluated the accuracy of σ_{n2n} and σ_{np} calculations in terms of the formulas obtained. The formulae deduced are shown to be possibly used for prediction of the (n,p) and (n,2n) reaction cross-sections at E_n~14-15 MeV for those nuclei on which there are no experimental data.

Simplifying assumption and approximations used when deriving the formulae for σ_{np} and σ_{n2n} calculations at E_n~14-15 MeV enable to see the limits of their applicability and to explain the cases of discrepancy between the results of comparison of the experimental cross-section values and the values predicted in terms of the empirical systematics.

The BOSPOR-80 library has gained ground in our country and was included in the INDL/V file of the IAEA Nuclear Data Section in the ENDF/B format.

Recently some new experimental data have been obtained and theoretical methods of threshold reaction cross-section analysis and predictions have been further developed. For this reason and with allowance for the experience of its operation the BOSPOR-80 library was revised and its new extended version BOSPOR-86 [3] was created. Now it includes the errors of the cross-sections recommended. They were evaluated with due account of the analysis of the experimental data errors, theoretical calculation uncertainties and discrepancies between the data recommended from other libraries. Moreover, for the

154

cross-sections of some most important in neutron metrology threshold reactions with the charged particle emission (16 (n,p) and (n,a) reactions) their analytical approximation was carried out near the reaction threshold, thus allowing us to improve the agreement between the results of cross-section evaluation and the integral data.

At the previous meeting on nuclear data for radiation damage [10] significant discrepancies were pointed out between the experimental integral data and the reference spectra-averaged cross-sections of the ^{47}Ti(n,p)^{47}Sc, ^{60}Ni(n,p)^{60}Co and ^{63}Cu(n,a)^{60}Co reactions from the ENDF/B-V file; these cross-sections were recommended to be revaluated. Table 2 gives the comparison between the experimental data and the calculated results of the U-235 and Cf-252 spectra averaged cross-sections of these reactions from BOSPOR-86 and ENDF/B-V, as well as the average cross-sections of the ^{47}Ti(n,p)^{47}Sc reaction, jointly evaluated by V.Mannhart, D.Smith and W.Medows [11].

For the ^{47}Ti(n,p)^{47}Sc reaction the experimental data and calculations show a reasonable agreement where as for the ^{60}Ni(n,p)^{60}Co reaction the discrepancy still exist.

Table 2.

Cross-sections of the ^{47}Ti(n,p)^{47}Sc, ^{60}Ni(n,p)^{60}Co and ^{63}Cu(n,a)^{60}Co reactions for the Cf-252 and U-235 fission spectra.

neutron field	Reaction	Experiment	Calculation		
			BOSPOR-86	ENDF/B-V	Evaluation
Cf-252	^{47}Ti(np)^{47}Sc	19,43±0,31[12]	18,87	24,066	19,73
	^{60}Ni(np)^{60}Co	2,39±0,13[12]	3,553	3,444	–
	^{63}Cu(na)^{60}Co	0,6897±0,013[12]	0,694	0,7581	–
U-235	^{47}Ti(np)^{47}Sc	17,7±0,6 [11]	16,90	21,589	–
	^{60}Ni(np)^{60}Co	2,3±0,4 [13]	2,639	2,529	–
	^{63}Cu(na)^{60}Co	0,50±0,06[13]	0,510	0,540	–

3. Evaluation of neutron radiative-capture cross-sections on the ^{23}Na, ^{37}Cl, ^{55}Mn, ^{63}Cu, ^{139}La and ^{186}W isotopes.

Activation detectors on the basis of such reactions as ^{186}W$(n,\gamma)^{187}$W, ^{23}Na$(n,\gamma)^{24}$Na, ^{37}Cl$(n,\gamma)^{38}$Cl, ^{55}Mn$(n,\gamma)^{56}$Mn, ^{63}Cu$(n,\gamma)^{64}$Cu and ^{139}La$(n,\gamma)^{140}$La, along with other activation detectors are widely used for measuring of neutron fluxes and spectra in nuclear power reactors and critical assemblies. Accuracy of the data obtained by means of such detectors directly depends on accuracy of the activation reaction cross-sections. Thus, the problem of evaluation of the reaction cross-sections used in activation measurements was always of great importance.

In 1982 under the aegis of IAEA the International Reactor Dosimetry File, IRDF-82, was established. It was recommended to be used when solving the wide range of problems concerning reactor dosimetry.

In 1985 a new version of this file, IRDF-85, appeared. The IRDF-85 library includes 60 sets (MAT) of evaluated data on cross-sections of various neutron reactions. 18 data sets contain information on cross-sections of the neutron reactions resulting in hydrogen and helium production. In 4 sets the data concern radiation damage cross-sections for iron, chromium and nickel. The library section containing information on cross-sections of the reactions used in neutron metrology, includes 38 data sets. They present the evaluated energy dependence of the cross-sections of 51 reactions on 35 isotopes.

Of all the reactions under consideration in the IRDF-85 library there are data on the cross-sections of only two reactions: ^{23}Na$(n,\gamma)^{24}$Na (MAT=6311) and ^{63}Cu$(n,\gamma)^{64}$Cu (MAT=6435). The data sets MAT=6311 and MAT=6435 were included in the IRDF-85 library from the ENDF/B-V American dosimetry file [14]. This file was passed to the users in 1978. A partial revision of the ENDF/B-V American dosimetry file, performed in 1981 and 1984 did not touch upon the data sets mentioned above. Thus, the evaluated data on the ^{23}Na$(n,\gamma)^{24}$Na and ^{63}Cu$(n,\gamma)^{64}$Cu reaction cross-sections

contained in the IRDF-85 library, are based on the information obtained before 1978.

The users can find the available data on the $^{55}Mn(n,\gamma)^{56}Mn$ reaction cross-section in the American ENDF/B-IV library [15] (MAT=1197) and in the Japanese JENDL-2 library [16] (MAT=2251). Evaluation of the reaction cross-section in the ENDF/B-IV library was carried out in 1974, as for the JENDL-2 library, it obtained the evaluated data in 1982.

For the $^{139}La(n,\gamma)^{140}La$ and $^{186}W(n,\gamma)^{187}W$ reactions there are cross-section data in the ENDF/B-V (MAT=9707) [17,18] and ENDF/B-IV (MAT=1131) libraries, respectively. Evaluation of neutron cross-sections for the La-139 isotope (MAT=9707) was made by R.E.Schenter and F.Schmittroth in 1980. For the W-186 isotope the data contained in MAT=1131 were evaluated in 1973.

Attention to the $^{37}Cl(n,\gamma)^{38}Cl$ reaction was caused by the fact that the detector based on this reaction is one of a few activation detectors giving information on a neutron spectrum in the Kilo-electron-Volt energy range. According to the CINDA catalogue at present there is no evaluated data on the cross-section of this $^{37}Cl(n,\gamma)^{38}Cl$ reaction.

The reason to review and evaluate the cross-section values of 6 above mentioned dosimetry reactions [19] consists in the fact that recently some new experimental data and methods of cross-section analysis within the frame of the present-day theoretical knowledge have appeared.

When evaluating the radiative capture cross-sections all the collection of the experimental data on neutron cross-sections for each target isotope was taken in to account.

The neutron radiative capture cross-section was in agreement with the total cross-section, with the cross-sections of elastic and inelastic scattering and other competing processes.

The resonance capture integral values and the thermal cross-sections (E=0,0253 eV) served as the main criteria of evaluation quality. For evaluated cross-sections' testing in the regions of higher energies the average cross-section

values were calculated in five various benchmarks: CFRMF, BIG-TEN, SIGMA-SIGMA, the U-235 thermal neutron induced fission neutron spectrum, the Cf-252 spontaneous fission neutron spectrum. The average radiative capture cross-section values calculated were compared with the available experimental data and the data of other evaluations.

3.1 General principles of evaluation of neutron radiative capture reaction cross-sections.

All the range of neutron energies from 10^{-5}eV up to 20 Mev, where the radiative capture cross-section was evaluated can be conditionally divided into three energy regions: the resolved resonance region, the unresolved resonance region and the smooth-cross-section region.

A. Resolved resonance region.

Cross-section evaluation in this region is based, mainly, on the resonance parameters, presented in [20] and supplemented as far as possible with the new experimental data available. Figures of cumulative number of resonances were used when choosing the highest energy boundary of the resolved resonance region without substantial omission of the s-, p- or d-wave resonances, contributing to the radiative capture cross-section. For many resonances given in [20] the values of spin and parity were not identified. These values were assigned by us, proceeding from a number of physical assumptions, including: the (2j+1) spin distribution of resonances, approximately equal level density values for levels with near the same spin, but opposite parity, weak deviation from a linear dependency of cumulative number of resonances with energy. When possible, we considered the value of the capture area under resonance:

$$A_\gamma^\nu = g\frac{\Gamma_n^\nu \cdot \Gamma_\gamma^\nu}{\Gamma_{tot}^\nu}$$

Such identification is surely rather conditional, however it doesn't disagree with all the known collection of experimental data. The choice of neutron and radiative

158

widths for resonances, where they were known, was based on the average radiative and reduced neutron widths and was also rather conditional but not contradicting the data available. Besides the experimental data with high energy resolution enabling to distinguish the capture area for separate resonances, there are usually the data with relatively low energy resolution but determining the average cross-section values in the region of resolved resonances with high accuracy. The radiative capture cross-sections derived in terms of the resonance parameters and averaged in the region of resolved resonances were compared with such data to evaluate the resonance omission. When such an omission was observed we introduced a group of fictitious resonances with the parameters which adjusted the average cross-sections up to the necessary level.

B.Unresolved resonance region.

The unresolved resonance region was chosen, as a rule, from the upper limit of the resolved resonance region up to the threshold of inelastic scattering.

The choice of parameters and the description of cross-sections in the region of unresolved resonances were carried out by means of the EVPAR code [21].

As initial approximation in calculations we used the average resonance parameters evaluated for the region of resolved resonances. Then, if necessary, the parameters were corrected so as to describe the experimental data available in this region. In this case, as in the range of resolved resonances, a number of simple physical assumptions was used connecting average distances between the levels with different spins and parities. As at the neutron energy, exceeding several hundred keV, the f-wave capture cross-section value became considerable and the existing format restrictions did not allow to introduce the average resonance parameters for the f-wave, its contribution was considered as a background component in the smooth cross-section file.

C. Smooth cross-sections region.

Cross-sections for neutrons with energies above the region of unresolved resonances are presented in the point-wise representation.

As the EVPAR code makes it possible to take into account only the s-, p-, d- and f-waves' contribution into the cross-section within the frame of the statistical theory, its applicability is restricted by the region, where the contribution of much higher waves is negligible. These boundaries for various nuclei are within the energy range from 1 MeV up to several MeV. Calculations in the smooth cross-section range were performed with the same parameters as those used for the region of unresolved resonances and with the schemes of inelastic scattering levels from the latest issues of "Nuclear Data Sheets".

For cross-section evaluation in the region of neutrons of much higher energy the optical and statistical calculations were usually used according to the ABAREX code [22]. The direct-semidirect processes' contribution was considered in the frame of the most simple parametrized scheme. For some reactions the cross-sections smoothly joined those presented in the IRDF-85 and JENDL-2 files. Note, however, that the detailed shape of cross-section dependence in this region is insignificant for the problem of unfolding fission reactor neutron spectra of any hardness.

As the total cross-section evaluation results along with the dosimetry reaction cross-section values must be included in the general purposes data file, it has been performed within the same approach as the capture cross-section evaluation. When calculating cross-sections of elastic scattering reaction (in the region of unresolved resonances), the potential scattering radius value was taken from [20] and varied, if necessary, proceeding from the condition of simultaneous description of the total cross-section and the cross-section of elastic scattering reaction.

D. Reference spectra cross-section testing.

A comparison of the resonance integrals of radiative capture for the evaluated cross-section data with the corresponding experimental results allows us to judge the quality of the radiative capture cross-section evaluation performed only in the region of resolved resonances.

For testing the evaluated data in other energy regions the average cross-section values were calculated in five various reference neutron fields (benchmarks): CFRMF, BIG-TEN, SIGMA-SIGMA, the spectrum of U-235 fission by thermal neutrons, the neutron spectrum of Cf-252 spontaneous fission [23]. The first three benchmarks are the neutron reference fields of intermediate energies. The average neutron energy in these benchmarks is equal to 0,76 MeV (CFRMF), 0,58 MeV (BIG-TEN) and 0,76 MeV (SIGMA-SIGMA). For CFRMF and BIG-TEN facilities the average energy values correspond to the centrally located neutron spectrum. By these benchmarks the radiative capture cross-sections in the upper region of resolved resonances and in the region of unresolved resonances can be tested.

The spectrum of U-235 fission by thermal neutrons and the neutron spectrum of Cf-252 spontaneous fission are the classical fast neutron spectra. The average neutron energies of these spectra are known to be equal to 1,97 MeV (U-235) and 2,13 MeV (Cf-252). Thus, the U-235 and Cf-252 neutron fission spectra are convenient for testing cross-sections in the energy range exceeding ~0,1 MeV, i.e. in terms of the earlier adopted terminology, in the smooth cross-section region of radiative capture.

The average cross-section values calculated in five enumerated benchmarks were compared with the available data of integral experiments and the results of other evaluations. Unfortunately we failed to find any experimental data on neutron radiative capture cross-sections on the Cl-37 and W-186 isotopes for none of the benchmarks under consideration. The experimental data on the ^{139}La$(n,\gamma)^{140}$La reaction cross-section were found only for the CFRMF neutron spectrum [24]. As for the rest three reactions under evaluation, there exists much more ample experimental information [25-30].

When calculating the average cross-section values of five enumerated benchmarks, the data on neutron spectra for these neutron fields were obtained from the IRDF-85 library. For the spectrum of U-235 fission by thermal neutrons two spectrum evaluations, contained in the IRDF-85 library, were used: NBS and ENDF/B-V.

Table 4 and 6 present the testing results of the cross-sections evaluated in the U-235 and Cf-252 spectra. Along with the average cross-section values in the spectrum the energy boundaries for 90% response ranges are given, thus making it possible to speak about the energy interval of the reaction cross-section region being tested.

E. Cross-section evaluation results.

^{23}Na$(n,\gamma)^{24}$Na reaction. The results of the ^{23}Na$(n,\gamma)^{24}$Na cross-section evaluation in the 640 group presentation are depicted in Fig.8 in comparison with the IRDF-85 evaluation and the experimental data available. As it was mentioned earlier, the ^{23}Na$(n,\gamma)^{24}$Na reaction cross-section data were comprised into the IRDF-85 library from the ENDF/B-V dosimetry file of 1984.

The comparison of thermal cross-sections and resonance integrals of radiative capture from [20] and the IRDF-85 with the present evaluation results shows (Table 3), that they are in agreement within the limits of the errors assigned. However for the energy region exceeding 330keV evident discrepancies (up to 30-50%) exist in many groups, thus resulting in some disagreements in the integral cross-sections for the hard spectrum benchmarks (Tables 4-6). For the neutrons with energies exceeding 600 keV the cross-sections of the present evaluation were chosen to be coinciding with the IRDF-85 data.

Fig.8. The ^{23}Na(n,γ)^{24}Na reaction cross-section.

———— present evaluation,

------- IRDF-85 evaluation.

Experimental data: ■ -[31], ▭ -[32], ⊕ -[33],
○ -[34], ⊕ -[35], △ -[36], □ -[37], ⬤ -[38],
◊ -[39].

Table 3.

Radiative capture cross-sections (σ_γ^0) for thermal energy neutrons $(E_n=0,0253$ eV) and radiative capture resonance integral values (I_γ) as a results of different evaluation.

Reaction	Evaluation Data	σ_γ^0, barn	I_γ, barn
$^{23}Na(n,\gamma)^{24}Na$	Mughabghab et.al.[20] IRDF-85 [2] Present evaluation	0,530±0,005 0,528 0,527	0,311±0,010 0,316 0,314
$^{37}Cl(n,\gamma)^{38}Cl$	Mughabghab et.al.[20] Experimental data[45] Present evaluation	0,433±0,006 0,433	0,30 ±0,04 0,213±0,009 0,211
$^{55}Mn(n,\gamma)^{56}Mn$	Mughabghab et.al.[20] JENDL-2 [16] Present evaluation	13,3 ±0,2 13,32 13,30	14,0 ±0,3 14,6 14,6
$^{63}Cu(n,\gamma)^{64}Cu$	Mughabghab et.al.[20] IRDF-85 [2] Present evaluation	4,50 ±0,02 4,50 4,48	4,97 ±0,08 5,63 4,98
$^{139}La(n,\gamma)^{140}La$	Mughabghab et.al.[20] ENDF/B-V [17] Present evaluation	8,93 ±0,04 9,00 8,91	11,8 ±0,8 12,0 12,1
$^{186}W(n,\gamma)^{187}W$	Mughabghab et.al.[20] ENDF/B-IV [15] Present evaluation	37,9 ±0,6 37,61 37,89	485 ± 15 520 481,7

Table 4.

Microscopic integral cross-sections in the U-235
thermal neutron induced fission neutron spectrum.
(Calculated values refer to the NBS spectrum evaluation)

Reaction	Evaluation Data	$\bar{\sigma}$,mbarn	90%responce ranges, MeV
^{23}Na$(n,\gamma)^{24}$Na	Experimental data	–	–
	IRDF-85 [2]	0,2817	0,053–4,30
	Present evaluation	0,3282	0,055–4,10
^{37}Cl$(n,\gamma)^{38}$Cl	Experimental data	–	–
	Present evaluation	0,5054	0,105–3,30
^{55}Mn$(n,\gamma)^{56}$Mn	Experimental data	–	–
	JENDL-2 [16]	3,002	0,021–3,60
	Present evaluation	2,983	0,019–3,60
^{63}Cu$(n,\gamma)^{64}$Cu	Experimental data[26]	9,30 ±1,40	–
	IRDF-85 [2]	10,08	0,055–3,80
	Present evaluation	10,82	0,063–3,70
^{139}La$(n,\gamma)^{140}$La	Experimental data	–	–
	ENDF/B-V [17]	6,564	0,066–3,60
	Present evaluation	7,209	0,066–3,70
^{186}W$(n,\gamma)^{187}$W	Experimental data	–	–
	ENDF/B-IV [15]	37,29	0,092–3,00
	Present evaluation	32,81	0,076–3,10

Table 6.

Microscopic integral cross-sections in the Cf-252
spontaneous fission neutron spectrum.

Reaction	Evaluation Data	$\bar{\sigma}$,mbarn	90%responce ranges, MeV
^{23}Na$(n,\gamma)^{24}$Na	Experimental data[28] IRDF-85 [2] Present evaluation	0,335±0,015 0,2712 0,3139	– 0,055–4,70 0,060–4,50
^{37}Cl$(n,\gamma)^{38}$Cl	Experimental data Present evaluation	– 0,4827	– 0,115–3,50
^{55}Mn$(n,\gamma)^{56}$Mn	Experimental data[28] JENDL-2 [16] Present evaluation	2,96 ±0,21 2,840 2,815	– 0,027–3,90 0,026–3,90
^{63}Cu$(n,\gamma)^{64}$Cu	Experimental data[25] IRDF-85 [2] Present evaluation	10,55±0,32 9,650 10,35	– 0,066–4,00 0,076–3,90
^{139}La$(n,\gamma)^{140}$La	Experimental data ENDF/B-V [17] Present evaluation	– 6,325 6,971	– 0,080–3,80 0,084–3,90
^{186}W$(n,\gamma)^{187}$W	Experimental data ENDF/B-IV [15] Present evaluation	– 35,56 31,29	– 0,010–3,00 0,088–3,20

$^{37}Cl(n,\gamma)^{38}Cl$ reaction. The results of the ^{37}Cl neutron capture cross-section evaluation in the region of resolved resonances (10^{-5} eV-100 keV) are based on Macklin's data [40]. The cross-section evaluation for the neutrons energy range from 100 keV up to 20 MeV was performed within the frame of optical and statistical calculations, with the direct-semidirect capture being considered, on the basis of the experimental data available [41-43]. Table 3 shows great discrepancy between the resonance capture integral value, presented by Mughabghab [20] and evidently based on Gleason's investigations [44], on the one hand, and the present evaluation results, on the other. The resonance capture integral obtained in the course of present evaluation by calculations in terms of the resonance parameters evaluated, shows a good agreement with the results of independent measurement [45] (I_γ=0,213±0,009).

$^{55}Mn(n,\gamma)^{56}Mn$ reaction. There is a great spread in experimental data for this reaction. The region of resolved resonances was chosen from 10^{-5} eV up to 100 keV, the region of unresolved resonances - from 100 keV up to 800 keV. For neutrons with the energy of 800 keV - 1,3 MeV the evaluated data were obtained by the EVPAR code calculations with the average resonance parameters, taken from the region of unresolved resonances. For neutrons of higher energy the data were mainly taken from the JENDL-2 library. A good agreement of cross-section values is observed in the thermal neutron energy region, but the resonance capture integral value appears to be somewhat higher than the one, given in [20] (Table 3). A prominent discrepancy (up to 20%) exists when comparing with the integral cross-sections for reference spectra of the BIG-TEN-type assembly.

$^{63}Cu(n,\gamma)^{64}Cu$ reaction. Comparison of the capture cross-section evaluated in the given work with the data from IRDF-85 and the available experimental data [31-32, 46-53] is shown in Fig.9. The region of resolved resonances was chosen from 10^{-5} eV up to 50 keV, as for the region of unresolved resonances, it covered the range from 50 keV up
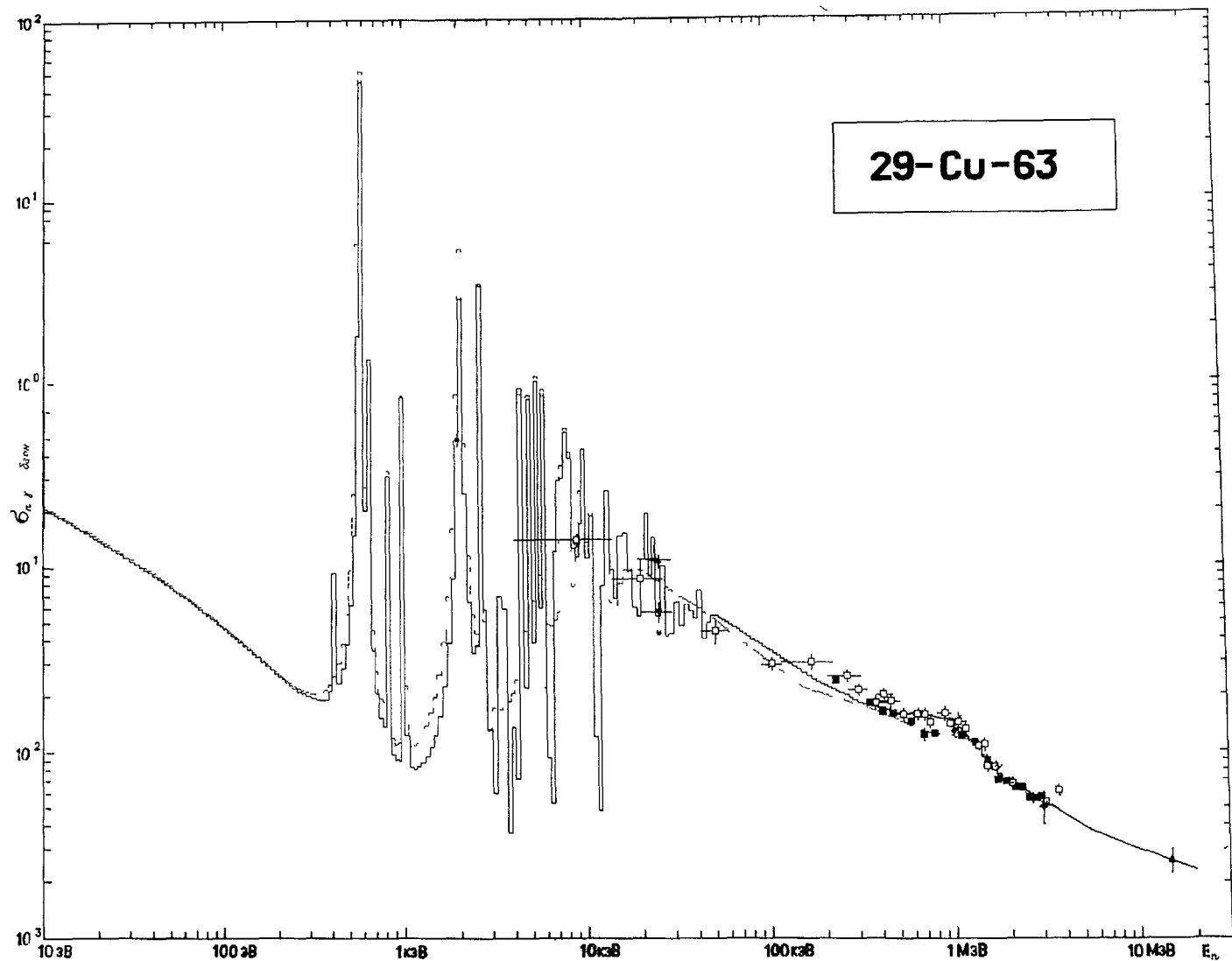
Fig.9. The $^{63}Cu(n,\gamma)^{64}Cu$ reaction cross-section.
——————— present evaluation,
- - - - - - IRDF-85 evaluation.

Experimental data: ▭ -[31], ▽ -[32], △ -[33], ♦ -[46], ◊ -[47], ▢ -[48], ▮ -[49], ✳ -[50], ⚜ -[51], ▼ -[52].

to 200 keV. For the neutron energy exceeding 2.5 MeV the cross-section values for evaluation were taken from IRDF-85. Unlike the IRDF-85 data, the cross-section value obtained in the present work is significantly lower for E_n=300 eV- 3 keV and somewhat higher for E_n=20 keV - 1 MeV. A distinct disagreement should be noted between the data on neutron capture cross-section for ^{63}Cu, ^{65}Cu and natural isotopic mixture at E_n=25 keV [54]. It points to the fact that the accuracy, characteristic of the known ^{63}Cu capture cross-sections for neutrons of this energy, cannot be high. The present evaluation improves the agreement with the data available in all the integral experiments except the BIG-TEN-type assemblies, where the predicted integral cross-section value turns out to be by 4% higher than that observed during the experiments.

^{139}La(n,γ)^{140}La reaction. In the present evaluation the region of resolved resonances was chosen from 10^{-5} eV up to 20 keV, the region of unresolved resonances covered the range from 20 keV up to 150 keV. Point-wise cross-section representation was used for higher energies. Table 3 shows cross-sections for thermal neutrons with the energy of 0.0253 eV and resonance capture integrals in terms of various evaluations. It should be noted that in the neutron energy range from 3 up to 80 keV the presently evaluated cross-section values are by 10 - 15% higher than the evaluation results according ENDF/B-V.

^{186}W(n,γ)^{187}W reaction. The region of resolved resonances covered the range from 10^{-5} eV up to 8.5 keV, the region of unresolved resonances - from 8,5 keV up to 120 keV. The resonance parameters evaluation in the unresolved region was based on new experimental data on the total cross-section and the radiative capture cross-section from works [55-58]. Within the energy range from 120 keV up to 1,6 MeV and in the region of unresolved resonances the cross-section evaluation was performed by means of the EVPAR code, with the competition of neutron inelastic scattering channels being taken into account. The scheme of

^{186}W levels was taken from work [59]. The evaluation results in the energy range of 120 keV - 1,6 MeV are in good agreement with the experimental data [53,57,58]. For the cross-section evaluation in the neutron energy range of 1,6 MeV - 4 MeV the results of the joint description of the available experimental data [53, 58, 60, 61] by the method of least squares were used. For neutrons with the energy exceeding 4 MeV the evaluation was based on the theoretical description of cross-sections in the model of direct-semidirect radiative capture. Energy cross-section dependence obtained from theoretical calculations was normalized to the radiative capture cross-section value for neutrons with 14,5 MeV energy; this value being evaluated proceeding from the experimental data [43, 62, 63].

The data in Table 3 indicate that reevaluation of the radiative capture cross-sections for the ^{186}W isotope results in improving the agreement with the available experimental data on the thermal cross-section (E_n=0,0253 eV) and resonance capture integral.

According to the present evaluation results the average radiative capture cross-section values in the spectrum of ^{235}U fission by thermal neutrons and in the spectrum of spontaneous ^{252}Cf fission are by 13,5% lower than it proceeds from the ENDF/B-IV evaluation data. Comparing with the data from the ENDF/B-IV library, the average capture cross-section values in the CFRMF, BIG-TEN and SIGMA-SIGMA spectrum also are much lower in terms of the new evaluation. The data on the average cross-sections for these spectra differ by 7,3%, 9,7% and 7,4%, respectively.

REFERENCES

1. Perey F.G. Least-Squares Dosimetry Unfolding: The Program STAYSL. Report ORNL/TM-6062 (ENDF-254), October, 1977.

2. Cullen D.E., McLaughlin P.K. The International Reactor Dosimetry File (IRDF-85). Report IAEA-NDS-41, Rev.1, Vienna, April, 1985.

3. Manokhin V.N., Pashchenko A.B., Plyaskin V.I. e.a. Activation Cross-Sections Induced by Fast Neutrons.

Handbook on Nuclear Activation Data. Vienna, 1987, p.305-411;

Badikov S.A., Pashchenko A.B. Approximation of Reaction Cross-Sections with Charged Particle Emission near Threshold. Problems of Atomic Science and Engineering. Ser.: Nucl. Const., 1987, No.3, p.34.

4. Nolthenius H.J. UNC 32/33 Computer programs for calculating group cross-section covariances from uncertainty parameters in the ENDF/B-V format. Report ECN-86161, ECN, Petten, November, 1986.

5. Rieffe H.Ch. "FITOCO. A program for the conversion of fine group flux density and cross-section data to coarse group values". Report ECN-92, ECN, Petten, April, 1981.

6. Bondars Kh.Ja., Veinbergs Ja.K., Lapenas A.A. Activation cross-sections of some threshold reactions. Nucl.Const., 1974, p.63.

7. Bychkov V.M., Zolotarev K.I., Pashchenko A.B. Creation of computerized library of evaluated threshold reaction cross-sections (BOSPOR-80) and testing BOSPOR-80 by means of integral experimental data. Problems of Atomic Science and Engineering. Ser.: Nucl. Const., 1981, No.3(42), p.60.

8. Bychkov V.M.,Manokhin V.N.,Pashchenko A.B.,Plyaskin V.I. Cross-sections of (n,p), (n,α), (n,2n) threshold reactions. Problems of Atomic Science and Engineering. Ser.: Nucl.Const., 1979, No.1(32), p.27; 1979, No.2(33), p.51; 1979, No.4(35), p.21.
Bychkov V.M.,Manokhin V.N.,Pashchenko A.B.,Plyaskin V.I. Cross-sections of neutron-induced threshold reactions. Moscow, Energoizdat, 1982.

9. Zelenetsky A.V., Ignatyuk A.V., Pashchenko A.B. Analysis of α-claster emission of neutron-induced nuclear reactions. To be published in Nuclear Physics.

10. Nuclear Data For Radiation Damage Assessment and Related Safety Aspects. (Proc. of the Advisory Group Meeting, Vienna, 12-16 October 1981). Report IAEA-TECDOC-263, 1982, p.329.

11. Mannhart W., Smith D.L., Meadows J.W. The D2screpancy Between Differential and Integral Data on ^{47}Ti(n,p).

(Proc. of Internat.Conf. on Nuclear Data for Basic and Applied Science, Santa Fe, 1985), 1985, p.577.

12. Mannhart W. Californium-252 Spectrum Averaged Neutron Cross-Sections. Handbook on Nuclear Activation Data, Vienna, 1987, p.413.

13. Calamand A. Cross-sections for Fission Neutron Spectrum Induced Reactions. Report INDC(NDS)-55/L, 1973.

14. Day Day N., Lemmel H.D., Pronyaev V.G. ENDF/B-V (Rev.2) Dosimetry File, IAEA-NDS-24, Vienna, 1984.

15. ENDF/B Summary Documentation, BNL-NCS-17541 (ENDF-201), compiled by Kinsey R.R., June, 1975.

16. Summary of JENDL-2 General Purpose File, ed. by T.Nakagawa, JAERI-M-84-103, 1984.

17. ENDF/B Summary Documentation, BNL-NCS-17541 (ENDF-201), compiled by Kinsey R.R., July, 1979.

18. ENDF/B-5 Fission products file. Editor Lemmel H.D., IAEA-NDS-25, Vienna, 1979.

19. Zolotarev K.I., Pronyaev V.G. Reevaluation of neutron capture reaction cross-sections and application of results for neutron metrology problems.To be published.

20. Mughabghab S.F.,Divadeenam M.,Holden N.E.Neutron Cross-sections.Vol.1.Neutron resonance parameters and thermal cross-sections.Part A.Z=1-60,New York-London,Academic Press,1981;

Mughabghab S.F. NEUTRON CROSS-SECTIONS. Vol.1. Neutron resonance parameters and thermal cross-sections. Part B Z=61-100, New York - London, Academic Press, 1984.

21. Manturov G.N. et.al. Problems of Atomic Science and Engineering. Ser.: Nucl.Const., No.1, 1983, p.50.

22. Moldauer P.A. Lectures presented at Workshop on Nuclear Model Computer Codes, 16 Jan - 3 Feb 1984, Trieste.

23. Grundl J., Eisenhauer C. Benchmark neutron fields for reactor dosimetry. In Neutron Cross Sections for Reactor Dosimetry. Vol.1, Review papers. Tech Doc. IAEA-208, Vienna, 1978, pp.53-104.

24. Weisbin C.R. Executive Summary. In Benchmark Data Testing of ENDF/B-V, BNL-NCS-31531 (ENDF-311), 1982, pp.1-28.

25. Mannhart W. Californium-252 spectrum averaged neutron cross-sections. In Handbook on Nuclear Activation Data, Tech Rep. Ser. No.273, Vienna, 1987, pp.413-437.

26. Fabry A., McElroy W.N., Kelligg et.al. Review of Microscopic Integral Cross Section Data in Fundamental Reactor Dosimetry Benchmark Neutron Fields. In Neutron Cross Sections for Reactor Dosimetry, vol.1, Review papers, Tech Doc.IAEA-208, Vienna, 1978, pp.233-263.

27. Anderl R.A., Millsap D.A., Rogers J.W. Addendum to integral data-testing report for ENDF/B-V cross-sections EGG-Phys. 5668, Jan 1982.

28. Dezso Z., Chikai J. Average cross-sections for the ^{252}Cf neutron spectrum. Proceeding of International Symposium of ^{252}Cf Utilization, Paris, April 1976.

29. Greenwood R.C., Helmer R.G., Rogers J.W. et.al. Radiometric reaction rate measurements in CFRMF and BIG-TEN. Proceedings of the Second ASTM_EURATOM Symposium on Reactor Dosimetry, NUREG/CP-0004, vol.3, 1977, pp.1207-1221.

30. Barr D.W. Reaction rate measurements in BIG-TEN. Report HEDL-TIME-75-130, 1976, pp.2-7.

31. Macklin R.L., Lazar N.H., Lyon W.S. Phys.Rev., v.107, 1957, p.504.

32. Booth R., Ball W.P., MacGregor M.H. Phys.Rev., v.112, 1958, p.226.

33. Perkin J.L., O'Connor L.R., Coleman R.F. Proc.Phys.Soc., v.72, 1958, p.505.

34. Bame S.J., Cubitt R.L. Phys.Rev., v.113, 1959, p.256.

35. Csikai J., Peto G., Buczko M. et al. Nucl.Phys., v.A95, 1967, p.229.

36. Menlove H.O., Coop K.L., Grench H.A. et al. Phys.Rev., v.163, 1967, p.1299.

37. Rigoleur C.Le., Bluet J.C., Beil H., Leroy J.L. EANDC(E)-140U, 1971.

38. Sigg R.A. Journal "Dissertation abstracts International" B, v.37, 1976, p.2237.

39. Anderson P., Zerro R., Bergquist I. Journal Physica Scripta (SWD), v.21, 1980, p.21.

40. Macklin R.L. Phys.Rev.C, v.29, n.6, 1984, p.1996.

41. Dovbenko A.G., Kolesov V.E., Koroleva V.P. Atomic Energy, 1967, v.23, p.151.

42. Leipunsky A.I. et al. Proceedings of Second Internat. Conference on Peaceful Application of Atomic Energy, Geneva, 1958, v.15, p.18.

43. Schwerer O. et al. Nucl.Phys., 1976,v.A264, p.105.

44. Gleason G. Radioanal. and Radiochem. Lett., v.23, 1975, p.317.

45. R.Van der Linden et.al. Journal of Radioanalytical chemistry, v.11, 1972, p.133.

46. Hughes D.J., Spatz D.B. Phys.Rev., v.91, 1953, p.1423.

47. Vervier J.F. Nuclear Phys., v.9, 1959, p.569.

48. Tolstikov V.A.,Koroleva V.P.,Kolesov V.E.,Dovbenko A.G. Nuclear-physical investigations in USSR, 1968, No.6.

49. Zaikin G.G., Korzh I.A., Sklyar N.T., Totsky I.A. Nuclear-physical investigations in USSR, 1968,No.6,p.103

50. Shuman R.P. Report WASH-1127, 1969, p.72.

51. Diksig M., Strohal P., Peto J. Acta Phys. (Hun), v.28, 1970, p.257.

52. Anand R.P., Bhattacharya D., Jhingan M.L., Kondaiah E. Nuov.Cim., v.50A, 1979, pp.251-252.

53. Voignies J., Joly S., Grenier G. Nucl. Sci. Eng., v.93, No.1, 1986, pp.43-56.

54. Belanova T.S., Ignatyuk A.V., Pashchenko A.B., Plyaskin V.I. Neutron radiative capture. Moscow, Energo-atomizdat, 1986.

55. Guenther P.T. et al. Phys.Rev.C, v.26, 1982, p.2433.

56. Kononov V.N. et al. Nuclear Physics, 1987, v.46(1), p.51

57. Bokhovko M.V. et al. Problems of Atomic Science and Engineering. Ser.: Nucl.Const., 1986, No.1, p.39.

58. Macklin R.L. et al. Nucl.Sci.Eng., v.84, 1983, p.98.

59. Nuclear Data Sheets, v.55, 1988, p.583.

60. Lindner M. et al. Nucl.Sci.Eng., v.59, 1976, p.381.

61. Miskel J.A. et al. Phys.Rev., v.128, 1962, p.2717.

62. Valkonen M. Report Univ. of Jyvaeskylae, JU-RR-1/1976.

63. Magnusson G. et al. Physica Scripta, v.21(1), 1980,p.21.

CONCLUSIONS AND RECOMMENDATIONS

Workshop 1

NUCLEAR AND ATOMIC DATA FOR RADIATION DAMAGE CALCULATIONS AND HELIUM AND OTHER TRANSMUTATION PRODUCT CROSS-SECTION DETERMINATIONS IN HIGH ENERGY NEUTRON FIELDS

Chairman: S. Cierjacks (Federal Republic of Germany)

1. The working group recognized that radiation damage by atomic displacements and the generation of helium and other transmutation products will represent a severe problem in future fusion reactors. The search for appropriate materials requires high-intensity neutron sources which most closely simulate the high-energy spectra and the other irradiation conditions in the various fusion reactor components (especially the first wall). For this purpose, 14 MeV, t-hydrogen d-lithium and spallation sources have been proposed (see IFMIF Meeting, San Diego, February 1989). From these the latter two sources produce continuous spectra with an average neutron energy close to 14 MeV and a significant portion of neutrons in a high-energy tail (up to ~50 MeV for d-lithium and up to ~1 GeV for spallation sources). In contrast to the other proposed high-energy sources, spallation sources are presently in operation (e.g., LANSCE, LANL, US; IPNS, ANL, US; KENS, KEK, Japan; ISIS, RAL, UK) or under construction (SINQ, PSI, Switzerland). Although not yet giving the ultimately requested intensity for radiation damage studies, these sources continue to rapidly develop, driven mainly by solid and liquid state physics.

2. Independent of whether d-lithium or spallation sources will ultimately be used for large-scale radiation damage studies for fusion reactor materials or not, the generation of atomic displacements, helium, and heavier transmutation products must now be studied at greatly extended energies up to 1 GeV, in order to judge the suitability of these sources for fusion-materials radiation damage studies.

3. While being aware of, and supporting, the conclusions and recommendations on radiation damage and damage correlation estimates

177

from the 1981 IAEA Advisory Group Meeting on Nuclear Data for Radiation Damage Assessment and Safety Aspects, the group concentrated discussions on the aspects of neutron fields with largely extended neutron energies.

4. Concerning helium and higher transmutation product cross section measurements the following recommendations are made.

a) The existing high-energy cross section data for helium production and neutron monitor reactions should be compiled as discussed at the present meeting (Appendices I.1-I.3). It is recommended to extend the range of data up to 1 GeV. Requests have been made that the Bologna, KFA and ANL groups investigate the possibility of extended model calculations for some of the most suitable monitor reactions.

b) It is recommended that an evaluation of the two proton monitor reactions $^{12}C(p,3p3n)^{7}Be$ and $^{27}Al(p,3p3n)^{22}Na$ is stimulated. Other reactions such as $^{56}Fe(p,n)^{56}Co$ and $^{65}Cu(p,n)^{65}Zn$ are considered to represent an important means to deal with mixed high-energy neutron-proton fields, typical especially for spallation sources.

c) Many measurements of the present activation reactions leading to long-lived activities of interest in fusion radioactivity calculations are limited in accuracy due to large uncertainties in the half-lives and decay data of the product nuclides. Therefore, it is recommended a reexamination of these data for a broad range of applications is stimulated.

d) The present status of the data on production of transmutation products other than H and He should be improved. It is recommended to gather existing measurements and to foster comparisons with calculations from suitable high-energy nucleon-meson transport codes. In addition to the existing results (for example, from CEC), new experiments are recommended. In this case, thin target measurements are proposed in order to avoid large spectra uncertainties due to the strong depth dependence in thick targets.
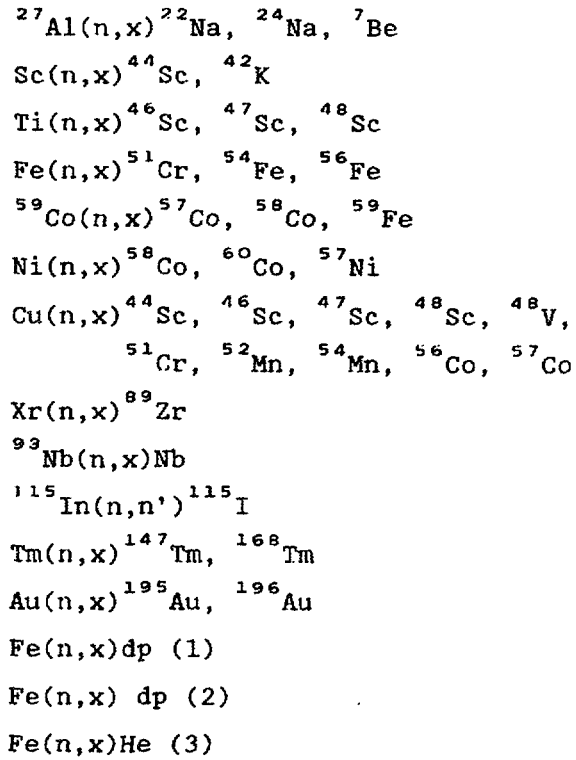
e) The inconsistencies experienced in the Ispra work presented at this meeting suggest that tests of the most important monitor reactions are necessary. Such tests should be carried out with well-defined spectra from time-of-flight measurements, and widely varying spectra, with maximum energies ranging between ~100 and 1000 MeV, should be used.

5. Radiation damage cross section calculations have been discussed with the following conclusions:

a) It is recommended to measure "effective" displacement threshold energies for atoms in compound materials.

b) It appeared highly desirable to find suitable experiments for comparison with basic radiation damage calculations, relating the basic quantities such as Frenkel pairs, etc., to the "macroscopic damage effects" such as radiation-induced hardening, electrical resistivity, etc.

c) Radiation damage cross sections should be made available over the entire energy range from ~1 keV to 1 GeV for one or more recommended materials (e.g., iron and/or copper). Presently there is, however, a discontinuity in the overlapping range, for example, of low energy calculations with SPECTER and high-energy calculations with VNMTC. More theoretical work is recommended to match the two branches suitably in the overlapping range.

d) In addition to the damage due to He released in nuclear reactions, further damage is produced by transmutation products. The basic data needed for a theoretical calculation of this type of damage are the microscopic transmutation production cross-sections and recoil energy spectra. It appears desirable to develop a simple model of damage energy partitioning for the components of alloys and compounds (for example, steel). It is recommended that users are provided with information on available methods (computer codes) for the calculation of these quantities and, as far as possible, to collect the above mentioned data and to create a compilation in a standard form (e.g., ENDF-6 format).

6. Nuclear data needed in activation calculations for fusion reactors have been brought to the attention of the group:

a) The large majority of data needs is taken care of by a number of international efforts.

b) All Member States should be encouraged to contribute to the improvement of the data for the ~250 important neutron-induced reactions listed by the UK group at Harwell (Appendix II).

c) Expertise in charged-particle reactions should be made available and assist in the compilation and dissemination of (x,n) reaction cross sections needed for future more complete activation calculations.

Appendix I.1

Activation Reactions Used in High Energy Neutron Dosimetry
(for spallation sources)

F. Hegedues
Institut Paul Scherrer
CH-5232 Villigen, Switzerland

$^{27}Al(n,x)^{22}Na$, ^{24}Na, ^{7}Be

$Sc(n,x)^{44}Sc$, ^{42}K

$Ti(n,x)^{46}Sc$, ^{47}Sc, ^{48}Sc

$Fe(n,x)^{51}Cr$, ^{54}Fe, ^{56}Fe

$^{59}Co(n,x)^{57}Co$, ^{58}Co, ^{59}Fe

$Ni(n,x)^{58}Co$, ^{60}Co, ^{57}Ni

$Cu(n,x)^{44}Sc$, ^{46}Sc, ^{47}Sc, ^{48}Sc, ^{48}V,
    ^{51}Cr, ^{52}Mn, ^{54}Mn, ^{56}Co, ^{57}Co

$Xr(n,x)^{89}Zr$

$^{93}Nb(n,x)Nb$

$^{115}In(n,n')^{115}I$

$Tm(n,x)^{147}Tm$, ^{168}Tm

$Au(n,x)^{195}Au$, ^{196}Au

$Fe(n,x)dp$ (1)

$Fe(n,x)$ dp (2)

$Fe(n,x)He$ (3)

181

Activation Reactions Used in High Energy Neutron Dosimetry
(for spallation sources)

L.R. Greenwood
Argonne National Laboratory
Argonne, Illinois 60439, USA

$^{27}AL(n,x)\,^{22}Na,\,^{24}Na,\,^{7}Be$

$Fe(n,x)\,^{51}Cr,\,^{52}Mn,\,^{54}Mn$

$^{59}Co(n,x)\,^{52}Mn,\,^{54}Mn,\,^{56}Mn$

$Ti(n,x)\,^{46}Sc,\,^{47}Sc,\,^{48}Sc,\,^{48}V,\,^{44}Sc$

$Ni(n,x)\,^{57}Co,\,^{58}Co,\,^{57}Ni,\,^{56}Co,\,^{52}Mn,\,^{54}Mn$

$Cu(n,x)\,^{48}V,\,^{46}Sc,\,^{47}Sc,\,^{48}Sc,\,^{56}Co,\,^{57}Co,$
$\qquad\quad^{58}Co,\,^{52}Mn,\,^{54}Mn$

$^{65}Cu(p,x)\,^{65}Zn$

$^{56}Fe(p,x)\,^{56}Co$
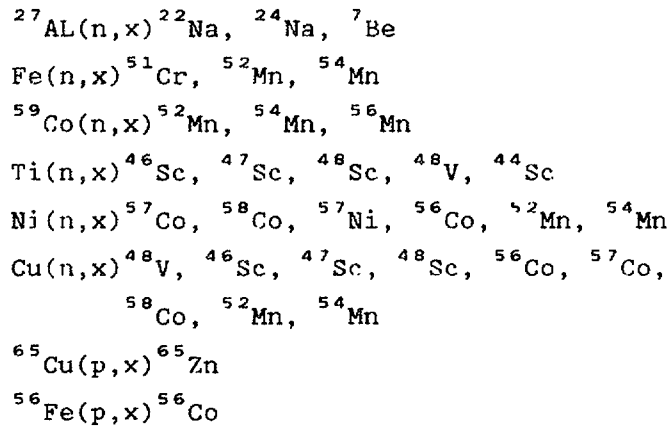
Appendix I.3

Activation Reactions Used in High Energy Neutron Dosimetry

R. Dierckx
European Communities, JRC Ispra, Italy

$$Co(n,\gamma)^{60}Co$$

$$Nb(n,\gamma)^{94}Nb$$

$$Nb(n,n')^{93\mu}Nb$$

$$Fe(n,x)^{54}Mn$$

$$Au(n,3n)^{195}Au$$

$$Ni(n,x)^{54}Mn$$

$$Ni(n,x)^{56}Co$$

$$Ni(n,x)^{57}Co$$

$$Ni(n,x)^{58}Co$$

$$Ni(n,x)^{60}Co$$

$$Ti(n,x)^{44}Ti$$

$$Ti(n,x)^{42}Ar$$

$$Ti(n,x)^{46}Sc$$

Appendix II

Reactions Important for Activation

R.A. Forrest
Nuclear Physics Division
Harwell Laboratory, UKAEA, Oxon. UK

Number	Reaction		
		48	$^{44}Ca(n,a)$
		49	$^{44}Ca(n,na)$
1	$^{11}B(n,d)$	50	$^{44}Ca(n,g)$
2	$^{13}C(n,g)$	51	$^{45}Ca(n,a)$
3	$^{13}C(n,a)$	52	$^{46}Ca(n,na)$
4	$^{14}C(n,na)$	53	$^{46}Ca(n,g)$
5	$^{14}N(n,p)$	54	$^{48}Ca(n,2n)$
6	$^{14}N(n,d)$	55	$^{45}Sc(n,a)$
7	$^{14}N(n,np)$	56	$^{45}Sc(n,p)$
8	$^{16}O(n,a)$	57	$^{45}Sc(n,g)\&$
9	$^{17}O(n,a)$	58	$^{46}Sc(n,na)$
10	$^{17}O(n,na)$	59	$^{45}Ti(n,2n)$
11	$^{20}Ne(n,a)$	60	$^{46}Ti(n,a)$
12	$^{23}Na(n,a)$	61	$^{46}Ti(n,np)\&$
13	$^{24}Mg(n,p)\&$	62	$^{46}Ti(n,d)\&$
14	$^{24}Mg(n,na)$	63	$^{46}Ti(n,2n)$
15	$^{26}Mg(n,g)$	64	$^{47}Ti(n,a)$
16	$^{27}Al(n,2n)\&$	65	$^{47}Ti(n,2n)$
17	$^{27}Al(n,a)\&$	66	$^{48}Ti(n,a)$
18	$^{27}Al(n,na)$	67	$^{49}Ti(n,a)$
19	$^{28}Si(n,na)$	68	$^{49}V(n,a)\&$
20	$^{28}Si(n,np)$	69	$^{51}V(n,a)$
21	$^{28}Si(n,d)$	70	$^{51}V(n,na)$
22	$^{30}Si(n,g)$	71	$^{50}Cr(n,a)$
23	$^{31}Si(n,g)$	72	$^{50}Cr(n,na)$
24	$^{31}P(n,g)$	73	$^{50}Cr(n,g)$
25	$^{32}P(n,p)$	74	$^{50}Cr(n,np)$
26	$^{34}S(n,g)$	75	$^{50}Cr(n,d)$
27	$^{34}S(n,a)$	76	$^{52}Cr(n,a)$
28	$^{35}Cl(n,a)$	77	$^{54}Cr(n,g)$
29	$^{35}Cl(n,p)$	78	$^{54}Mn(n,2n)$
30	$^{37}Ar(n,np)$	79	$^{55}Mn(n,2n)$
31	$^{37}Ar(n,d)$	80	$^{55}Mn(n,g)$
32	$^{40}Ar(n,g)$	81	$^{54}Fe(n,np)$
33	$^{40}Ar(n,2n)$	82	$^{54}Fe(n,d)$
34	$^{39}K(n,p)$	83	$^{56}Fe(n,g)$
35	$^{39}K(n,a)$	84	$^{56}Fe(n,2n)$
36	$^{41}K(n,p)$	85	$^{57}Fe(n,g)$
37	$^{40}Ca(n,a)$	86	$^{58}Fe(n,g)$
38	$^{40}Ca(n,2p)$	87	$^{59}Fe(n,g)$
39	$^{40}Ca(n,g)$	88	$^{58}Co(n,g)$
40	$^{40}Ca(n,np)$	89	$^{59}Co(n,g)\&$
41	$^{40}Ca(n,d)$	90	$^{60}Co(n,p)$
42	$^{42}Ca(n,2n)$	91	$^{60}Co(n,g)$
43	$^{42}Ca(n,a)$	92	$^{58}Ni(n,p)\&$
44	$^{43}Ca(n,2n)$	93	$^{58}Ni(n,g)$
45	$^{43}Ca(n,na)$	94	$^{58}Ni(n,2n)$
46	$^{43}Ca(n,2p)$	95	$^{58}Ni(n,np)$
47	$^{44}Ca(n,2n)$	96	$^{58}Ni(n,d)$

184

Number	Reaction
97	^{60}Ni(n,2n)
98	^{60}Ni(n,p)
99	^{60}Ni(n,np)
100	^{60}Ni(n,d)
101	^{61}Ni(n,g)
102	^{62}Ni(n,g)
103	^{62}Ni(n,a)
104	^{63}Ni(n,a)
105	^{64}Ni(n,2n)
106	^{63}Cu(n,p)
107	^{63}Cu(n,g)
108	^{63}Cu(n,a)&
109	^{64}Zn(n,2n)
110	^{64}Zn(n,p)
111	^{64}Zn(n,na)
112	^{64}Zn(n,2p)
113	^{64}Zn(n,np)
114	^{64}Zn(n,d)
115	^{64}Zn(n,g)
116	^{66}Zn(n,a)
117	^{66}Zn(n,2n)
118	^{92}Zr(n,g)
119	^{93}Zr(n,a)
120	^{94}Zr(n,2n)
121	^{94}Zr(n,na)
122	^{94}Zr(n,g)
123	^{96}Zr(n,2n)
124	^{92}Nb(n,2n)&
125	^{93}Nb(n,2n)&
126	^{93}Nb(n,p)
127	^{93}Nb(n,g)&
128	^{95}Nb(n,2n)&
129	^{92}Mo(n,2n)&
130	^{92}Mo(n,g)&
131	^{92}Mo(n,np)&
132	^{92}Mo(n,d)&
133	^{94}Mo(n,p)&
134	^{94}Mo(n,2n)&
135	^{95}Mo(n,np)&
136	^{95}Mo(n,d)&
137	^{98}Mo(n,g)
138	^{100}Mo(n,2n)
139	^{103}Rh(n,g)&
140	^{103}Rh(n,na)&
141	^{104}Pd(n,g)
142	^{105}Pd(n,g)
143	^{106}Pd(n,g)&
144	^{107}Pd(n,g)
145	^{108}Pd(n,g)&
146	^{107}Ag(n,g)^{m}
147	^{107}Ag(n,p)&
148	^{107}Ag(n,2n)&
149	^{109}Ag(n,2n)^{m}
150	^{109}Ag(n,g)^{m}
151	^{110}Cd(n,g)&
152	^{111}Cd(n,g)
153	^{112}Cd(n,g)^{m}
154	^{112}Sn(n,a)
155	^{116}Sn(n,a)^{m}
156	^{117}Sn(n,n')^{m}
157	^{119}Sn(n,n')^{m}
158	^{120}Sn(n,g)^{m}
159	^{122}Sn(n,g)^{m}
160	^{124}Sn(n,g)
161	^{125}Sn(n,g)
162	^{121}Sb(n,p)^{m}
163	^{121}Sb(n,g)
164	^{121}Sb(n,2n)
165	^{123}Sb(n,g)&
166	^{123}Sb(n,2n)&
167	^{124}Sb(n,g)
168	^{125}Sb(n,p)&
169	^{126}Sb(n,p)&
170	^{122}Te(n,g)^{m}
171	^{136}Cs(n,g)
172	^{137}Ba(n,p)
173	^{139}La(n,a)&
174	^{139}La(n,h)
175	^{140}Ce(n,2n)&
176	^{140}Ce(n,a)&
177	^{148}Nd(n,g)
178	^{150}Nd(n,g)
179	^{150}Nd(n,2n)
180	^{150}Sm(n,g)
181	^{151}Sm(n,g)
182	^{152}Sm(n,g)
183	^{152}Sm(n,2n)
184	^{151}Eu(n,g)
185	^{151}Eu(n,2n)^{m}
186	^{152}Eu(n,g)
187	^{153}Eu(n,g)&
188	^{153}Eu(n,2n)^{g}
189	^{154}Eu(n,g)
190	^{158}Gd(n,g)
191	^{160}Gd(n,2n)
192	^{159}Tb(n,2n)&
193	^{158}Dy(n,p)&
194	^{165}Ho(n,2n)&
195	^{165}Ho(n,g)^{m}
196	^{166}Ho(n,n')^{m}
197	^{164}Er(n,2n)
198	^{177}Hf(n,g)^{n}
199	^{178}Hf(n,n')^{n}
200	^{178}Hf(n,2n)&
201	^{178}Hf(n,g)^{n}
202	^{179}Hf(n,n')^{n}
203	^{179}Hf(N,2n)^{n}
204	^{180}Hf(n,2n)^{n}
205	^{180}Hf(n,g)
206	^{180}Hf(n,3n)^{n}
207	^{181}Hf(n,g)&
208	^{179}Ta(n,2n)&
209	^{181}Ta(n,na)^{g}
210	^{181}Ta(n,2n)^{m}
211	^{181}Ta(n,g)&
212	^{181}Ta(n,t)^{n}

Number	Reaction		
		234	$^{191}Ir(n,g)^n$
		235	$^{191}Ir(n,na)$
213	$^{181}Ta(n,nd)^n$	236	$^{191}Ir(n,2n)$&
214	$^{182}Ta(n,p)$&	237	$^{192}Ir(n,n')^n$
215	$^{182}Ta(n,g)$	238	$^{193}Ir(n,2n)^n$
216	$^{180}W(n,2n)$&	239	$^{192}Pt(n,g)$&
217	$^{182}W(n,a)^n$	240	$^{194}Pt(n,2n)$&
218	$^{182}W(n,na)^n$	241	$^{197}Au(n,a)$&
219	$^{182}W(n,g)$&	242	$^{197}Au(n,2n)$&
220	$^{183}W(n,g)$	243	$^{195m}Hg(n,2n)$
221	$^{184}W(n,g)$&	244	$^{196}Hg(n,2n)^m$
222	$^{186}W(n,g)$	245	$^{203}Tl(n,2n)$
223	$^{186}W(n,na)$&	246	$^{204}Pb(n,p)$
224	$^{185}Re(n,g)^m$	247	$^{204}Pb(n,t)$
225	$^{187}Re(n,2n)^m$	248	$^{204}Pb(n,2n)$&
226	$^{187}Re(n,g)$&	249	$^{204}Pb(n,n')^m$
227	$^{188}Os(n,g)$&	250	$^{206}Pb(n,2n)$
228	$^{188}Os(n,p)$&	251	$^{206}Pb(n,a)$
229	$^{189}Os(n,g)$&	252	$^{208}Pb(n,g)$
230	$^{190}Os(n,g)$&	253	$^{208}Bi(n,2n)$
231	$^{190}Os(n,a)$	254	$^{209}Bi(n,2n)$
232	$^{192}Os(n,g)$	255	$^{209}Bi(n,g)$
233	$^{192}Os(n,2n)$&	256	$^{210}Po(n,2n)$

& indicates the sum of cross sections forming all isomeric states.

If particular isomeric products are required these are shown by:

g ground state   m 1st isomer   n 2nd isomer

EVALUATION OF PRELIMINARY RESULTS OF
THE REAL-88 INTERLABORATORY EXERCISE

Chairman: **H.J. Nolthenius** (Netherlands)

The last phase of the REAL-88 exercise was discussed, especially the topics related to the purpose of this Advisory Group Meeting:

A) IRDF-90 (to be released in the first half of 1990)

The participants of the workshop were informed on the present status of updating of the International Reactor Dosimetry File. The main changes are as follows: 15 new evaluations for threshold reactions have been included: 2 threshold reactions have been considerably modified (TI47P, NI60P); furthermore 4 new reactions have been added to the library. The uncertainty data are generally lower than in the previous edition. The capture cross sections remained unaltered. It should be ensured that

1. Irregularities of the capture reaction cross sections which were detected are corrected (mentioned in the report "The role of the REAL-88 exercise in the radiation damage characterization of nuclear facilities" of this Advisory Group Meeting).

2. The gas production cross sections of the IRDF-85 be updated.

3. Recent damage cross sections be incorporated.

4. The library be made available both in interpolable point data and 640 (SAND II) group format.

5. A report be issued (in the frame work of the REAL-88 exercise) on the differences between the IRDF-85 and IRDF-90.

B) Processing of cross section uncertainties

6. The comparison of multigroup cross section uncertainties calculated by the program package NJOY and UNC32/33 should be organized.

7. The feasibility of supplying multigroup uncertainty data in a more suitable format for neutron spectrum adjustment should be investigated.

C) Contents of the REAL-88 reference file

The reference file will contain cross section libraries, input data sets for different adjustment tasks, a STAY'SL-type adjustment code, cross section processing codes and several utility programs, and a complete output set.

8. Both the IRDF-85 and IRDF-90 640-group cross section libraries should be present in the neutron spectrum adjustment reference file of the REAL-88 exercise. The IRDF-85 should be used for testing the user's adjustment procedure, while the IRDF-90 should be used for adjustment tasks in daily practice.

9. The situation with respect to the development of the STAY'SL-type code on PCs should be clarified before inserting it into the reference file.

10. As cross section processing codes, the UNC32/33 and FITOCO, both in standard FORTRAN-77 versions, should be included.

11. Among the utility programs should be present the STAYDEXP for calculating the (output) damage exposure parameters, and spectrum characterizing parameters. In special cases the code BLOWUP might be useful.

12. The ENDF pre-processing code package (RECENT, LINEAR, GROUPIE, etc.) need not be included in the reference file. It should be distributed separately.

D) Miscellaneous

13. The participants of the workshop suggested to organize in early 1991 a second Specialists' Meeting on the Requirements and Status of Covariance Data in Evaluated Data Files to review the progress since the Rome Meeting in 1986. They agreed that one

of the most important tasks is to make available the covariance information on the scattering cross sections.

14. It is reiterated that the users should perform a separate and detailed study of the effect of neutron self-shielding in activation detectors, and of the influence of covers around the detectors (e.g., Cd, Gd and/or the stainless steel wall of the reactor PV surveillance irradiation capsules). The impact of cover-material cross sections on the developed neutron spectrum should be investigated in detail.

15. The systematic differences which are detected between the STAY'SL and LSL adjustment procedures should be explained.

16. Neutron spectrum adjustment computations should be made more user-friendly.

E) The "Post-REAL" situation

After the distribution of the REAL-88 reference file, the "evaluators" will continue their work on the following items:

- testing the IRDF-90 in neutron spectrum adjustment calculations
- definition of new test cases for neutron spectrum adjustment runs using up-to-date information (probably also for fusion spectra)
- recommendations to organize the continuation of this workshop during the 7th ASTM-EURATOM Symposium on Reactor Dosimetry, and the following meeting at the time of the next AGM (probably in 1993), to discuss the state-of-art of neutron spectrum adjustment and radiation damage prediction.

LIST OF PARTICIPANTS

AUSTRIA

H.K. Vonach
Institut für Radiumforschung
   und Kernphysik
Boltzmanngasse 3
A-1090 Vienna

CZECHOSLOVAKIA

B. Osmera
Nuclear Research Institute
CS-250 68 Rez u Prahy

GERMANY, Fed. Republic of

S. Cierjacks
Institut für Angewandte Kernphysik
Kernforschungszentrum Karlsruhe
Postfach 3640
D-7500 Karlsruhe

HUNGARY

Mrs. E. Zsolnay
Budapest Training Reactor
Department of Physics
Technological University
Muegyetem-Rkp. 3
H-1521 Budapest

E. Szondi
Department of Physics
Technological University
Muegyetem-Rkp. 3
H-1521 Budapest

ITALY

Mrs. M. Petilli
ENEA - Centro Studi Nucleari
   - Cassaccia
Santa Maria di Galeria
C.P. 2400
I-00100 Roma AC

V. Sangiust
Politecnico di Milano - CESNEF
Instituto di Ingegneria Nucleare
Via Ponzio 34/3
I-20133 Milano

NETHERLANDS

H.J. Nolthenius
Netherlands Energy Research
   Foundation (ECN)
P.O. Box 1
1755 ZG Petten

SWITZERLAND

F. Hegedüs
Institut Paul Scherrer
CH-5232 Villigen PSI

U.S.S.R.	A.B. Pashchenko
	Centr po Jadernym Dannym
	Fiziko-Energeticheskij Institut
	Ploschad Bondarenko
	249 020 Obninsk, Kaluga Region

V.V. Gann
Physics-Technical Institute
Academy of Sciences of the
    Ukrainian SSR
Khar'kov 310108

A.I. Ryazanov
Institut Atomnoi Energii
    I.V. Kurchatova
Ploschad I.V. Kurchatova
SU-123182 Moscow D-182

UNITED KINGDOM

M.G. Sowerby
Nuclear Physics and Instrumentation
    Division
Building 418
Harwell Laboratory
Didcot, OXON OX11 ORA

U.S.A.

L.R. Greenwood
Argonne National Laboratory
Fusion Power Program, Building 205
Argonne, Illinois 60439

F.J. Ruddy
Westinghouse Research and Development
    Center
1310 Beulah Road
Pittsburgh, Pennsylvania 15235

INTERNATIONAL ORGANIZATIONS

R. Dierckx
Physics Division B44
Euratom CCR
Commission of the European Communities
Joint Research Establishment
Ispra Establishment
I-21020 Ispra (Varese), Italy

W. Matthes
Joint Research Centre
Commission of the European
    Communities
Ispra Establishment
21020 Ispra (Varese), Italy

G. Tsotridis
Netherlands Energy Research
    Foundation (ECN)
P.O. Box 2
1755 ZG Petten, the Netherlands

192

V.A. Konshin
IAEA Division of Physical and Chemical
    Sciences
Wagramerstr. 5, P.O. Box 100
A-1400 Vienna, Austria

J.J. Schmidt
IAEA Nuclear Data Section
Wagramerstr. 5, P.O. Box 100
A-1400 Vienna, Austria

N. Kocherov (Scientific Secretary)
IAEA Nuclear Data Section
Wagramerstr. 5, P.O. Box 100
A-1400 Vienna, Austria

HOW TO ORDER IAEA PUBLICATIONS

■ An exclusive sales agent for IAEA publications, to whom all orders
and inquiries should be addressed, has been appointed
in the following country:

UNITED STATES OF AMERICA   UNIPUB, 4611-F Assembly Drive, Lanham, MD 20706-4391

■ In the following countries IAEA publications may be purchased from the
sales agents or booksellers listed or through
major local booksellers. Payment can be made in local
currency or with UNESCO coupons.

ARGENTINA	Comisión Nacional de Energía Atómica, Avenida del Libertador 8250, RA-1429 Buenos Aires
AUSTRALIA	Hunter Publications, 58 A Gipps Street, Collingwood, Victoria 3066
BELGIUM	Service Courrier UNESCO, 202, Avenue du Roi, B-1060 Brussels
CHILE	Comisión Chilena de Energía Nuclear, Venta de Publicaciones, Amunategui 95, Casilla 188-D, Santiago
CHINA	IAEA Publications in Chinese: China Nuclear Energy Industry Corporation, Translation Section, P.O. Box 2103, Beijing IAEA Publications other than in Chinese: China National Publications Import & Export Corporation, Deutsche Abteilung, P.O. Box 88, Beijing
CZECHOSLOVAKIA	S.N.T.L., Mikulandska 4, CS-116 86 Prague 1 Alfa, Publishers, Hurbanovo námestie 3, CS-815 89 Bratislava
FRANCE	Office International de Documentation et Librairie, 48, rue Gay-Lussac, F-75240 Paris Cedex 05
HUNGARY	Kultura, Hungarian Foreign Trading Company, P.O. Box 149, H-1389 Budapest 62
INDIA	Oxford Book and Stationery Co., 17, Park Street, Calcutta-700 016 Oxford Book and Stationery Co., Scindia House, New Delhi-110 001
ISRAEL	Heiliger & Co. Ltd. 23 Keren Hayesod Street, Jerusalem 94188
ITALY	Libreria Scientifica, Dott. Lucio de Biasio "aeiou", Via Meravigli 16, I-20123 Milan
JAPAN	Maruzen Company, Ltd, P.O. Box 5050, 100-31 Tokyo International
PAKISTAN	Mirza Book Agency, 65, Shahrah Quaid-e-Azam, P.O. Box 729, Lahore 3
POLAND	Ars Polona-Ruch, Centrala Handlu Zagranicznego, Krakowskie Przedmiescie 7, PL-00-068 Warsaw
ROMANIA	Ilexim, P O. Box 136-137, Bucharest
SOUTH AFRICA	Van Schaik Bookstore (Pty) Ltd, P.O. Box 724, Pretoria 0001
SPAIN	Díaz de Santos, Lagasca 95, E-28006 Madrid Díaz de Santos, Balmes 417, E-08022 Barcelona
SWEDEN	AB Fritzes Kungl. Hovbokhandel, Fredsgatan 2, P.O. Box 16356, S-103 27 Stockholm
UNITED KINGDOM	HMSO, Publications Centre, Agency Section, 51 Nine Elms Lane, London SW8 5DR
USSR	Mezhdunarodnaya Kniga, Smolenskaya-Sennaya 32-34, Moscow G-200
YUGOSLAVIA	Jugoslovenska Knjiga, Terazije 27, P.O. Box 36, YU-11001 Belgrade

---

■ Orders from countries where sales agents have not yet been appointed and
requests for information should be addressed directly to:

**Division of Publications
International Atomic Energy Agency
Wagramerstrasse 5, P.O. Box 100, A-1400 Vienna, Austria**